UNCLASSIFIED

AD **272 244**

Reproduced
by the

ARMED SERVICES TECHNICAL INFORMATION AGENCY
ARLINGTON HALL STATION
ARLINGTON 12, VIRGINIA

HE-150-192

UNIVERSITY OF CALIFORNIA

INSTITUTE OF ENGINEERING RESEARCH

BERKELEY CALIFORNIA
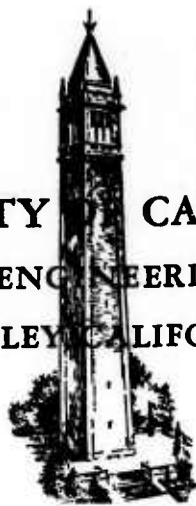
SPHERE DRAG IN A LOW DENSITY SUPERSONIC FLOW

by

Jerome Aroesty

SPHERE DRAG IN A LOW DENSITY SUPERSONIC FLOW

by

Jerome Aroesty

Submitted in partial satisfaction of the
requirements for the degree of Doctor of
Philosophy in Engineering Sciences

FACULTY INVESTIGATORS:

S. A. SCHAAF, PROFESSOR OF ENGINEERING SCIENCES
L. TALBOT, ASSOCIATE PROFESSOR OF AERONAUTICAL SCIENCES
G. J. MASLACH, PROFESSOR OF AERONAUTICAL ENGINEERING

Approved _S a Schaaf_

ABSTRACT

Sphere drag coefficients were measured in the Berkeley Low Density Wind Tunnel at Mach numbers of 2, 4, and 6, and free stream Reynolds numbers between 10 and 10,000 for both insulated and cold wall conditions. The measurements indicate that sphere drag in this regime is strongly dependent on the Reynolds number behind a normal shock wave, and only weakly dependent on Mach number. In addition, it was found that a decrease in T_w/T_o from 1 to 0.26 was accompanied by a 5 - 10% decrease in the drag coefficient.

The tests were performed using two different force measuring techniques. A precision microbalance was used to obtain data for insulated spheres, and a moving model technique was used to obtain data for small spheres falling freely through a wind tunnel jet. These latter tests were performed using both cold and insulated models.

The results obtained on insulated spheres at Mach numbers of 2 and 4 were in good agreement with the measurements of other investigators. The results of the cold wall tests indicate that for Mach numbers greater than 5 in air, sphere drag coefficients are a function only of T_w/T_o and the post normal shock Reynolds number.

TABLE OF CONTENTS

LIST OF SYMBOLS

A   film length in cm per four timing marks

B   coefficient of linear term in the framing rate equation

$$\frac{dN}{dt} = C(A + BN)$$

C   dimensional constant in framing rate equation

C_D sphere drag coefficient

$$\frac{\text{drag force}}{q_\infty \; \frac{\pi \, D^2}{4}}$$

D   sphere diameter

$f''(0)$ shear parameter of boundary layer theory

local shear stress $\sim f''(0) \cdot$ function of (x)

$g'(0)$ heat transfer parameter of boundary layer theory

local heat flux $\sim g'(0) \cdot$ function of x

Kn   Knudsen number, $\quad \lambda_\infty/D$

M   Mach number

$\overline{M}$ magnification factor   ft/in

n   exponent in viscosity-temperature formula $\mu \sim T^n$

Re_∞ Reynolds number based on diameter and free stream condition

Re_2 Reynolds number based on diameter and post normal shock

condition

S   molecular speed ratio, $\quad U/\sqrt{2RT}$

T_∞ static temperature

T_o stagnation temperature

T_w wall temperature

U   velocity

w   specific weight, $\#/\text{in}^3$

σ' normal momentum exchange parameter

σ tangential momentum exchange parameter

ρ density

I. INTRODUCTION

As new values of gasdynamic, thermal and chemical parameters become significant, and as new facilities and instruments are developed, a problem which is often considered is the determination of the drag force acting on an isolated sphere in a uniform stream. The current investigation is concerned with the experimental determination of sphere drag coefficients in the supersonic rarefied gas regime which is characterized primarily by relatively thick viscous layers and by the corresponding large viscous contributions to the drag force[1].

The present experiments had a two-fold purpose; the first objective was to supply empirical drag information for Mach numbers of 2, 4, 6, free stream Reynolds numbers varying from 10 to 10,000, and free stream Knudsen numbers varying from 0.3 to 0.001 for the case when both the sphere wall temperature and the stagnation temperature were at ordinary room levels. The second objective was to determine whether any significant change in drag coefficient could be produced by a reduction in the sphere wall temperature from 300° K to 80° K while the free stream Mach number, Reynolds number, Knudsen number, and stagnation temperature were held fixed.

The experiments were performed in the Berkeley Low Density Wind Tunnel, where previous studies of sphere drag in a supersonic low density flow were made over a portion of the present range of parameters. During the performance of the current series of tests, no provision had yet been made for increasing the wind tunnel supply temperature beyond ordinary room temperature levels. The thermal properties of air are well known for the range of pressures

and temperatures encountered during these experiments, and it is certain that no dissociation, ionization, condensation, or other real gas phenomena were present.

In terms of complete simulation of the free flight case, it is clear that the stagnation temperature levels of the wind tunnel tests were significantly lower and the chemical composition somewhat different from those encountered in flight. Since stagnation temperature, sphere temperature and chemical composition are all important in determining the presence of real gas effects, a complete simulation would probably include these parameters as well as Reynolds number, Mach number, Knudsen number and the ratio T_w/T_o. If hypersonic free flight in the low density regime is accompanied by large departures from thermodynamic equilibrium[2] which arise from the relative inability of parts of the flow held to provide sufficient numbers of collisions for the appropriate equilibrium to occur, then this too will affect the drag force, and should be considered in simulation studies. However, it is quite possible that adequate simulation for a gross property such as drag could be obtained with the duplication of only a few important parameters. For the range of parameters encountered during the current investigation, partial simulation of the hypersonic flight of a sphere in the upper atmosphere can be achieved by requiring that Re_2 be identical for both free flight and wind tunnel tests, and that T_w/T_o be < 1 for both cases.

II. PREVIOUS THEORETICAL WORK

Theoretical calculations of the drag coefficient of a sphere in a supersonic rarefied gas flow are available for the free molecule flow regime[3] and the near-free-molecule or transition regime[4,5,6,7].

These calculations, which are applicable only to larger values of the Knudsen number than those encountered during the present experiments, reveal salient points about the structure of a very rarefied gas flow. In a free molecule flow, the role of intermolecular collisions is to maintain the uniform Maxwellian velocity distribution of the free stream. This requires that the sphere diameter be very small compared to the distance between collisions in order for the effect of the body on the otherwise uniform flow to be neglected.

At any point in the flow the distribution function possesses a true two sided character, since molecules which are in the solid angle Ω subtended by the sphere and which have recoiled from the sphere, possess a completely different distribution function than those molecules in the remaining $4\pi-\Omega$ solid angle. The distribution function of the recoiling molecules helps determine the net transport of energy and momentum to the sphere, but does not in any significant way affect the distribution function of incoming molecules. The drag coefficient for free molecule flow can be written

$$C_D = C_{D_o} + C_{D_{recoil}} \tag{II-1}$$

where C_{D_o} is related to the momentum imparted by the incoming molecules, $C_{D_{recoil}}$ is related to the momentum imparted by molecules which recoil from the sphere.

The nature of the particle-surface interaction is of fundamental importance in determining $C_{D_{recoil}}$, while C_{D_o} is a function of molecular speed ratio alone. Values of C_D, C_{D_o} and $C_{D_{recoil}}$ are presented in Figure 1 for the range of Mach number and wall temperature encountered during the experiments. The estimates of C_D and $C_{D_{recoil}}$ are made on the basis of purely diffuse reflection corresponding to emission from the wall with a wall Maxwellian distribution. For hypersonic flow corresponding to $S \geq 6$ in this case, C_{D_o} is constant at a value of 2. This value is twice the drag coefficient calculated by hypersonic Newtonian theory in the absence of centrifugal corrections[8]. The difference between the two results may be interpreted in the following way. Resolving C_{D_o} into two components, corresponding to normal and tangential momentum,

$$C_{D_o} = C_{D_o press} + C_{D_o skin friction}.$$ Hypersonic Newtonian theory neglects $C_{D_o skin friction}$ because the model is based on an inviscid thin shock layer which is incapable of sustaining any shear. Since $C_{D_o press}$ and $C_{D_o skin friction}$ are both equal to one, it is clear that the additional consideration of tangential momentum transfer to the sphere is responsible for the larger value of the Newtonian free molecule drag coefficient than that obtained by a purely inviscid analysis.

Molecular beam experiments indicate that normal momentum transfer to a surface at an arbitrary angle is a function of the wall temperature, while transfer of tangential momentum is relatively insensitive to this parameter. This can be seen by considering the results using the three parameter interaction model, σ, σ', α which is discussed in reference 9. The pressure on any surface in free

molecule flow can be written as

$$p = \rho V^2 f(S, \sigma', \theta, T_w, T_w/T_\infty) \qquad \text{(II-2)}$$

while the shear τ can be written as

$$\tau = \sigma \rho V^2 \bar{f}(\theta, S) . \qquad \text{(II-3)}$$

This result indicates that the only manner in which the wall temperature can change the free molecule drag coefficient is through a change in the normal momentum transfer. It is interesting to contrast this behavior with the behavior predicted by laminar boundary layer theory (valid for small Kn but large Re). Solutions of similar compressible boundary layer flows indicate that the shear stress at the wall is a function of wall temperature. If the boundary layer approximation is considered as a leading term in a solution of the Navier Stokes equations, then it follows that wall temperature can affect the normal momentum transfer to the surface only through the induced pressure, which can be comparatively small for blunt body flows. This fundamental change in the role of the wall temperature in determining aerodynamic coefficients as the mean free path varies suggests that extrapolation of results from one regime to another may yield the proper gross coefficients but will not reflect the true physics of the flow.

While free molecule flow past a sphere seems to be well understood, except for the problem of surface-particle interactions,

the asymptotic approach to this regime as the Knudsen number decreases is not nearly so well defined. First collision and first iterate solutions[4,5,6,7] indicate that for this geometry there is a likelihood that the drag coefficient can be written as

$$C_D = C_{D_{FM}} \left[1 - \frac{A}{Kn} \right] \tag{II-4}$$

where A is given by

$$\frac{0.26 \left[\frac{\gamma}{6} \right]^{1/2} M \left[\frac{T_\infty}{T_w} \right]^{1/2} - \frac{1}{\sqrt{2}} (1.30)}{C_{D_{FM}}}$$

in the calculations of Charwat and Baker[4]. The above solution is valid only for supersonic flow and a cooled body.

A result of both first iterate and first collision calculations is that the primary effect of collisions between molecules leaving the body and incoming molecules is to shield the body from some of these incoming molecules and thus to decrease the drag coefficient. In view of the approximations involved in the computations, perhaps the most significant result is that for particles reflecting diffusely from a very cold wall, and hypersonic flow, the Reynolds number and temperature ratio enter into the drag coefficient in the form:

$$C_D = C_{D_{FM}} \left[1 - \frac{0.15 \, Re}{C_{D_{FM}}} \left(\frac{T_\infty}{T_w} \right)^{1/2} \right] \tag{II-5}$$

As far as the utility of equation (II-4) for engineering estimates is concerned, it is probably true that in the region of theoretical validity the uncertainty in the nature of the particle-surface interaction is of larger magnitude than the correction to free molecule flow values given by the term in $1/Kn$, particularly in the light of the restrictive assumptions necessary to the various calculations.

While solutions are available for sphere drag in a supersonic highly rarefied gas flow, there are no theoretical solutions which are valid at lower Knudsen numbers. A boundary layer solution, constructed by patching together an inviscid flow and a laminar boundary layer flow, has not yet been presented for this problem. In fact, an inviscid calculation which is valid over the supersonic as well as subsonic parts of the flow field has not yet been performed. If this theoretical inviscid solution were in hand, it would then be possible to consider the still formidable question of the calculation of displacement thickness and shear stress for a compressible non-similar boundary layer with heat transfer. Since "local similarity"[10] is of questionable validity for the calculation of shear, and since integral techniques are not very suitable to compresible flows with heat transfer[8], a series expansion analogous to the Blasius series of incompressible sphere flow would be a more reliable mode of solution.

Calculation of a non-similar laminar compressible boundary layer entails the solution of a set of partial differential equations for the particular inviscid flow under consideration. For the case of adiabatic flow, when $\mu \sim T$ and $Pr = 1$, the use of the Stewartson transformation reduces the non-similar compressible flow to a non-similar

incompressible flow. Fortunately, the transformed incompressible flow corresponds to boundary layer flow over an axisymmetric blunt body, whose properties may be calculated by the use of the series solutions tabulated in reference 44. Thus, for this case all the relevant differential equations have been solved. Because the solutions are given in the incompressible plane it is then necessary to transform into the appropriate compressible laminar flow. A requirement for the use of the solutions given in reference 44 is that both the sphere radius R and the incompressible velocity U_i be expanded in an oddpower series in X_i, with the leading term in each series corresponding to rotationally symmetric stagnation point flow.

Because of the lack of theoretical knowledge of the complete inviscid flow field, and because the present application did not warrant an exact solution of the boundary layer equations, a simple integral technique was utilized to provide estimates of the skin friction drag. The method of Rott and Crabtree[43], as applied to adiabatic flow for the case of $\mu \sim T$ and $Pr = 1$ yielded the estimates

$$C_{D_{SF}} \sim \frac{1}{\sqrt{Re_2}} \quad (2) \quad \text{at} \quad M = 6$$

$$C_{D_{SF}} \sim \frac{1}{\sqrt{Re_2}} \quad (5/2) \quad \text{at} \quad M = 2$$

These coefficients 2 and 5/2 must be regarded as only representing the order of magnitude of the boundary layer coefficients, because of the use of several simplifying assumptions. The empirical formula, $C_p = C_{p_{max}} \cos^2 \theta$ was used in the region from $\theta = 0$ to $90°$, and the

integration of shear stress was arbitrarily stopped at $\theta = 90°$.

Speculation concerning the properties of the boundary layer solution is reinforced somewhat by consideration of known properties of various laminar compressible flows with heat transfer.

1) The similar solutions of reference 11 for $Pr = 1$, $\mu \sim T$, indicate that surface shear stress is a function of wall temperature. The two effects, steepening of the velocity profile and varying of viscosity, act in different ways, but the combined effect is to cause a moderate reduction in shear as the wall is cooled.

2) The flat plate laminar shear stress formula of Young[12],

$$C_F = \frac{0.664}{\sqrt{Re_x}} \left[0.45 + 0.55 \frac{T_w}{T_\infty} + 0.09 \ (\gamma-1) \ M^2 \ Pr^{1/2} \right]^{\frac{n-1}{2}} \qquad (II-6)$$

indicates that wall temperature and Mach number can affect shear stress only at sufficiently high temperature levels such that $n \neq 1$. The results of reference 13 show this quite clearly for the case of flow past a wedge. Of course, the effects of pressure gradient are not considered.

3) The theory of reference 10, which has been shown to be satisfactory for prediction of the heat transfer on highly cooled bodies[14], suggests that the surface heat rate at all stations on a hemisphere section is independent of Mach number and a function only of conditions at the stagnation point if the Mach number is sufficiently high. If this result can be extended to shear stress at the wall, then it would be a corrollary that the integrated shear force could be represented as

$$C_{D_{shear}} \sim \frac{F\left[\gamma,\ T_w,\ T_o\right]}{\sqrt{Re_2}} \tag{II-7}$$

$$M > 10$$

The validity of this "local similarity" technique is not verified for shear, and in fact, it is almost certain to be much less suitable for predicting skin friction than it is for determining heat rates. This is in view of the large variation of $f''(0)$ (the shear parameter) with β and T_w/T_o compared to the very small variation of $g'(0)$ (heat transfer parameter) over the values of β that are relevant to a 3-dimensional blunt body flow[11].

If an analogy between shear stress and heating rate can be drawn from reference 10, then it would be in the form of

$$\frac{[\tau/\theta]}{[\tau/\theta]_o} = \frac{\dot{q}}{\dot{q}_o} = f(\theta,\ M_\infty)\ , \tag{II-8}$$

in keeping with the technique adopted by Lees, where $g'_w(0)$ and $f''_w(0)$ are kept at their stagnation values.

Reference 10 considers the variation in the ratio q/q_o with Mach number and angular position on a hemisphere cylinder, using an empirical pressure formula to calculate external properties. The results indicate that this ratio q/q_o is perhaps 60% larger on the supersonic parts of the hemisphere at $M = 2$ than it is at $M = 6$. Since this is the region that must contribute a substantial portion of the viscous drag force, the inference can be drawn that the skin friction drag on a sphere may show an increase as the Mach number is decreased. However,

this is a thoroughly speculative statement. A more reliable inference is that the skin friction drag coefficient will be a function of free stream Mach number until hypersonic flow is attained, as well as the Reynolds number based on conditions behind a normal shock wave.

There has been a great deal of study recently given to the extension of boundary layer results to lower Reynolds number flows by the consideration of various higher order effects which were neglected in the original boundary layer analysis. If a systematic technique is adopted, the boundary layer solution is the leading term in the expression for C_F, with the next higher order effects generally being proportional to $1/Re$ (for blunt bodies).[15] Since no results for flow over an entire sphere (until separation) have yet been calculated using the various proposed methods, and since the objective at present seems to be primarily to investigate the stagnation point region, very little relevant information can yet be drawn from these theories.

The effect of the base region on a sphere becomes unimportant as the Mach number increases, but at a Mach number of 2, it may contribute a substantial (20%) amount to the total drag. A theoretical investigation of low Reynolds number base flow on a sphere has not yet been accomplished, although theories and experiments are available for a cone cylinder and spheres at higher Reynolds numbers[19,25]. In view of the lack of specific knowledge concerning the viscous wake region, no valid estimates are possible concerning the effects of the wake on the separation point and the pressure distribution over the sphere base.

In addition, it is not presently certain just how the separation point is affected by Mach number, Reynolds number and wall temperature.

The results of incompressible boundary layer theory indicate that it is not possible to extimate the drag coefficient and separation point accurately without using the empirical pressure distribution around a sphere. While the supersonic case may be different, it should be noted that it is only the local boundary layer order shear stress which varies like $1/\sqrt{Re_2}$, while the integrated skin friction drag must be a function of the separation point, which in turn may be a complicated function (as yet unknown) of the parameters. The variation in the separation point could conceivably be more significant in determining the drag coefficient than the higher order corrections to boundary layer theory, particularly at low Mach numbers.

In the light of the still unsolved problems of supersonic low Reynolds number flow over a sphere, only a form for the variation of C_D can be postulated-- $C_D = A + B/\sqrt{Re_2} + C/Re_2$, (equation II-9), where A, B, C are $f(M, T_w, T_o)$. If A is identified with the pressure drag, $B/\sqrt{Re_2}$ is identified with the boundary layer order shear stress and the induced pressure effect on the drag, and C/Re_2 contains all higher order effects, then it is only known that A must be a number somewhat close to 1, and B must be positive. The magnitude and sign of C/Re is unknown in view of its purely tentative nature. In addition, as $M \rightarrow \infty$, A and B should become relatively independent of the free stream Mach number.

In summation, the statement can be made that theoretical calculations of sphere drag at supersonic velocities are available for the high Knudsen number regime, whereas only crude arguments are available for flows at lower Knudsen numbers.

III. PREVIOUS EXPERIMENTAL WORK

While theoretical calculations have been made of sphere drag in a supersonic rarefied gas stream only for the limit of large Knudsen number, experimental work has been devoted to the small or moderate Knudsen number regime. This inability of theory and experiment to provide solutions in a region of common validity reflects both the complexity of the continuum theory and the difficulty of achieving satisfactory measurements at large Knudsen numbers.

There is an extensive literature dealing with sphere drag measurement at supersonic speeds and Reynolds numbers of 10^5 - 10^6. Since some of the data obtained during the current investigation were taken at Reynolds numbers of 10^4, there is some value in discussing this literature, particularly since these earlier works provide the only detailed experimental studies of the base and wake region.

The earliest known investigation of a Reynolds number effect on the drag of spheres in a supersonic stream was the work of Eula[16], who found that the total drag coefficient is invariant with Reynolds number in a Reynolds number region between 10^5 and 8×10^5 at M = 1.85 and M = 2.13. Subsequent experiments at Goettingen and Pennemunde[17,18] at Mach numbers between 1.2 and 4.3 confirmed Eula's results. The objective of these measurements was to detect a critical Reynolds number where transition might occur. Lehnert[19] inferred from Schlieren photographs of spheres at M = 3.26 and Reynolds numbers between 1×10^5 and 5×10^6 that laminar boundary layers and laminar flow separation existed even at such high Reynolds numbers, which explains the lack of any super-sonic analog to the well known decrease in sphere drag at low subsonic

14.

speeds at a critical Reynolds number of 3 to 6 x 10^5. Lehnert also pre-
sented some results on the structure of the wake flow which are at least
partially relevant to the present investigation. He found that the point
of emanation of the trailing edge shock wave moved closer to the sphere
rear stagnation point as the Reynolds number was increased, varying from
1.7 sphere diameters at Re = 5 x 10^4 to 0.7 sphere diameters at Re = 1 x 10^6.
Corresponding to this increase in the wake length as the Reynolds number
decreased was an increase in the sphere base pressure, a correlation which
had been noted earlier for cone cylinders by Kurzweg[10]. An attempt to
artificially form transition from laminar to turbulent flow by the use of
a trigger ring did not trip the boundary layer, but did manage to deform
the boundary layer sufficiently so that the base pressure was lowered
somewhat from its undisturbed value. In addition, Lehnert scrutinized
spark shadowgraphs of spheres in free flight, and found that wake transi-
tion location varied from 1.2 sphere diameters at Re = 7 x 10^4 to 0.2
sphere diameters for Re > 4 x 10^5 at M ~ 2 to M ~ 4.5. Erdman[21] had
shown earlier that the pressure was constant over the entire base region
at low supersonic speeds for Re > 10^5. This enabled Lehnert to estimate
base drag coefficients from a single base pressure measurement. The
measurements indicated that base drag coefficients decreased from ~ 0.3
at M = 1.6 to 0.03 at M = 4.2, and showed an increase with increasing
Reynolds number for Re < 2 x 10^5.

Kavanau's[25] work on base and wake pressures of cone cylinders
at lower Reynolds numbers indicated that both the critical distance and
base pressures are not monotonic in Reynolds number, but exhibit a
difference in behavior when the Reynolds number is sufficiently large

such that transition occurs upstream of the critical point. This is related to the increased ability of the wake region to provide adequate mixing and sufficient pressure rise due to the much greater efficiency of turbulent mixing over laminar mixing. In all of Lehnert's work transition does occur upstream of the critical region, with the result that the critical region moved downstream and the base pressure increased as the Reynolds number decreased. At the Reynolds number of the current experiments, it is likely that the critical region may move upstream and the base pressure may decrease as the Reynolds number is lowered since only laminar mixing is possible in the region between the sphere and the critical region. Kavanau's work also showed that the critical region is further from the base at M ~ 2 than at M ~ 4. Although extrapolation of Lehnert's or Kavanau's studies is a questionable endeavor, some qualitative inferences may be drawn:

1. If sphere drag models are supported by cross-stings, it is possible that boundary layer velocity profiles may be sufficiently distorted as to cause somewhat different base pressure levels from the no-sting case. This is important only at low supersonic Mach numbers (M ~ 2). Skreekanth[26] attempted to measure this interference effect of cross sting supports on sphere drag coefficients at M = 2 and found that the effect was generally negligible for free stream Reynolds numbers less than 60.

2. In view of the large distance between the sphere rear stagnation point and the formation of the trailing shockwave, there is a possibility that wind tunnel data obtained at

low Mach numbers (M < 2) and low Reynolds numbers will be affected by flow non-uniformities and also by sphere mounting techniques. If the Crocco-Lees mixing theory[22] is valid for this problem, then there is a likelihood that only disturbances which are upstream of the "critical point" can affect the sphere base flow. Since the "critical point" is near the origin of the trailing shock wave, and since this origin can be several sphere diameters downstream of the sphere, this requires that the external flow be uniform over this length, and in addition requires that no disturbances occur within this distance. The violation of either of these two requirements could yield a drag coefficient which is a function of sphere diameter as well as Reynolds number and Mach number, in apparent violation of similarity considerations. This effect will be more significant at low supersonic Mach numbers than at large supersonic Mach numbers, because of the relative unimportance of base drag for M > 3.

Free flight investigations at Reynolds numbers of 10^5 and 10^6 and Mach numbers of 2 - 10 have been presented by Hodges[23] and Charters and Thomas[24]. (See Figure 1). An essential difference between the flow structure at these large Reynolds numbers and the flow structure at the Reynolds numbers encountered during the present investigations is that the transition zone in the wake is very close to the sphere rear stagnation point at large Reynolds numbers, while it can be downstream of the critical point at low Reynolds numbers. In addition, the low Reynolds number case possesses a much thicker viscous layer, the shock standoff

distance is substantially larger, and the shear stress makes a sizable contribution to the drag force. However, these three latter considerations are really only a difference in degree, rather than a fundamental change in the flow structure. The first effect mentioned, the movement of the transition zone toward the body suggests, however, that there is a fundamental difference in the base zone and the separation point.

It is quite likely that only for low supersonic Mach numbers is a scaling procedure based on $C_{D_{low\ Re_2}} - C_{D_{high\ Re_2}} \sim \dfrac{1}{\sqrt{Re_{2_{low}}}}$ not adequate, since it is for this flow condition that the base effects become significant. Kavanau's[25] correlation of base pressures on cone cylinders in the form $p_b/p_\infty = f(\sqrt{Re_\infty}/M^2)$ is certainly not included in the above scaling.

Drag measurements at Reynolds numbers less than 10^4 have been achieved in a number of different facilities, including low density wind tunnels[26,27,28,29,30], pressurized ballistic ranges[31,32], free flight[33] in the upper atmosphere, plasma wind tunnels[34], and "hot-shot" wind tunnels[35].

The first tests in a low density wind tunnel were performed by Kane[27] in 1950-1951. These data, which were later extended by Sherman and Jensen[28,29], covered the Reynolds number range 15 to 800, and the Mach number range 2.2 to 3.2. The sphere wall temperatures and the stagnation temperature were both at ordinary room levels. It is important to note that some knowledge of both the temperature levels and the temperature ratio T_w/T_o begins to be necessary as viscous effects become significant. During the period of these early measurements, there was still some uncertainty in the interpretation of various pressure probe

readings in the low Reynolds number regime. Because of this uncertainty in the determination of flow conditions, early values of C_D and Reynolds number may be somewhat questionable, while values of the drag force were probably quite good. Since the first tests, which were of spheres mounted on cross-stings, seemed to indicate that this mounting technique changed the velocity profile, the tests of Sherman and Jensen were performed with tail sting mounted spheres. These tests indicated an effect of model diameter, in addition to a Reynolds number effect. The work of Lehnert[19] and Kavanau[25] suggests as a possible explanation that this apparent model size effect was due to disturbances in the wake region caused by the relative non-uniformity of the flow field over the region between the sphere base and the critical point. These non-uniformities were intensified by the lack of any means of eliminating either under or over expansion of the stream leaving the jet.

Free flight tests of sphere drag were performed by May and Witt[31,32] in a low pressure ballistic range. Tests were performed by firing small spheres from a shotgun into a ballistic range, and then photographing the spheres by a series of still cameras as various reference lines were crossed. Although knowledge of flow conditions is excellent for this kind of test, there is a problem in attaining sufficient accuracy in distance measuring techniques to determine the small change that the drag force makes to the very large initial velocity. In addition, there is no knowledge of the temperature of the sphere in the region where data is taken, a lack which may not be very significant at the Reynolds number of the tests.

Liu[33], who had utilized sphere drag coefficients in the falling sphere method of determining upper air density, presented data in 1959 which had been obtained by upper atmosphere rocket firings of inflatable spheres.

The presentation of sphere drag data in the form of lines of constant C_D versus M and Re_∞ is suggested by Liu. Although this technique is convenient for use, it requires a great deal of uncertain extrapolation and interpolation in view of the limited range of Mach numbers that are available, and fails to reflect a Mach number independence principle at $M > 5$ if Re_2 is used as the independent variable.

Skreekanth[26] measured sphere drag in a low density wind tunnel using a microbalance and sting mounted spheres. The model and supply temperatures were both at nominal room temperature values. A model size effect was not detected, perhaps owing to the relatively small diameter spheres that were tested, and also to the uniform nature of the flow field. The tests were at $M \sim 2$ and $3 < Re_\infty < 60$.

Wegener and Ashkenas[30] presented data of sphere drag obtained in a $M = 4$ low density wind tunnel under conditions of $Re \sim 50$ to 1000 and T_o, $T_w = 300°$ K. The measurement technique was to support a small stabilized sphere on fine wire in the air stream, measure the deflection angle of the wire, and after correcting for the stabilization technique and wire drag, inferring the force on the sphere. The nozzle was a conical nozzle with boundary layer correction, and calibration indicated a Mach number gradient of 0.1/inch. In addition, at larger sphere sizes (1/2 to 3/8 inch) the core diameter and the model diameter are comparable. Both of these effects seemed to contribute to a small but measurable model size

effect. The near parabolic pitot pressure profiles presented in reference 30 also suggest that the sphere drag coefficient measurements at $M < 4.008$ may be somewhat affected by the apparent almost fully viscous nature of the free stream.

While all of the data presented in the preceding paragraphs were obtained at ordinary temperature levels in air, recent work described in reference 34 presents the results of several measurements of sphere drag in a low density N_2 hypervelocity wind tunnel utilizing a plasma generator as a heat source. At a Mach number of 9.4, $T_o \sim 3000°$ K and $Re_\infty = 240/in$, $T_w/T_o \sim 0.3$, four different drag coefficient points were obtained during the course of calibration of the wind tunnel. All estimates of flow properties were based on thermal equilibrium throughout. Since these tests were run at sufficiently low temperatures to eliminate the possibility of dissociation, and since the wind tunnel calibration was quite extensive, it is felt that these are valid estimates of the flow parameters.

Reference 35 presents the results of experiments performed at estimated values of $M = 11 \sim 59$, $Re_\infty = 10,000 \sim 20$, $T_o = 9000°$ K $\sim 2600°$ K, and $Kn_\infty \sim 0.001$ to 3 for air; and $M = 38.5 \sim 64.7$, $Re_\infty = 14,400$ to 74, $Kn_\infty = 0.002$ to 1, $T_o = 4000°$ K $- 2000°$ K for helium. In both series of tests, the wall temperature was probably close to room temperature level. The actual force measurements, which were accomplished by the use of a moving model and a Fastax camera, were accurate, but any estimates of flow properties must be considered as largely tentative because of the extremely high temperatures, the "bootstrap" technique, and the sensitivity of the data reduction to the extrapolation parameter. The validity of the data is intimately related to the question of whether flow phenomena in a

"hot shot" tunnel, where a great deal of electrical energy is discharged into a small slug of working gas, and the gas is then permitted to burst a diaphragm and then expand into a conical nozzle of 45° included angle, is sufficiently well understood that meaningful aerodynamic measurements can be taken. At the present time the answer to this question has not yet been presented.

IV. EXPERIMENTAL PROCEDURE AND APPARATUS

Since the present experiments possessed a twofold purpose, and since two completely different force measuring techniques were utilized, it is most natural to separate the experimental procedure into three sections, the first dealing with procedure and equipment that was common to both techniques, and the remaining two sections dealing with procedure and equipment that is related to each of the force measuring techniques.

A.   Common Equipment and Procedure

The Berkeley Low Density Wind Tunnel #4 is an open jet continuous flow, non return type wind tunnel which is capable of providing supersonic flow at static pressure levels of less than 100 microns. Complete descriptions of the wind tunnel and instrumentation are available in reference 36. Tests were run in four different wind tunnel nozzles, a $M \sim 2$ nozzle (No. 6), a large $M \sim 4$ (No. 14), a smaller $M \sim 4$ nozzle (No. 8), and a $M \sim 6$ nozzle (No. 9). All of these nozzles were designed to achieve a test core of uniform isentropic parallel flow imbedded in a relatively thick boundary layer. Descriptions of nozzle design and fabrication techniques are available in references 36, 37, and 38. Since the installation of a stagnation point heater had not yet been completed during the period of the current experiments, the wind tunnel stagnation temperature was at room temperature levels.

The early drag measurements in the Berkeley wind tunnel attempted to determine flow properties by the use of three local measurements, but subsequent work[39,40] had shown that these local measurement techniques were subject to substantial viscous effects. The confirmation of isentropic flow from the stagnation chamber to the test section had

been reported in 1952[37]. All of the nozzles used during the current tests had been calibrated and utilized by previous investigators, so that there was confidence in the isentropic nature of the flow. The presence of isentropic flow (only when the static pressure at the nozzle exit plane is equal to the static pressure of the test chamber) eliminated the need for the local measurements and utilizes in their stead one local measurement and two measurements of stagnation conditions. Impact pressures were measured locally with a source shaped impact probe, and both stagnation pressure and temperature were measured in the settling chamber.

A description of the pressure instrumentation is included in reference 36. The essential nozzle characteristics in terms of M and Re/in are almost solely determined by the flow rate for a given nozzle. Boundary layer thicknesses, static pressures, and Mach numbers vary as the flow rate is changed. Figure 2 exhibits the Mach number - Re_2/in characteristics of the four different nozzles. Since flow nonuniformities are present in each nozzle, the decision was made to maintain the same axial position for all tests made with a given nozzle; this axial test position generally being selected on the basis of previous calibration. This did not completely eliminate the possibility of free stream non-uniformity affecting the critical wake region, which could be several sphere diameters downstream of the sphere base.

B.   Force Measurements

1.   Drag Balance Studies

The first goal of the current investigation was to provide drag coefficient information for spheres over the operating range of the four supersonic nozzles described in the preceding section. Sphere wall

temperature and wind tunnel supply temperature were both at a nominal value of 300° K, insuring that near adiabatic wall conditions were simulated. Drag force was measured using a null type beam balance incorporating a crossed strip flexure pivot. A Schaevitz linear variable differential transformer was used to sense the null position of the beam, and the force on the model was computed from a simple static moment summation about the pivot center. Precision quartz and steel springs were utilized to oppose the moment created by the aerodynamic force. From a measurement of the spring extension it was possible to compute the aerodynamic moment acting on the pivot center. From a knowledge of the geometry of the balance, model, and model support system it was possible then to compute the force acting on the model alone.

Detailed information concerning balance design and operation is contained in references 41 and 48. Figure 3 exhibits a schematic of the balance system. Earlier work[28,29] at low supersonic Mach numbers had cast suspicion on the use of either cross sting or tail sting supported models, in view of the decided sting effect on the base flow field that had been demonstrated by Kavanau[25]. In order to reduce the likelihood of any distortion of the base flow, the decision was made to support the spheres in the following fashion:

Each model was drilled with either three or four small holes (0.010") on the great circle of the sphere. Wires were then inserted into these holes, and small pieces of hypodermic tubing were forced into the holes to fasten the wires to the sphere. This tubing was trimmed so that it was either flush or beneath the surface of the model. These wires were then connected to an aluminum yoke by adjustable brass support

rods. This yoke was circular in shape and possessed an inside diameter larger than the largest nozzle exit diameter. This yoke was then mounted on the drag balance by a steel rod which was held in the sting support system of the balance. Figure 4 is a photograph of the complete model-wire-yoke assembly as it appeared on the balance. The yoke was then completely shielded from any backflow by a large sheetmetal shield, and the wires and support rods were shielded by 1/4" diameter adjustable brass tubes with partially capped ends. Only one inch of each wire was exposed to the flow in order to reduce wire contributions to the drag force. A photograph of the entire system, including shields, is given in Figure 5.

The original intention was to perform the tests for three-wire mounted spheres and four-wire mounted spheres, and thus determine exactly the total effect of one wire (and shield) on the drag force of a sphere. However, reduction of early data revealed that the scatter in the experiment was sufficiently large so that it was difficult to assess the effect of one wire on the sphere. In addition, wire diameter was limited by the substantial deflection of thin wires by central aerodynamic loads and the consequent additional moment about the pivot center due to the movement of the model center of gravity. Thus, it was necessary that wire diameter be a compromise between strength and minimum disturbance.

A constant wire diameter of 0.003" was used for all models between 1" and 1/4", and a nominal 0.001" wire was used for the 1/8" models. Rather than attempt to assess the total effect of one wire and shield, it was decided that wire drag alone would be measured under the identical conditions as the sphere plus wire drag tests. In this fashion, the wire drag could be subtracted as a tare force, but no real estimate

could be made of the effect of the interference of the wire on the sphere flow field.

It was assumed (on the basis of the work discussed in reference 19) that this effect was very small for such small disturbances, and well within the scatter of the data. The wire effect could be significant if transition were likely, but all previous work had failed to reveal any transition over a tripped sphere at Mach ~ 2. There was, of course, a possibility that these small disturbances distorted the velocity profile somewhat near separation, and hence affected the base flow. However, the ratio of wire diameter to sphere diameter was of $0(10^{-2})$, so that any such effect would be quite small.

For all tests performed with the 1/4" model, an attempt was made to correct for the total effect of the wire and shield assembly by obtaining drag measurements on a two-wire mounted model, and then on a four-wire mounted model. The difference between the two gross drag coefficients at the same value of the Reynolds number was plotted in order to obtain a smooth curve of the total correction due to two wires. This correction (after smoothing) was considered to be a valid representation of the effect of two wires on the drag of the 1/4" sphere, and was treated as a correction to the gross drag coefficients.

The height of the sphere center above the base plate of the balance was measured carefully, and vertical symmetry of all mounting wires about this position was required in order to compute the moment balance about the pivot center.

For a given nozzle all tests were run at the same axial position downstream of the nozzle exit plane on the jet center line. The selection

of this operating point was governed by the availability of a relatively uniform region of flow. The operating procedure was as follows: The model was mounted on the balance and the wind tunnel then pumped down at no-flow by the ejector system. The null reading of the spring extender at no-flow was then noted. The flow was then established in the tunnel by the use of the flowrator, and an impact probe was positioned in the flow by the traverse mechanism. This impact probe was stationed at a point slightly upstream of the sphere forward stagnation point, where it was known that free stream impact pressure could be measured. Stagnation pressure, impact pressure, and stagnation temperature were then recorded after the jet had been balanced. The impact probe was then moved out of the stream and the jet was balanced again. The counter on the drag balance was read after the spring extender had been utilized to bring the beam back to its null position. This procedure was repeated at each flow rate.

For the wire tare determination an attempt was made to simulate the interaction of the sphere shock wave and boundary layer with the wire by setting up a dummy sphere and then measuring the drag on the wire alone. These tests were run in a similar fashion to the tests of the combined sphere and wire assembly. (See Figure 6).

Spring calibrations were made in the manner described by reference 48. A cathetometer was used to estimate whether wire deflection was significant enough to cause any appreciable shift in the center of gravity of the model. Although the shift in the center of gravity was measurable, it was certain that no additional spurious non-aerodynamic moment had been measured.

The reduced data is shown in Table 1. The data reduction technique is given in Section V-A. Forces were measured in the range of 50 grams to 20 milligrams merely by selection of the proper spring. Spring calibrations were made before and after use, and it soon became evident that linearity and spring constant were almost invariant from run to run.

2. Moving Model Studies

The second objective of these studies was to determine whether severe wall cooling produced any significant change in sphere drag coefficient at supersonic velocities and low Reynolds number. Although steady cooling of fixed models by circulating of a coolant had been utilized for local measurements of heat transfer and pressure at low Reynolds number[41], it was felt that this technique was not readily adaptable to gross force measurements on small spheres ($1/32'' < d < 1/4''$).

A moving model technique was adopted, whereby models were released from a reservoir above the edge of the wind tunnel jet and permitted to fall through the jet. As the spheres passed through the section of uniform flow, their trajectory was photographed with a high speed motion picture camera. Horizontal distances were measured on the resulting films and knowledge of sphere diameter and density was then used to calculate horizontal force by the application of Newton's second law. The reservoir was capable of being maintained either at room temperature or at reduced temperatures by the circulation of coolant. The use of this technique of force measurement on both cooled and uncooled spheres introduced a consistent, relatively simple system with no support or interference problems. This simplicity in experimentation was gained at the expense of somewhat diminished accuracy and more difficult data reduction. The following assumptions were implicit in the

use of the moving model technique:

1) Characteristic times for development of boundary layers, wakes and shock waves were shorter than the time or traverse of a sphere through the jet section. Times of traverse were of $O(10^{-2})$ sec, while a characteristic flow time d/U was of $O(10^{-5})$ sec.

2) The effect of the small vertical relative velocity of the jet with respect to the model was completely negligible in the development of the sphere flow field. Since $v_{sphere}/U_{jet} - u_{sphere}$ was $O(10^{-3})$, this was equivalent to a misalighment of the flow with the horizontal axis of $O(10^{-3})$ rad. Misalignments of this small magnitude would not influence the rlow field or drag force measurably.

3) The sphere wall temperature was not changed significantly by the aerodynamic heating encountered during the trajectory through the jet. Estimates were made of the extent of temperature variation by assuming an average heat transfer coefficient for the entire trajectory and using the known solutions for the transient cooling of a sphere. In order to insure that the estimates be conservative ones, the average heat transfer coefficient was selected at the maximum value anticipated, the stagnation point value at $Re_2/inch = 1200$. For the range of diameters and materials encountered during these tests, these estimates indicated that the sphere wall temperature was not changed by more than a few degrees from its initial value.

This system of measurement, whereby acceleration from near zero horizontal velocity to a velocity of 0(10) ft/sec requires slower exposure speed and less precision than the kind of tests which are run in ballistic ranges, where the deceleration of very fast moving spheres (0(10) ft/sec) is observed. A 16-millimeter Fastax camera was used at a shutter speed of approximately 50 microseconds, corresponding to a framing rate of 3000 frames/sec.

Description of Operating Procedure

A schematic of the complete moving model test system is shown in Figure 7. The sphere constant temperature reservoir and release mechanism are shown in some detail in Figure 8. Multiple tests were achieved by releasing several spheres simultaneously, and were utilized to decrease the effort of data reduction.

The following procedure was used during the tests, and was invariant from run to run:

The sphere reservoir was mounted above the wind tunnel jet, and the release mechanism was set at the top edge of the jet on the center line. A piece of flashed opal glass was marked with three vertical and one horizontal reference lines. This transluscent screen was mounted vertically at the far edge of the jet and was never more than 4 inches from the jet center line. Six 750 PR lamps were used to illuminate the rear of the opal glass screen in order to provide a uniformly bright background for the models. The reference lines were used to provide a fixed reference system which was not subject to effects of film shrinkage and movement.

Several spheres were placed in each of eight consecutive chambers of the model reservoir. The maximum sphere diameter was 1/4" and the minimum sphere diameter was 1/32". The upper limit was determined by the requirement that sufficient acceleration for accurate measurements be obtained, and the lower limit was determined by the difficulty of handling and observing small spheres. Several attempts were made to test 1/64" diameter spheres, but no successful results were achieved.

After the spheres were placed in the reservoir, the Fastax camera, which was mounted outside the wind tunnel, was focused on a point midway between the tunnel centerline and the reference screen. All coolant tubing to the reservoir was connected, but no liquid nitrogen was permitted to flow until the wind tunnel was at a lower pressure. The wind tunnel was then sealed and evacuated to operating pressure by the ejector system and auxiliary pumps.

A predetermined flow rate was set and the jet balanced in order to insure uniform flow. An impact tube was placed on the tunnel center-line at a point one inch downstream of the release mechanism and the various flow measurements were taken. After the impact tube had been removed from the flow by the traversing mechanism, 16 mm Plus X film was loaded into the Fastax camera. A setting of 130 volts was utilized with a "Goose" booster auxiliary power supply, and a delay system was set in order that the models could be released during the slowly varying part of the film acceleration cycle. A nominal framing rate of 3000 frames was used, with some small variation from run to run. A controlled crystal oscillator was set to make timing marks on the film at the rate of 900.2 cycles/sec. With the camera loaded, and the spheres in the release mechanism, a run was ready to commence.

The six 750 PR lamps were turned on manually approximately 1/2 second before the starting relay was actuated. The starting relay on the "Goose" unit was then actuated. The solenoid on the release mechanism released the models at 0.7 sec after the film had started to move through the camera. The models fell through the jet and their trajectories were recorded on the film, which was already at a mean constant speed by this time. This rather short sequence of events constituted a complete run.

The first four such runs in a given nozzle were conducted with models that were at room temperature levels. Two flow rates were run in each nozzle, in order to provide additional variation in Reynolds number. Thus, at M = 6, for instance, the first two runs were at a flowrator setting of 55#/hr and the second two runs were at a setting of 20#/hr.

After these first four runs, liquid nitrogen was pumped through the constant temperature reservoir in order to cool the models to a surface temperature of 80° K. A thermocouple which was mounted on the release mechanism was utilized as an indication of the temperature of the entire assembly. The individual chambers had been designed to insure that the spheres were completely surrounded by a constant temperature enclosure. Once the models were cooled down to liquid nitrogen levels by radiation, conduction and convection in their chambers, a set of runs was made at the same flow conditions as the earlier tests with uncooled models. The test procedure was identical with that described earlier in this section.

Since a requirement of this technique was that there be a uniform flow region sufficiently large to obtain useful data over the model path, it was necessary that only relatively large flow rates be utilized, since

the lower flow rates in a given nozzle generally exhibited a broadening of the boundary layer. In addition, it was known that the No. 14 M ~ 4 nozzle possessed a larger uniform core than the smaller No. 8 M ~ 4 nozzle. For this reason, these moving model tests were not performed in the No. 8 nozzle, but were performed in the No. 9 M ~ 6, No. 6 M ~ 2 and No. 14 M ~ 4 nozzles.

After a complete set of eight tests in a given nozzle had been performed, the distances were measured between film plane and the tunnel centerline, and also between the tunnel centerline and the reference screen.

A new nozzle was then installed and the entire operating procedure was repeated.

All runs were made with Plus X 16 mm reversal film at an opening of f.8 on a 1-1/2 f(1.9) lens. Depth of focus at the distances utilized during the tests was 8" for this opening. An enlarged print of a typical frame is shown in Figure 9. All films were developed by a commercial laboratory and were developed as positive films.

V. REDUCTION OF DATA

A. Fixed Model Technique

A complete description of the techniques used to calculate p,
M, Re_1, Re_2, and q is given in reference 48. In addition, the same
reference yields some detail about the reduction of force measurements
on the microbalance to drag coefficient form. Table 1 presents all of
the reduced data in tabular form.

B. Moving Model Technique

Each roll of film was first edited on an Eastman Kodak Recordat
Microfilm Reader. As no more than 10 feet of any roll consisted of use-
ful information, it was convenient to eliminate the unnecessary parts as
quickly as possible. After this editing process, the film was viewed on
a light table in order to locate the timing marks and to scribe them
carefully.

A Bausch and Lomb optical comparator was then used to measure
distance on the film. The use of the 25X magnification was judged the
most satisfactory compromise between convenience and accuracy. For each
model, distance data was obtained from a number of frames. As a frame
was selected for scrutiny, it was scribed with a number. The stagnation
point of each model was selected as a moving reference point and the
left side of one of the three reference lines drawn on the opal glass
screen was selected as a fixed reference line. Since only distances
normal to the fixed reference line were measured, it was necessary to
use only one of the two possible movements of the comparator stage.
After a frame was selected for observation, it was numbered, and then
the film was positioned so that the left hand side of the reference

line on the film was lined up with the right hand side of the reference
line on the comparator screen when the screen was set at 0°. The micro-
meter on the comparator was then used to measure the location. Next, the
moving stage was shifted until the right hand side of the comparator ref-
erence line was precisely lined up with the forward stagnation point of
the moving spheres. The micrometer on the comparator was then used again
to measure location. Since there were usually several models on each
frame, it was possible to measure one reference line and several different
model distances without any adjustment of the film. In order to eliminate
the effect of film shrinkage on the measurements, the distance between two
reference lines fixed in space was measured at least once for each roll of
film, and this was used to estimate the magnification factor. Careful
reading of the film on a comparator is tedious, time consuming work, and
it was found that the speed of film reading was increased by the use of
a tape recorder for recording the measurements, rather than transcribing
them as they were taken.

Once the film had been read on an optical comparator, it was
necessary to count the timing marks in order to evaluate elapsed time
as a function of the number of frames from the first frame of interest.
The distance between every fourth timing mark was measured, using a
scale. This distance, in centimeters, was then plotted against the
number of frames counted from the first frame. In general, a straight
line was drawn through the points, yielding a curve $\frac{dN}{dt} = C(A+BN)$. This
line represented the variation in framing rate due to the acceleration
of the film through the Fastax camera. Over a sufficiently small region
this fit was satisfactory, and since $BN/A << 1$, this was sufficiently
accurate to evaluate $t(N)$. This first order differential equation can

be solved exactly for $t(N)$, but the small magnitude of BN/A permits an approximate solution $tCA = N\left[1 - \frac{1}{2} \frac{BN}{A^2}\right]$ which is correct within 0.2% over the range of values encountered during the experiment. It was convenient to keep the time scale in units of N or frames, and to convert to seconds at a later stage in the data reduction.

Since A and BN are given in units of centimeter/four timing marks, then the constant C is equal to

$$\frac{\text{No of frames}}{\text{centimeter}} \cdot \frac{f}{4} \qquad \text{where } f \text{ is the frequency of the timing light generator}$$

$$C = \frac{1}{0.762} \times \frac{900.2}{4} \left[\frac{N}{cm} \cdot \frac{4 \text{ timing marks}}{sec}\right]$$

All differentiations were calculated using distances at the film plane, and the final conversion to values at the object plane was done at a later step, using the appropriate magnification factor. Once a time scale was established and the various distances recorded, the next step was the calculation of $S_{ref} - S_{mod}$ for each test sphere at each frame of interest. A suitable constant was usually added to this difference in order to insure that the distance term be positive. Table 2 consists of tabulated values of distance and time for all the tests.

The next step in the data reduction scheme was to smooth and differentiate the data. Hartree[46] suggests that the most effective smoothing technique may be the plotting of points on a convenient scale and then discarding points which are obviously wild. In view of the difficulty in plotting four digit numbers with sufficient accuracy, this approach was not adopted, but rather the smoothing and first differentiation

was accomplished by a purely numerical technique. The data was smoothed and the first differentiation was done by the use of the 704 computer using the routine described in Appendix 1.

The computer output was then plotted on a working curve similar to Figure 10. This is a plot of $\dfrac{d(S_{ref}-S_{mod})}{d(CAt)}$ vs CAt for run 146. The slope of this curve is proportional to the local acceleration. A fundamental requirement of the moving model technique was that the acceleration be constant over a sufficiently large region such that the slope could be estimated with some confidence. At this stage of the data reduction, it was possible to assess whether the model had been tested in a uniform region of the stream, and thus had a constant force acting on it for a sufficiently long time. In general, the velocity curves possessed substantial regions in the center (corresponding to over 100 frames) where the velocity varied linearly. (See Table 2.)

Whereas the first differentiation and smoothing of the raw data points was done numerically, the second differentiation and smoothing was done graphically. Since it was no longer necessary to plot four digit numbers accurately as in the initial smoothing, the graphical approach was acceptable at this stage. In addition, it provided the first opportunity to dismiss wild points from consideration. As discussed in Appendix 1, wild points in the original data propagated errors in slope to 3 points on each side of the bad one, so that it was quite easy to identify the presence of a wild point by a set of seven differentiated values which were displaced significantly from the surrounding points. Once a wild point was identified, it was corrected, and the first differentiation and smoothing process was done over. This was quite

convenient since it was necessary to change only one IBM data card, corresponding to the corrected point, in the set.

A sphere which had undergone constantly varying aerodynamic forces would possess an acceleration curve which was also constantly varying. This would make the choice of a single acceleration to represent the test a somewhat questionable procedure, in view of the fact that flow properties were evaluated at only one station in the stream. Because of this, velocity curves which did not exhibit a substantial region of constant acceleration were discarded. The decision was made to draw a single straight line through the local values of the velocity corresponding to the uniform region. Essentially, this is equivalent to selecting a single average acceleration to represent the motion of the sphere in the uniform core of the jet. It was felt that the slope of this straight line represented the average acceleration in the test section within ±2%. The actual acceleration is equal to this geometric slope $d^2(S_{ref}-S_{mod})/d^2(tAC)$ multiplied by $(AC)^2 \bar{M}$, where $\bar{M}$ is the magnification factor.

From this slope, knowledge of sphere density, sphere diameter and dynamic pressure q_∞ in the test section, the drag coefficient was calculated using the following relation:

$$C_D = (\text{Slope}) \times \frac{\rho_{mod} \times \text{Dia} \times \bar{M}(AC)^2}{q_\infty} \times \frac{2}{3}$$

Values of w_{mod}, Dia, $\bar{M}$, A, q_∞, and C_D are tabulated for each run in Table 3.

Figures 11, 12, and 13 exhibit the data points for both wall temperatures at each nominal Mach number, 2, 4, and 6. Although it is possible to draw faired curves through the data points and hence estimate the effect of cooling on sphere drag, it was decided that a statistical analysis would be desirable to aid in the detection of any significant differences which might be attributed to cooling.

As discussed in Section IV-B-2, any systematic error that arose due to the use of the moving model technique was present in all the sets of data, since testing and reduction was invariant from run to run. In the belief that random errors in measurement and reduction yielded errors in value of the drag coefficient which were about normally distributed, a regression analysis was carried out for each set of data corresponding to a given nominal Mach number and a given wall temperature. This is described in Appendix 2. Another useful simplifying assumption was made; that the value of the independent variable $1/\sqrt{Re_2}$ was identical with its true value. This greatly reduced the complexity of the regression analysis and could certainly be justified by both the negligible error in the estimated value of Re_2 compared to the magnitude of the error in the estimated value of C_D, and in addition, by the fact that C_D is a slowly varying function of Re for the range of variables tested.

VI. ACCURACY

Since the two force measuring techniques were completely dissimilar, it is necessary to evaluate the accuracy of the results separately for the drag balance studies and the moving model studies.

A. Drag Balance Studies

The primary cause of uncertainty in the drag balance measurements is the magnitude and effect of the nonuniformity of the flow produced in the various nozzles. This nonuniformity of the stream in which the spheres are imbedded results in some uncertainty in the magnitude of the parameters that are selected to characterize the flow (p, M, q, T), and in addition may affect the structure of the flow field surrounding the sphere. This latter effect is particularly important at $M \sim 2$, where disturbances in the wake region may cause significant variations in the base drag. It is thus quite unfortunate that the flow in the No. 6 nozzle ($M \sim 2$) is the least uniform of the various nozzles tested. If the work of Lehnert and Kavanau[19,25] can be extended to these tests, then it appears likely that a uniform region of perhaps 3 - 5 sphere diameters is needed to insure an undisturbed near wake and undisturbed base pressure.

In addition to this inherent nonuniformity, results reported in references 26 and 42 suggest that flow in $M \sim 2$ nozzles operating with thick boundary layers are sensitive to flow obstructions (such as models, shields or probes) which are downstream of the exit plane.

At $M \sim 4$ and $M \sim 6$, it is felt that base effects are not so important as at $M \sim 2$, and hence nonuniformities or disturbances in the wake region will not result in a significant effect on the drag. In addition to this, the flow is more uniform in both $M \sim 4$ nozzles and the

M ~ 6 nozzle than it is in the M ~ 2 nozzle. If the small effects of measurement errors in pressure and temperature are considered as well as the nonuniformities of the flow, then estimates of the flow properties are subject to the following uncertainty:

Nominal Mach No.	2	4	6
Uncertainty in Mach Number	±4%	±1%	±2%
Uncertainty in Dynamic Pressure	±6%	±3%	±4%
Uncertainty in Reynolds Number	±6%	±4%	±5%

While the above estimates are rather conservative, and probably infer the 95% confidence limits for most of the data, they are probably not valid at the lower flow rates achieved within each nozzle, where it is known that nonuniformities are more significant and measurements more difficult.

Force measurements could be obtained within accuracy of ±0.5% for the entire range of forces under completely static conditions by the proper choice of quartz springs. Under dynamic conditions (as in the wind tunnel tests) this estimate of the error in force measurements is generally valid, except under conditions of fluctuating ejector performance. The uncertainty in drag coefficient, which considers both uncertainty in force measurement and uncertainty in flow properties, is estimated at ±7% at M ~ 2, ±4% at M ~ 4, and ±5% at M ~ 6.

B. Moving Model Tests

The uncertainty in the force measurements of the moving model tests is closely related to flow uniformity. While it is inherently subject to random errors, it is felt that the technique utilized during the current tests was capable of estimating forces with an uncertainty

of ±2%. Measurement of distances on the optical comparator was accurate
to ±0.0001 inch on the film scale, corresponding to an actual dimension
of ±0.002 inch during the tests. Measurements of time were read correctly
within 1%, and measurements of model density were correct within 0.5%.
While it is true that a force measurement taken from only three displacement-
time data points could be subject to an error as large as ±10% for a small
heavy model, the several averaging processes built into the differentiation
schemes and the use of 12 to 35 data points reduce the uncertainty in force
measurement to a level of ±2%. If the uncertainty in flow parameters over
the length of path is considered, the errors in the moving model tests will
be of the following order:

Nominal Mach No.	2	4	6
Uncertainty in Mach Number	±4%	±2%	±3%
Uncertainty in Dynamic Pressure	±6%	±3%	±5%
Uncertainty in Reynolds Number	±6%	±5%	±6%
Uncertainty in C_D	±7%	±6%	±5%

VII. RESULTS

A. Force Balance Studies:

The results of the experiments performed with a fixed model mounted on a drag balance are shown in Table 1 and are presented in Figures 14, 15, 16, and 17 in the form of C_D vs. Re_2 curves. Since there were significant differences in the results obtained with the different nozzles, it is instructive to examine all of the data obtained in a given nozzle for possible model size and support effects.

Nozzle No. 6 - The results of tests performed in the No. 6 nozzle are shown in Figure 14. The presentation of the data in terms of a single independent variable, Re_2, is suggested by the discussion of boundary layer solutions given in Section II, but is certainly not quite so suitable at lower supersonic Mach numbers where base effects are important, and where the blunt body inviscid flow field is still a function of free stream Mach number. The results obtained in this nozzle, which provided a Mach number variation of $M \sim 2.1$ to $M \sim 1.6$, were substantially different from those obtained in any of the other nozzles. An examination of Figure 14 reveals two salient points:

1). Two drag measurements performed on a fixed diameter sphere at a given value of the Reynolds number, the one test of a sphere mounted by four wires, the other test of a sphere mounted by three wires, consistently indicate that the three-wire mounted model possesses a somewhat higher drag coefficient (2 - 8%) than the four-wire mounted model. This is significant for the 3/8, 1/2, and 3/4" diameter sphere at larger Reynolds numbers, but does not seem to be present in the data obtained with the 1" diameter model. The data obtained with the 1/4" diameter model was the only data which was

corrected for model support effects by measuring drag coefficients on a two-wire supported model, a four-wire supported model, and then extrapolating to the case of an unsupported model.

Any explanation of this systematic variation in the drag coefficient with the method of support must be purely speculative. The first hypothesis was that the wire deflection was sufficiently large to cause a shift in the model center of gravity, and hence cause an additional non-aerodynamic moment which would appear as an increment in the drag force. This hypothesis was shown to be false by actual measurement of the model deflection under load, both in and out of the wind tunnel, by the lack of any systematic effect at other Mach numbers than 2, and by the absence of any significant variation in the data obtained with the 1" sphere.

The next hypothesis was that this is a purely aerodynamic phenomena related to the impinging of compression waves emanating from the wire shields shown in Figure 5 on the wake region of the model. This hypothesis, if true, would require the flow behind the 1" model to show the largest difference between the three-wire results and four-wire results. In addition, application of the theory of reference 22 would probably require base drag to be relatively unaffected by any compression wave impinging in the far wake, and since the distance between the shield tip and the model was 1", any disturbance off the shields would certainly impinge on the far wake of the 3/8 and 1/2" diameter models. Thus, it appears unlikely that this hypothesis is completely valid. No completely satisfactory explanation is yet possible of these results.

2). In addition to the significant variation in the results obtained at a fixed model diameter, Mach number, and Reynolds number with varying

number of support wires, there is also a non-systemic variation in C_D from model size to model size at a fixed value of the Reynolds number. The non-systematic nature of this variation eliminates the difference in Mach number as the responsible factor. This model size effect was observed by Sherman[28] and Jensen[29], who supported models by tail stings, and attributed the lack of correlation with Reynolds number alone at least partially to the effect of the supports on the critical wake region. This effect seems to be especially predominant for $Re_2 > 150$. It is possible that this model size effect, along with the sphere mounting effect, is a function of non-uniformity in the nozzle which is always present, and which may be affected by the additional interference of the model and the support assembly.

Nozzle No. 8 - $M \approx 3.7$-4. Results obtained in the No. 8 nozzle are shown in Figure 15. The data do not indicate either any significant systematic effect of the method of support or of model size. All of the data obtained in this nozzle (M ~ 4.0 to 3.7) seem to be contained in a scatter band of approximately ±3%, which includes random error and the variation due to Mach number.

Nozzle No. 14 - $M \approx 3.2$-4. The results of data obtained with the No. 14 nozzle are shown in Figure 16. This nozzle is essentially a scaled up version of the No. 8 nozzle, and was designed to utilize the full pumping capacity of the wind tunnel ejector system. Even at low flow rates, corresponding to reduced Mach numbers and low free stream Reynolds numbers (350/in), there is a relatively uniform core of 1-1/2 inches in diameter[38]. The data obtained with this nozzle indicate no systematic effect of either model diameter or mounting technique.

As in the other tests at $M \sim 4$ in the No. 8 nozzle, all of the data fall within a scatter band of approximately ±3%. At the lower flow rates, the Mach number corresponding to the low Reynolds number range of a fixed diameter model is 3.3, compared to 4.0 at the higher flow rates. There is thus a greater likelihood that there is variation within this ±3% which is due to the systematic effect of Mach number. However, the effect is so small as to be indistinguishable from random error.

Nozzle No. 9 - Figure 17 is a presentation of the data obtained in the No. 9 nozzle, which provides a nominal $M = 6$ flow. Once again, as in the tests performed at $M \sim 4$, there is no systematic support or model size effect. All the data, except for two or three wild points, fall within a scatter band of approximately ±3%. For values of the Mach number which are possible in this nozzle, there is little likelihood of small variations in the Mach number affecting the drag coefficient. Thus, it is probable that the variation within this scatter band of ±3% is due to random errors, rather than to any systematic Mach number effect. Figure 18 presents all of the data at all Mach numbers as a function of Re_∞. This figure shows the relative maganitues of the scatter quite clearly.

B.   Moving Model Studies

The results of the experiments performed with the moving model technique are shown in Table 3, and are presented in Figures 11, 12, and 13. It is desirable to consider the results, as before, at a fixed nominal value of the Mach number.

No. 6 Nozzle - $M = 2$ - the results of the tests performed in the No. 6 $M \sim 2$ nozzle are shown in Figure 11. As described in Appendix

2, a least squares polynomial fit in $1/\sqrt{Re_2}$ was utilized to describe the data, and to aid in the interpretation of the results. This curve, and various confidence limits are shown in Figure 11 for both the insulated and cold wall data. The limited amount of data and the restricted range of model size (1/4" to 1/32" diameter) combined with the greater random error of these experiments made it difficult to assess any model size effect. The regression curve of C_D on Re_2 for the insulated wall models agrees with the data obtained with the force balance measurements in the region of overlap. This agreement helps establish the validity of this moding model technique in this particular wind tunnel nozzle.

The results of the moving model tests performed on cold models (T ~ 80 K) are also shown in Figure 11. It is apparent from a comparison of the two regression lines that there is a small effect on the drag coefficient of the reduction in wall temperature from 300° K to 80° K at M ~ 2 < Re_2 < 150.

No. 14 Nozzle - M ~ 4 - The results of the experiments performed in the M ~ 4 No. 14 nozzle are shown in Figure 12. This nozzle was utilized to provide all the M ~ 4 data because of its larger region of uniform flow than the No. 8 nozzle. In the region of common validity, at T_{wall} ~ 300 K, there is satisfactory agreement between the regression curve of C_D on Re_2 obtained by the moving model technique and the data obtained by the force model measurements. Thus, the validity of the technique in this nozzle is established, and one may with greater confidence assess the effect of wall cooling. The regression curves of C_D on Re_2 for both cold wall and insulated wall indicate that a significant decrease

in the drag coefficient (8 - 10%) accompanies a reduction in sphere wall temperature from $T_w = 300$ K to $T_w = 75°$ K. Although the lower confidence limit of the insulated wall regression estimate is very close to the upper confidence limit of the cold wall estimate, particularly at $Re_2 > 100$, it is still likely that there is a significant difference in drag coefficient which is attributable to the reduction in wall temperature.

No. 9 Nozzle - M ~ 6 - The results of the experiments performed in the Mach No. 6, No. 9 nozzle are shown in Figure 13. Agreement between the regression estimate of the insulated wall tests and the data obtained by the fixed model technique is not quite as satisfactory in the region of overlap as either the M ~ 2 or M ~ 4 tests. The regression line seems to be approximately 5% lower than the data points for values of $Re_2 > 100$, but the difference is not very significant if one considers the few points in this region obtained by the moving model measurements.

The regression estimate of C_D on Re_2 for cold wall tests indicates that a significant (8 - 10%) decrease in drag coefficient accompanies a reduction in wall temperature from 300° K to 80° K.

VIII. DISCUSSIONS & CONCLUSIONS

Although the data obtained at M ~ 2 is not so clearly defined as that at M ~ 4 and M ~ 6, examination of Figures 14, 15, and 16 reveals a variation of the drag coefficient with Mach number. For values of $Re_2 < 200$, the drag coefficient exhibits a small increase with decreasing Mach number, at the same value of Re_2. Throughout the entire range of these studies, the drag coefficients measured at M ~ 4 are approximately 5% higher than those measured at M ~ 6. The drag coefficients measured at M ~ 2 are larger than those measured at M ~ 4 by as much as 12% for values of $Re_2 < 100$, but seem to fall slightly below the M ~ 4 data at $Re_2 > 200$. As a consequence, the slope of the C_D ~ Re_2 curve seems to be somewhat larger at M ~ 2 than at M ~ 4 or M ~ 6.

This variation of C_D with Mach number suggests that any comparison of these data with earlier work must be on the basis of relatively constant Mach number. The early work at Berkeley, the recent work of Sreekanth at Toronto, and the ballistics range data of May and Witt are all shown in Figure 19, as well as all of the results of the present investigation at M ~ 2. Comparison of the present work with that performed at Berkeley in 1951 is difficult because of the inadequate knowledge of stream and probe properties which plagued the early experiments in low density wind tunnels. However, there is reasonable agreement among all the data except for several high points reported in reference 27 at $Re_2 < 15$. In the region near $Re_2 \sim 15$, the results of reference 26 agree fairly well with the results of the present investigation. The data obtained by the moving model technique is also shown in Figure 19. Both adiabatic and cold wall tests produced significantly more random error

than the balance tests, and it is certainly true that the regression estimate shown in Figure 11 is a more reliable indication of the variation of C_D with Re_2 than is examination of individual data points. While it is true that a small reduction in drag coefficient accompanies a change in wall temperature from $T_w/T_o \sim 1$ to $T_w/T_o \sim 0.26$ at $M = 2$, this reduction does not seem to be as significant at $M \sim 2$ as it is at $M \sim 4$ and $M \sim 6$.

Figure 20 presents a summary of the experimental values of the sphere drag coefficients obtained at a nominal Mach number of 4. Although the work of reference 29 was stated as being in the range of $M \sim 2.8$ to $M \sim 3.2$, there is considerable question concerning this and other stated values of the flow parameters because of the use of uncorrected 5° cone probes to measure static pressure. For the Mach and Reynolds number region of these tests, the viscous correction to cones of this small angle is quite significant, and consequently there is considerable uncertainty surrounding these results. In addition, it appears as if there was no attempt made to balance the jet leaving the nozzle in any of the work reported in references 27, 28, or 29, leaving the possibility of an under-expanded or overexpanded jet which was completely determined by the ejector characteristics. The recent work of Wegener and Ashkenas[30] is also presented in Figure 20. The adiabatic wall data of the present tests are in fair agreement with their work, being approximately 3 - 5% higher at the same value of Re_2. This small increase may be related to the fact that there is a Mach number range of 3.31 to 4.1 which is included here at the nominal value of $M \sim 4$, while the data of reference 30 was obtained in a range of $3.8 < M < 4.1$. All of the data obtained at $M \sim 4$

by the moving model technique is also presented in Figure 20. The con-
sistently large scatter of these experiments requires (as at M ~ 2) that
estimates of the results of the cold wall tests can best be made from the
regression curve, Figure 12, rather than from examination of individual
data points.

The drag coefficient of the cooled models is approximately
5 ~ 10% less than that of the adiabatic models, indicating that at M ~ 4,
reduction in wall temperature from 300° K to 80° K is moderately effective
in reducing drag. The work of reference 45 provides additional data taken
in the Jet Propulsion Laboratory Low Density Wind Tunnel at M ~ 4. In
these tests, the same technique which had been used for adiabatic spheres
and which was reported in reference 30 was applied to heated spheres.
The results are also shown in Figure 20, and indicate that an increase
in the ratio T_w/T_o from 1 to 2.6 is accompanied by an increase in drag
coefficient of 8 - 10% in the range $30 < Re_2 < 50$. These results on
uninsulated spheres at M ~ 4 are highly suggestive that for this Mach
number, where base and wake effects are not very significant in deter-
mining drag a boundary layer solution would yield reasonable values of
the skin friction and the variation of the drag coefficient with
temperature. The empirical correlation proposed in reference 45,

$$C_D \approx 1 + \frac{9}{8} \frac{(\rho_2/\rho_\infty)^{1/2}}{Re_2^{1/2}} \quad f''(0)$$

where f''(0) is taken at its
stagnation point value

implies that the variation of drag coefficient with wall temperature at
M = 4 may be estimated merely by selecting the value of the stagnation

point shear parameter which corresponds to the value of T_w/T_o. While this correlation is the result of a rather simple analysis, it does yield the observed result that an increase in temperature is accompanied by an increase in drag.

Figure 21 is a summary of available sphere drag data at low Reynolds numbers and hypersonic speeds. The characterization of the present experiments at $M \sim 6$ as hypersonic experiments has no real a priori justification, except for the knowledge that both inviscid supersonic blunt body flows and "local similarity" boundary layer flows exhibit little change with Mach number in the range $5 < M < \infty$ if a perfect gas with constant γ is assumed. The work of reference 35 reports further results for sphere drag in air at stagnation temperatures of 9600° K, for helium at stagnation temperatures of 3000° K, as well as the results shown in Figure 21, which are for $T_o \sim 2600°$ K in air. The decision to include here only the work done at $T_o \sim 2600°$ K in air is predicated on the belief that it was only for these results, where dissociation effects are small, is there a valid comparison with the present work.

The work of reference 34 is also shown in Figure 21. These experiments were performed in a well calibrated arc-heated nitrogen stream at approximately 3000° K. The temperature of the spheres was maintained at 900° K, corresponding to a ratio $T_w/T_o = 0.3$.

The adiabatic experiments at $M \sim 6$ indicate that even at $Re_2 \sim 1000$, the drag coefficient variation with Re_2 is still significant, and there is perhaps a 10 or 15% contribution to the drag due to viscous effects. The results obtained here at $T_w/T_o \sim 0.26$ indicate that the drag force is reduced by 10% from the adiabatic values. There is good

agreement between the data of reference 34 and the regression estimate of the cold wall data which was obtained during the present investigations. This agreement between the results of two different ecperiments, the one at $T_o \sim 3000°$ K at $M \sim 9.4$, and the other at $M \sim 5.9$ and $T_o \sim 300°$ K suggests that in hypersonic flow of air at stagnation temperatures less than $3000°$ K (corresponding to the onset of appreciable dissociation), the drag coefficient of spheres is a function only of Re_2 and T_w/T_o.

Comparison of the present work with that of reference 35 indicates that substantial discrepancy exists between results cited there and the present results. As discussed earlier, the lack of understanding of the processes occurring in a hot shot wind tunnel, the inability to obtain measurements of local impact pressure, and the nature of the "bootstrap" technique which was used as an integral part of data reduction and experimentation, all contribute to a large uncertainty in the true magnitude of Re_2, and a somewhat lesser uncertainty in the value of C_D. Since the results cited in reference 35 are strongly dependent on the choice of extrapolation parameter and were hampered by a lack of knowledge of the variation of C_D with Re_2, it would be of interest to recalculate the flow properties in the "hot shot" tunnel using the estimate of C_D vs. Re_2 shown in Figure 21. In this fashion it might be possible to estimate the true values of local stream properties without recourse to a "bootstrap" technique.

IX. CONCLUSIONS

The results of the experiments performed on fixed adiabatic spheres served to delineate further the variation of the drag coefficient in the low Reynolds number supersonic regime. While these results were satisfactory at $M \sim 4$ and $M \sim 6$, several discrepancies at $M \sim 2$ were noted which were in qualitative agreement with results first observed in the earliest low density wind tunnel measurements. Although no completely valid explanation of these discrepancies has been presented, it is felt that further tests in a larger, more uniform $M \sim 2$ nozzle, using the unshielded wire technique of reference 30 would provide valuable information concerning this discrepancy.

The use of the moving model technique to measure drag forces on small spheres in a low density wind tunnel must be viewed as only a partial success. The significant increase in random error over the fixed model tests and the great difficulty in data reduction both tend to diminish the utility of this technique as a means of measuring drag coefficients on insulated or heated spheres. However, in view of the difficulty of obtaining drag measurements on highly cooled small models in any other fashion, it can be a useful technique in the measurement of drag forces if it is used in conjunction with a relatively simple statistical analysis. If cognizance is taken of the fact that this technique permitted the measurement of sphere drag forces as low as 5 milligrams in a wind tunnel context, with a probable error of the regression estimate of less than ±5%, then its use can certainly be justified.

REFERENCES

1. S.A.Schaaf, "Recent Progress in Rarefied Gas Dynamics Research," ARS Journal, 30, 5, May 1960, 443-447.

2. L.Talbot, "Recent R search on the Shock Structure Problem," Paper 61-1, Western States Section, Combustion Institute, April 10-11,1961.

3. S.A.Schaaf, P.L.Chambre', "Flow of Rarefied Gases," Vol. III, Part H, High Speed Aerodynamics and Jet Propulsion Series, Princeton University Press, 1958.

4. R.Baker, A.Charwat, "Transitional Correction to the Drag of Spheres in Free-Molecule Flow," Physics of Fluids, 1, 73-81, March/ April 1958.

5. D.R.Willis, "A Study of Some Nearly Free Molecular Flow Problems," Princeton Aero Lab Report 440, 1959.

6. D.R. Willis, "A Study of Nearly Free Molecular Flow," RAND Report 339, June 1959.

7. P.Welander, "The Drag of a Sphere Which Moves at High Speed Through a Rarefied Gas," Proc. 1st Int'l Symposium on Rarefied Gas Dynamics, Nice, France, Pergamon Press, London, 1960, pp 317-328.

8. W.Hayes, R.Probstein, Hypersonic Flow Theory, Academic Press, New York, 1958.

9. S.A.Schaaf, "Mechanics of Rarefied Gases," Handbuch der Physik, (in press).

10. L.Lees, "Laminar Heat Transfer Over Blunt Nosed Bodies at Hypersonic Flight Speeds," Jet Propulsion, 26, 4, 259, 1956.

11. C.B.Cohen, E.Reshotko, "Similar Solutions for Compressible Laminar Boundary Layer with Heat Transfer and Pressure Gradient," NACA TN 3325, 1955.

12. A.D.Young, Modern Developments in Fluid Dynamics, Edited by L. Howarth, Oxford Press, London, 1953.

13. S.A.Schaaf, E.S.Moulic, M.T.Chahine, G.J.Maslach, "Aerodynamic Characteristics of Wedges in Low Density Supersonic Flow," ARS Journal, 31, 2, 194, 1961.

14. O.Tewfik, "Heat Transfer, Recovery Factor, and Pressure Distributions Around a Cylinder Normal to a Supersonic Rarefied Gas Stream," Univ. of Calif. Eng. Proj. Report HE-150-169, 1959 (Ph.D.Thesis).

15. M.VanDyke, "Higher Order Approximations in Boundary Layer Theory," Paper presented before ARS Meeting, August 1961.

16. A.Eula, "L'Influenca del Numero di Reynolds ai Grandi numeri di Mach," L'Aerotechnica Vol. XX, No. 1, p. 20, 1940.

17. O. Walchner, "Systematische Geschossmessungen in Windkunal," AVA Report 41/8/6, Goettingen.

18. R.Lehnert, "Drei kumponentenmessungen an Kugeln im Ueberschall," Peenemunde Archive Report 66/46, 1942.

19. R.Lehnert, "Base Pressure of Spheres at Supersonic Speeds," NAVORD Report 2774, U.S.Naval Ordnance Lab, February 1953.

20. H.H.Kurzweg, "Interrelationship between Boundary Layer and Base Pressure," J. Aero. Sci., 743, 1951.

21. S.Erdman, "Widerstand von Kugeln und Kugeln aus der Drurck verteilung bei Ueberschall geschwindiskert," Lilienthal-Gesellschaft fuer Luftfahrtfurshung Bericht 139 2 Tech, 1941.

22. L.Crocco, L.Lees, "A Mixing Theory for the Interaction Between Dissipative Flows and Nearly Isentropic Streams," J. Aero. Sci., 649, 1952.

23. A.J.Hodges, "The Drag Coefficient of Very High Velocity Spheres," J. Aero. Sci., 24, 10, 755-758, 1957.

24. A.Charters, B.Thomas, "The Aerodynamic Performance of Small Spheres From Subsonic to High Subsonic Velocities," J. Aero. Sci., 12, 4, 468, October 1945.

25. L.Kavanau, "Base Pressure Studies in Rarefied Supersonic Flows," J. Aero. Sci., 23, 3, 193, 1956.

26. A.Skreekanth, "Drag Measurements in Circular Cylinders and Spheres in the Transition Region at a Mach Number of 2," UTIA Report No. 74, April 1961.

27. E.D.Kane, "Sphere Drag Data at Supersonic Speeds and Low Reynolds Numbers," J. Aero. Sci., 18, 5, 259, 1951.

28. F.S.Sherman, "Note on Sphere Drag Data," J. Aero. Sci., 18, 566, 1951.

29. N.A.Jensen, "Supplementary Data on Sphere Drag Tests - No. 2," Univ. of Calif. Eng. Proj. Report HE-150-92, 1951.

30. P.Wegener, H.Ashkenas, "Wind Tunnel Measurement of Sphere Drag at Supersonic Speeds and Low Reynolds Numbers," J. Fluid Mech., 10, 4, 550, 1961.

31. A.May and A.Witt, "Supersonic Drag of Spheres at Low Reynolds Numbers in Free Flight," J. Appl. Phys., 28, 910, 1957.

32. A.May and A.Witt, "Free Flight Determinations of the Drag Coefficients of Spheres," J. Aero. Sci., 20, 635, 1953.

33. V.C.Liu, "Rarefied Gas Dynamical Considerations in the Rocket-Sounding Measurements," Paper 7-1, Aerodynamics of the Upper Atmosphere Symposium, RAND Report R-339, 1959.

34. L.Potter, M.Kinslow, G.Avery, A.Bailey, "Description of Preliminary Calibration of a Low Density Hypervelocity Wind Tunnel," AEDC TN-61-63, August 1961.

35. D.F.Masson, et.Al., "Measurement of Sphere Drag from Hypersonic Continuum to Free Molecular Flow," RAND Res. Memo RM-2678, 1960.

36. G.J.Maslach, F.S.Sherman, "Design and Testing of an Axi-Symmetric Hypersonic Nozzle for a Low Density Wind Tunnel," WADC Tech. Report TR-341, 1956.

37. J.M.Owen, F.S.Sherman, "Design and Testing of a Mach 4 Axially Symmetric Nozzle for Rarefied Gas Flows," Univ. of Calif. Eng. Proj. Report HE-150-104, 1952.

38. L.L.Lynes, "Design, Fabrication, and Evaluation of Axisymmetric Nozzles," Univ. of Calif. Eng. Proj. Report HE-150-174, 1959.

39. L.Talbot, "Viscosity Corrections to Cone Probes in a Rarefied Supersonic Flow at a Nominal Mach Number of 4," NACA TN 3219, 1954.

40. F.S.Sherman, "New Experiments on Impact-Pressure Interpretation in Supersonic and Subsonic Rarefied Air Streams," NACA TN-2995, 1953.

41. R.N.Latz, "Design of a Two Component Microbalance for Low Density Wind Tunnels," Univ. of Calif. Eng. Proj. Report HE-150-124, 1954.

42. D.C.Ipsen, "Experiments on Cone Drag in a Rarefied Air Flow," Jet
        Propulsion, 1076, December 1956 (Also unpublished data).

43. N.Rott, L.Crabtree, "Simplified Laminar Boundary Layer Calculations
        For Bodies of Revolution and for Yawed Wings," J. Aero. Sci.,
        19, 553, 1952.

44. H.Schlicting, Boundary Layer Theory, McGraw Hill Book Co., New York,
        1955, Chapter X.

45. M.T.Chahine, "Similarity Solution for Stagnation Point Heat Transfer
        in Low Density, High Speed Flow," JPL, CalTech Research
        Summary 36-8, Sec. VII, May 1, 1961.

46. D.Hartree, Numerical Analysis, Oxford Univ. Press, London, 1952.

47. K.Brownlee, Statistical Theory and Methodology in Science and
        Engineering, J. Wiley & Sons, New York, 1960.

48. D.Tellep, "Lift on Flat Plates in Low Density Supersonic Flow," Univ.
        of Calif. Eng. Proj. Report HE-150-131, 1955.

APPENDIX A

The regression analysis of the data points is based on the assumption that the data arose from an experiment adequately represented by the model of equation (II-9). Each family of data points was first fit to a simple straight line in $1/\sqrt{Re}$, $C_{D_{i_1}} = A_1 + N_1/\sqrt{Re_i}$ by the method of least squares. The same family of data points was then fit to a quadratic in $1/\sqrt{Re}$, $C_{D_{2i}} = A_2 + B_2/\sqrt{Re_i} + C_2/Re_i$, also using the method of least squares. The significance of the quadratic fit was judged on two different bases, the one completely statistical, and the other following from the gas dynamics analysis that led to the construction of the model. The viewpoint was adopted that the higher order polynomial in $1/\sqrt{Re}$ could be consistent with the assumed model only if the term which is associated with the boundary layer shear stress, $B_2/\sqrt{Re_i}$, possessed a positive value. If the coefficient B_2 did not possess a positive value, then the quadratic polynomial was removed from further consideration and the linear fit was adopted.

If the coefficient B_2 was determined to be positive, then the highest order term in the quadratic was examined for statistical significance in the following fashion (see Brownlee[47]).

The sum of the squares of the residuals was calculated for both the linear fit and the quadratic fit, i.e.,

$$SS_1 = \sum_{i=1}^{n} (C_{D_{ex}i} - C_{D_{i_1}})^2$$

$$SS_2 = \sum_{i=1}^{n} (C_{D_{ex}i} - C_{D_2})^2$$

An F statistic, which consists of the quotient of two variances is constructed. The variance is estimated by $SS_2/n-3$, corresponding to the sum of the squares of the error distributed over the $n-3$ remaining degrees of freedom. The reduction in variance due to the addition of a quadratic term in the regression formula is then estimated by subtracting SS_2 from SS_1. The F statistic is then calculated,

$$F = \frac{SS_1 - SS_2}{SS_2/n-3} \quad .$$

This statistic is distributed as $F(1, n-3)$ where 1 refers to the degrees of freedom of the numerator and $n-3$ refers to the number of degrees of freedom of the denominator. If this value of $F(1,n-3)$ is less than the tabulated value of $F_\alpha(1,n-3)$ corresponding to some required level of significance α, then there is no evidence at this level α that the coefficient C is not equal to zero. The probability of rejecting a true hypothesis is α. In non-statistical language, a value of $F < F_\alpha$ indicates that there is no significant advantage in considering the quadratic rather than the linear fit. A value of $\alpha = 95\%$ was selected for these tests. Table 4 contains the coefficients for both the linear and quadratic fit. In only one case, $M = 2$ at $T_w = 300°$ K, was the coefficient B_2 negative, eliminating the quadratic fit from consideration. All of the remaining cases except the $M = 4$, $T_w = 300°$ K case possessed values of F less than $F_{0.05}$, indicating that the coefficient C_2 was not different from zero at the 5% level. For $M = 4$, $T_w = 300°$ K, it was found that $C_2 \neq 0$ at both the 5% and 1% levels.

Confidence Limits

Once the estimate of the regression of C_D on Re was made, it was desired to establish confidence limits for this estimate. First it was necessary to evaluate the variance of the estimate at each point. For a quadratic fit,

$$\text{Variance} \ (C_{D_{\text{estimate}}}) = \text{Var} \ (A_2) + \text{Var} \ (B_2) \left[\frac{1}{\sqrt{Re_i}} - \frac{\overline{1}}{\sqrt{Re_i}} \right]^2$$

$$+ \ \text{Var} \ (C_2) \left[\frac{1}{Re_i} - \frac{\overline{1}}{Re_i} \right]^2$$

$$+ \ 2 \ \text{cov} \ (B_2 C_2) \left[\frac{1}{\sqrt{Re_i}} - \frac{\overline{1}}{\sqrt{Re_i}} \right] \left[\frac{1}{Re_i} - \frac{\overline{1}}{Re_i} \right]$$

The calculation of the variances and covariance of the coefficients in a quadratic are given in reference 47.

Confidence intervals are derived using the approximate t multiplier corresponding to the degrees of freedom of the error variance at the prescribed level of significance. Thus if the confidence interval is selected as $1 - \alpha$, then the estimate of the regression line is

$$C_{D_i} = A_2 + B_2 / \sqrt{Re_i} + C_2 / Re_i \quad \pm \quad t_\alpha \ \sqrt{V(C_{D_i})}$$

Figures 11, 12, and 13 show 95% confidence intervals. Since this is a somewhat severe test of an estimate, it was decided to utilize 50% confidence limits in the interpretation of the data. This corresponds to the probable error of the estimate in the sense that there is a 50% chance

that the performance of an identical experiment would yield a regression line that falls within the 50% confidence intervals. In all cases where C_2 was determined to be zero, pooled estimates of the error variance were made.

APPENDIX   B

704 Subroutine (DUZ) was used to smooth and differentiate the data points. The scheme operated in the following way:

Consider a set of data points

$$x_i, \quad t_i \qquad \text{where} \quad x_i \quad \text{is distance}$$

$$t_i \quad \text{is time}$$

$$i \; = \; 1, \; n \qquad i \quad \text{is the number of the point}$$

It is necessary that $n \geq 7$ for operation of this program. For $i = 1$ to $i = 4$ the derivative $\frac{\partial x}{\partial t_i}$ was obtained by evaluating the derivative of the least squares quadratic fit through the first 7 points. Thus if a second order polynomial $x = \alpha + \beta t + \gamma t^2$ is constructed through the first 7 points, then $\frac{\partial x}{\partial t_i} = \beta + 2\gamma t_i$.

For values of $i = 4 < m < n-3$, a quadratic in t is fit through the three adjoining points on both sides of point m, as well as through point m itself. The derivative of this quadratic fit is the evaluated at the point $m=i$ as before

$$\frac{\partial x}{\partial t}_{i=m} \; = \; \beta + 2\gamma t_{i=m}$$

For values of i less than n but greater than $n-4$, a least squares quadratic is drawn through the last 7 points. The value of the derivative is then obtained at each of the points of interest.

The accuracy of this scheme was tested empirically by differentiating the function e^x in the range $0 < x = \; < 2$, and the results

indicated that the derivative of a smooth analytic function could be obtained with an accuracy of 0.3%.

Since the experimental data was analytic in t, and since the region of interest could be represented exactly by a parabola, this differentiation scheme was quite acceptable. Some difficulties were encountered when a wild point appeared in the data, since it could influence the derivatives evaluated at the 6 surrounding points by the role that it played in the evaluation of the least squares coefficients. The presence of a wild point could be detected easily, however, when the local derivatives were examined graphically. If a wild point was detected, it was examined carefully in order to determine just how it arose, and after it was corrected, the set of data was differentiated again.

TABLE 1a. RESULTS OF DRAG BALANCE TESTS

M ≈ 4 - No. 14 Nozzle

Run No.	Diameter (inches)	No. of Wires	$C_{D_{total}}$	$C_{D_{tare}}$	$C_{D_{net}}$	Re_∞	Mach No.	Re_2
676	0.250	4	1.842	0.584	1.258	620	4.055	167.4
			1.851	0.590	1.261	579.5	4.033	108.9
			1.882	0.608	1.274	495	3.975	135.6
			1.9129	0.620	1.292	453.5	3.949	125.0
			1.922	0.632	1.290	413.7	3.914	114.6
			1.981	0.656	1.325	357	3.876	100.6
			2.0447	0.710	1.335	250	3.731	75.4
			2.146	0.738	1.408	192.5	3.586	62.2
			2.1525	0.754	1.398	162.5	3.333	58.5
			2.197	0.760	1.437	127.5	3.227	47.9
			2.167	0.760	1.407	90.1	3.153	34.7
669	0.250	2	1.554	0.291	1.262	614.7	4.049	165.9
			1.5904	0.306	1.284	485	3.993	132.9
			1.5618	0.296	1.265	570.7	4.014	155.0
			1.6119	0.311	1.300	441.0	3.969	120.8
			1.633	0.319	1.314	398.2	3.939	109.9
			1.6505	0.328	1.322	352.5	3.892	98.7
			1.709	0.356	1.353	245.5	3.745	74.01
			1.769	0.371	1.392	187.8	3.602	60.19
			1.778	0.377	1.401	151.4	3.485	50.9
			1.810	0.380	1.430	125.4	3.258	46.6
			1.878	0.380	1.498	86.97	3.191	33.02

TABLE 1a. - Continued

Run No.	Diameter (inches)	No.of Wires	$C_{D_{total}}$	$C_{D_{tare}}$	$C_{D_{net}}$	Re_∞	Mach No.	Re_2
680b	0.125	2	1.670	0.364	1.306	311	4.047	84.59
			1.680	0.366	1.314	259.8	4.033	70.6
			1.712	0.372	1.340	243	3.992	66.33
			1.742	0.373	1.369	222	3.962	61.05
			1.769	0.380	1.389	199	3.931	55.1
			1.780	0.386	1.436	177	3.891	49.6
			1.865	0.429	1.436	123	3.764	36.5
			1.913	0.466	1.447	95	3.617	30.2
			2.046	0.497	1.549	73.3	3.515	24.4
			2.131	0.479	1.652	58.5	3.402	18.7
			2.063	0.433	1.630	45.7	3.233	17.22
609	1.000	4	1.179	0.0496	1.128	1956	3.972	535.9
			1.149	0.0467	1.102	2532	4.044	686.2
			1.159	0.0475	1.111	2353	4.025	637.6
			1.193	0.0523	1.141	1626	3.916	450.4
			1.219	0.0549	1.164	1430	3.889	400.4
			1.230	0.0601	1.169	997	3.726	309.4
610B	1.000	4	1.348	0.065	1.273	332	3.352	118.5
			1.382	0.067	1.315	451	3.492	152.0
611	1.000	4	1.295	0.065	1.230	736	3.670	228.2
			1.320	0.067	1.253	463	3.437	159.7

TABLE 1a - Continued.

Run No.	Diameter (inches)	No. of Wires	$C_{D_{total}}$	$C_{D_{tare}}$	$C_{D_{net}}$	Re_∞	Mach No.	Re_2
642	1.000	3	1.215	0.041	1.173	1433	3.876	402.7
			1.212	0.046	1.165	1015	3.717	307.5
			1.312	0.0486	1.263	744.6	3.650	233.06
			1.325	0.0475	1.277	470	3.424	163.1
			1.365	0.0475	1.317	340	3.305	124.0
641	1.000	3	1.144	0.0351	1.108	2574	4.026	697.5
			1.155	0.0357	1.119	2373	4.019	645.2
			1.174	0.0373	1.136	1997	3.919	547.2
			1.183	0.0380	1.145	1815	3.952	499.1
			1.224	0.0393	1.185	1806	3.913	502.0
			1.243	0.0413	1.200	1453	3.879	406.8
634	0.500	3	1.300	0.144	1.156	1245	4.036	337.4
			1.319	0.147	1.172	1093	4.020	296.2
			1.337	0.153	1.184	926	3.981	252.8
			1.365	0.162	1.203	759	3.918	210.2
			1.396	0.1687	1.227	680	3.884	191.0
			1.516	0.1855	1.3305	476	3.768	140.4
			1.485	0.198	1.2807	381	3.617	121.2
			1.494	0.2015	1.293	305	3.525	101.2
			1.507	0.179	1.328	253	3.382	89.3
			1.463	0.180	1.283	160	3.271	59.2

69.

TABLE 1a - Continued

Run No.	Diameter (inches)	No.of Wires	$C_{D_{total}}$	$C_{D_{tare}}$	$C_{D_{net}}$	Re_∞	Mach No.	Re_2
617	0.500	4	1.349	0.192	1.156	1263	4.044	341.6
			1.359	0.196	1.164	1173	4.031	317.9
			1.381	0.204	1.176	975	3.987	266.2
			1.411	0.216	1.195	798	3.925	221.0
			1.435	0.225	1.210	706	3.898	197.0
			1.486	0.247	1.238	520	3.769	153.9
			1.552	0.264	1.287	370	3.643	116.6
618	0.500	4	1.556	0.260	1.296	378.5	3.626	119.6
			1.577	0.269	1.308	329.5	3.501	110.2
			1.602	0.239	1.363	242.5	3.365	86.1
			1.667	0.240	1.427	155.5	3.262	57.7
648	0.750	3	1.203	0.0632	1.139	1895	4.025	513.5
			1.214	0.0640	1.150	1766	4.014	480.3
			1.236	0.06689	1.169	1458	3.968	399.5
			1.245	0.0686	1.176	1343	3.942	370.6
			1.267	0.07114	1.196	1197	3.914	332.1
			1.2807	0.0730	1.207	1064	3.867	301.1
			1.3308	0.0784	1.252	733	3.712	222.8
			1.374	0.0876	1.286	562	3.636	177.0
			1.3739	0.0779	1.296	484	3.348	173.3
			1.363	0.0746	1.288	398	3.230	149.3
			1.385	0.0734	1.311	294	3.212	111.4

TABLE 1a - Continued

Run No.	Diameter (inches)	No.of Wires	$C_{D_{total}}$	$C_{D_{tare}}$	$C_{D_{net}}$	Re_∞	Mach No.	Re_2
652	0.750	4	1.2119	0.0818	1.130	1897	4.034	514.0
			1.227	0.0853	1.142	1769	4.023	479.4
			1.239	0.0892	1.149	1487	3.977	407.4
			1.249	0.0916	1.157	1353	3.951	372.7
			1.266	0.948	1.170	1199	3.921	332.1
			1.279	0.0973	1.181	1072	3.871	302.3
			1.333	0.1097	1.223	732	3.153	218.1
			1.342	0.1203	1.221	436	3.521	149.7
			1.385	0.1153	1.270	359	3.404	125.3
			1.420	0.1126	1.308	273	3.380	96.4
			1.356	0.1154	1.240	567	3.631	179.2
627	0.375	3	1.636	0.325	1.311	376.2	3.756	112.1
			1.705	0.338	1.367	289	3.605	92.5
			1.772	0.3625	1.409	223	3.513	74.7
			1.768	0.363	1.405	180	3.390	63.4
			1.773	0.324	1.449	128	3.244	47.9
			1.528	0.261	1.266	893	4.017	243.0
			1.511	0.256	1.254	954	4.030	259.0
			1.529	0.273	1.255	945.4	3.979	259.0
			1.543	0.280	1.260	673.8	3.951	185.6
			1.567	0.288	1.278	606.1	3.919	167.9
			1.588	0.298	1.290	529	3.879	148.6

TABLE 1a - Continued

Run No.	Diameter (inches)	No.of Wires	$C_{D_{total}}$	$C_{D_{tare}}$	$C_{D_{net}}$	Re_∞	Mach No.	Re_2
624	0.375	4	1.581	0.347	1.234	949	4.049	256.2
			1.600	0.355	1.245	883	4.042	238.9
			1.621	0.372	1.249	750	4.002	204.8
			1.642	0.381	1.261	680	3.977	186.3
			1.669	0.391	1.278	605	3.940	166.9
			1.705	0.400	1.304	533	3.890	149.2
			1.771	0.427	1.343	384	3.735	115.2
			1.755	0.455	1.300	289.8	3.611	92.44
			1.808	0.496	1.313	221.2	3.550	72.5
			1.876	0.499	1.369	174	3.416	60.4
			1.796	0.431	1.365	124.8	3.273	46.0

TABLE 1b. RESULTS OF DRAG BALANCE TESTS

M ~ 4 - No. 8 Nozzle

Run No.	Diameter (inches)	No.of Wires	$C_{D_{total}}$	$C_{D_{tare}}$	$C_{D_{net}}$	Re_∞	Mach No.	Re_2
677	0.250	4	1.843	0.614	1.229	610	4.066	165
			1.864	0.616	1.248	546	4.028	148
			1.890	0.622	1.268	469	3.950	128.9
			1.891	0.626	1.265	435	3.928	120.5
			1.948	0.634	1.314	389.5	3.896	108.7
			1.937	0.640	1.297	362	3.857	99.9
			1.976	0.648	1.328	326	3.841	93.2
			1.988	0.654	1.334	299.6	3.800	87.2
668	0.250	2	1.541	0.308	1.233	631	4.006	173
			1.538	0.308	1.230	563	3.960	154
			1.586	0.310	1.276	486	3.917	134.9
			1.616	0.314	1.302	451	3.874	127
			1.615	0.314	1.301	417.2	3.808	120.9
			1.677	0.319	1.298	366.5	3.797	106.62
			1.647	0.323	1.324	336.5	3.839	96.0
			1.652	0.326	1.326	309.6	3.765	91.6
637	1.000	3	1.164	0.0376	1.126	2665	4.068	716.9
			1.194	0.038	1.155	2138	4.014	581.5
			1.192	0.0375	1.154	1673	3.929	463.4
			1.198	0.0365	1.162	1513	3.886	424.4
			1.206	0.0360	1.1707	1360	3.855	386.2
			1.240	0.0342	1.2063	1199	3.816	345.3

TABLE 1b - Continued

Run No.	Diameter (inches)	No.of Wires	$C_{D_{total}}$	$C_{D_{tare}}$	$C_{D_{net}}$	Re_∞	Mach No.	Re_2
637 (Continued)	1	3	1.243	0.0320	1.211	1034	3.742	310.2
			1.174	0.038	1.136	2293	4.036	621.4
601	1	4	1.138	0.0509	1.087	2670	4.053	720.9
			1.148	0.0507	1.097	2308	4.019	626.6
			1.161	0.0489	1.112	1997	3.969	547.6
			1.178	0.0490	1.129	1759	3.945	485.5
			1.213	0.046	1.167	1354	3.866	381.8
			1.230	0.042	1.188	1028	3.730	309.4
			1.206	0.0409	1.165	1287	3.670	399.0
602	1	4	1.243	0.040	1.203	1024	3.736	307.7
			1.232	0.045	1.187	1196	3.798	352.8
			1.212	0.047	1.165	1341	3.841	382.2
			1.200	0.0483	1.152	1517	3.889	424.8
			1.186	0.0485	1.137	1686	3.921	467.0
			1.171	0.0490	1.122	1825	3.950	502.8
			1.167	0.049	1.118	1980	3.977	542.5
			1.155	0.049	1.106	2120	3.994	578.7
638	1	3	1.173	0.0376	1.134	2675	4.061	719.6
			1.193	0.0380	1.154	2310	4.014	628.3
			1.189	0.0390	1.150	2141	4.011	582.4
			1.203	0.039	1.164	2004	3.996	547.1
			1.217	0.0384	1.178	1832	3.967	502.9

TABLE 1b - Continued

Run No.	Diameter (inches)	No.of Wires	$C_{D_{total}}$	$C_{D_{tare}}$	$C_{D_{net}}$	Re_∞	Mach No.	Re_2
647	0.750	3	1.192	0.0677	1.124	1937	4.067	521.0
			1.196	0.0677	1.127	1935	4.073	520.5
			1.208	0.0671	1.141	1690	4.029	458.0
			1.227	0.0671	1.159	1558	4.013	423.8
			1.236	0.0675	1.167	1461	3.993	398.9
			1.252	0.067	1.185	1348	3.977	369.4
			1.253	0.066	1.187	1243	3.896	346.8
			1.261	0.067	1.193	1133	3.899	316.1
			1.299	0.065	1.234	981	3.873	276.6
			1.291	0.063	1.228	903	3.828	259.2
651	0.750	4	1.208	0.0903	1.118	1933	4.084	519.9
			1.219	0.0895	1.130	1695	4.034	459.3
			1.227	0.0892	1.137	1585	4.002	431.3
			1.241	0.0900	1.1507	1458	3.998	396.6
			1.250	0.0900	1.162	1363	3.974	373.5
			1.266	0.0890	1.177	1246	3.920	345.1
			1.276	0.0890	1.186	1156	3.892	323.7
			1.305	0.0870	1.218	1032	3.841	294.6
			1.321	0.0850	1.236	929	3.799	270.3

TABLE 1b - Continued

Run No.	Diameter (inches)	No.of Wires	$C_{D_{total}}$	$C_{D_{tare}}$	$C_{D_{net}}$	Re_∞	Mach No.	Re_2
633	0.500	3	1.290	0.150	1.140	1326	4.069	358
			1.314	0.153	1.160	1127	4.027	305
			1.325	0.156	1.168	1050	4.014	287
			1.331	0.156	1.175	999	3.992	272
			1.343	0.156	1.187	902	3.957	248
			1.356	0.157	1.198	839	3.931	232.4
			1.372	0.158	1.213	757	3.897	211.6
			1.388	0.156	1.232	669	3.854	190.0
			1.408	0.156	1.252	508	3.820	168.7
615	0.500	4	1.427	0.211	1.216	770	3.897	214.8
			1.454	0.209	1.245	677	3.843	193.3
			1.443	0.196	1.247	608	3.782	181.8
			1.427	0.210	1.217	756	3.932	208.6
			1.398	0.209	1.189	812	3.960	223.3
616	0.500	4	1.407	0.210	1.197	909	3.966	249.8
			1.392	0.209	1.191	1011	3.997	276
			1.383	0.208	1.175	1066	4.018	289.4
			1.346	0.200	1.146	1352	4.066	363.7
			1.373	0.204	1.169	1138	4.027	308.4
628	0.375	3	1.503	0.273	1.230	967	4.079	261
			1.527	0.276	1.251	858	4.041	232.5
			1.538	0.278	1.260	806	4.014	219.2
			1.536	0.282	1.254	749.6	3.997	204.4

TABLE 1b - Continued

Run No.	Diameter (inches)	No.of Wires	$C_{D_{total}}$	$C_{D_{tare}}$	$C_{D_{net}}$	Re_∞	Mach No.	Re_2
629	0.375	3	1.512	0.282	1.230	750	3.995	204.7
			1.524	0.285	1.239	689	3.968	188.7
			1.538	0.2846	1.253	622	3.932	172.3
			1.561	0.289	1.272	577	3.903	160.9
			1.565	0.289	1.276	507	3.857	143.5
			1.597	0.270	1.327	445	3.796	129.9
623	0.375	4	1.577	0.363	1.214	963.7	4.078	259
			1.598	0.369	1.229	858.7	4.040	232.7
			1.607	0.371	1.235	805.1	4.015	219.0
			1.618	0.377	1.240	754.9	3.998	206.1
			1.637	0.381	1.256	690	3.967	189.0
			1.645	0.3795	1.265	636	3.921	176.1
			1.653	0.386	1.266	583	3.894	163.2
			1.674	0.386	1.2889	508.9	3.850	145.0
			1.658	0.361	1.297	450.4	3.775	133.9
680	0.125	2	1.684	0.376	1.308	322	4.090	93.0
			1.681	0.377	1.304	285	4.033	77.52
			1.738	0.388	1.351	245	3.991	66.88
			1.758	0.396	1.362	225	3.973	61.65
			1.753	0.399	1.354	197.3	3.939	54.45
			1.761	0.401	1.360	167.1	3.894	46.69
			1.839	0.410	1.429	164.2	3.866	46.4
			1.848	0.402	1.446	148	3.813	42.77

TABLE 1c - RESULTS OF DRAG BALANCE TESTS

$M \sim 2$ - No. 6 Nozzle

Run No.	Diameter (inches)	No. of Wires	$C_{D_{total}}$	$C_{D_{tare}}$	$C_{D_{net}}$	Re_∞	Mach No.	Re_2
678	0.250	4	1.845	0.437	1.408	190	2.173	113.0
			2.016	0.507	1.509	156	2.141	94.8
			2.057	0.569	1.488	131.9	2.092	81.8
			2.157	0.618	1.539	114.4	2.064	71.6
			2.295	0.727	1.568	84.07	2.021	53.6
			2.364	0.789	1.575	64.5	1.945	42.4
			2.413	0.789	1.624	64.5	1.619	47.7
670	0.250	2	1.729	0.218	1.511	192	2.180	114.2
			1.784	0.254	1.530	156	2.160	93.9
			1.804	0.286	1.518	131	2.110	70.1
			1.854	0.309	1.545	114	2.080	71.0
			1.889	0.304	1.525	84	2.018	53.76
			1.979	0.407	1.572	64.8	1.958	42.2
679	0.125	2	2.782	0.561	2.221	21.05	1.641	15.5
			2.623	0.568	2.055	21.4	1.697	15.4
			2.027	0.459	1.568	94.4	2.176	56.4
			2.095	0.468	1.627	79.1	2.141	48.0
			2.172	0.469	1.703	65.83	2.089	40.82
			2.252	0.481	1.771	56.75	2.071	35.44
			2.322	0.489	1.833	43.15	1.986	27.9
			2.394	0.512	1.882	33.95	1.885	22.8

TABLE 1c - Continued

Run No.	Diameter (inches)	No.of Wires	C_D	C_D	C_D	Re_∞	Mach No.	Re_2
679 (Continued)	0.125	2	2.393	0.550	1.843	28.05	1.896	18.8
			2.357	0.567	1.790	24.8	1.866	16.8
			2.579	0.583	1.946	21.1	1.768	14.8
625	0.375	4	1.603	0.429	1.174	295.8	2.183	176.9
			1.706	0.464	1.242	238.5	2.160	143.6
			1.777	0.479	1.298	199.1	2.125	121.8
			1.825	0.488	1.337	179.1	2.108	110.1
			1.987	0.492	1.495	130.3	1.996	83.9
			2.127	0.514	1.613	99.9	1.912	66.5
			2.187	0.532	1.655	76.9	1.772	54.0
			2.214	0.566	1.647	59.4	1.672	43.1
			2.014	0.495	1.519	128.8	1.966	84.0
626	0.375	3	1.781	0.359	1.422	200	2.115	122.8
			1.795	0.366	1.429	181	2.082	112.6
			1.980	0.386	1.594	100.4	1.911	66.9
			2.037	0.400	1.637	75.4	1.804	52.32
			2.103	0.421	1.681	59.6	1.699	42.9
			1.904	0.368	1.536	127.0	1.997	81.8
			1.609	0.322	1.287	294	2.179	175.8
			1.718	0.347	1.370	239	2.154	144.3
614	0.500	4	1.311	0.246	1.073	394.7	2.179	235.6
			1.376	0.282	1.093	314.2	2.150	189.8
			1.433	0.270	1.162	260.4	2.112	156.5

TABLE 1c - Continued

Run No.	Diameter (inches)	No.of Wires	$C_{D_{total}}$	$C_{D_{tare}}$	$C_{D_{net}}$	Re_∞	Mach No.	Re_2
614 (Continued)	0.500	4	1.461	0.276	1.184	241.7	2.099	147.0
			1.584	0.290	1.273	170.0	2.014	110
			1.676	0.303	1.373	131.2	1.926	86.8
			1.719	0.324	1.395	98.4	1.830	67.7
			1.777	0.331	1.440	83.60	1.752	58.2
635	0.500	3	1.331	0.185	1.147	394	2.179	235
			1.395	0.212	1.183	317.8	2.155	191.9
			1.456	0.210	1.247	259.9	2.122	159.0
			1.476	0.207	1.269	244.2	2.097	151.2
			1.585	0.217	1.368	171.4	2.008	110.0
			1.650	0.227	1.423	130.98	1.926	86.8
			1.731	0.243	1.488	99.82	1.835	68.5
			1.753	0.248	1.505	85.06	1.726	60.7
649	0.750	3	1.1974	0.0815	1.115	586	2.181	349.3
			1.244	0.086	1.158	474	2.148	286.8
			1.288	0.088	1.200	398	2.124	243.6
			1.342	0.091	1.251	340.7	2.102	210.0
			1.432	0.104	1.328	258.4	2.016	165.4
			1.489	0.116	1.377	204.9	1.863	139.3
			1.502	0.115	1.386	158.6	1.697	114.2
			1.555	0.116	1.440	127.05	1.628	93.7
650	0.750	4	1.507	0.155	1.351	120.7	1.726	86.2
			1.460	0.154	1.306	153	1.827	105.3

TABLE 1c - Continued

Run No.	Diameter (inches)	No.of Wires	$C_{D_{total}}$	$C_{D_{tare}}$	$C_{D_{net}}$	Re_∞	Mach No.	Re_2
650 (Continued)	0.750	4	1.398	0.154	1.244	200.9	1.945	132.2
			1.157	0.109	1.049	589.4	2.181	352.2
			1.199	0.115	1.085	478.4	2.154	289.0
			1.247	0.118	1.129	401.4	2.124	245.7
			1.283	0.121	1.161	347.25	2.090	215.4
			1.360	0.139	1.221	259.6	2.018	165.9
636	1	3	1.167	0.0460	1.120	770	2.175	460.5
			1.2137	0.0487	1.165	626	2.149	378.1
			1.263	0.0505	1.213	520	2.119	318.2
			1.298	0.0515	1.246	480.5	2.105	296.5
			1.362	0.0571	1.305	336.4	2.015	215.2
			1.393	0.0610	1.332	263.5	1.916	175.5
			1.454	0.0650	1.388	194.6	1.822	134.3
			1.456	0.0655	1.391	169.7	1.746	120.1
613	1	4	1.139	0.0608	1.078	783.2	2.176	468.2
			1.1479	0.0618	1.086	775.7	2.173	463.9
			1.1969	0.0650	1.1317	629.2	2.147	379.9
			1.245	0.0675	1.178	516.9	2.109	317.9
			1.268	0.0685	1.200	479.7	2.106	295.9
			1.362	0.0760	1.286	335.1	2.023	213.8
			1.393	0.0809	1.312	260.1	1.926	172.6
			1.438	0.0871	1.350	195.8	1.803	136.0
			1.462	0.0876	1.374	167.5	1.728	119.6

TABLE 1d - RESULTS OF DRAG BALANCE TESTS

M ~ 6 - No. 9 Nozzle

Run No.	Diameter (inches)	No. of Wires	$C_{D_{total}}$	$C_{D_{tare}}$	$C_{D_{net}}$	Re_∞	Mach No.	Re_2
670b	0.250	2	1.383	0.238	1.145	2564	6.030	371
			1.4115	0.247	1.104	2174	6.001	315
			1.428	0.254	1.174	1969	5.982	287.4
			1.369	0.260	1.109	1790	5.953	263
			1.458	0.264	1.194	1641	5.933	242
			1.471	0.273	1.198	1406	5.895	209
			1.508	0.291	1.217	990	5.728	153.4
			1.546	0.302	1.244	762	5.562	123.0
677b	0.250	4	1.627	0.477	1.150	2521	6.039	365.5
			1.666	0.496	1.170	2161	6.016	313.3
			1.689	0.511	1.178	1933	5.992	280
			1.709	0.528	1.181	1759	5.978	257
			1.733	0.537	1.196	1541	5.950	226.6
			1.750	0.549	1.201	1364	5.928	201.2
			1.787	0.572	1.200	1109	5.874	165.2
			1.815	0.587	1.228	932	5.798	142.1
			1.843	0.606	1.237	732	5.633	115.07
681	0.125	2	1.479	0.288	1.191	1291	5.864	193.65
			1.485	0.290	1.195	1158	5.817	176.0
			1.497	0.287	1.210	1064	5.792	161.7
			1.513	0.298	1.215	967	5.757	147.9
			1.529	0.303	1.226	868.6	5.720	133.67

TABLE 1d - Continued

Run No.	Diameter (inches)	No. of Wires	$C_{D_{total}}$	$C_{D_{tare}}$	$C_{D_{net}}$	Re_∞	Mach No.	Re_2
681 (Continued)	0.125	2	1.547	0.311	1.236	769.5	5.687	120.81
			1.600	0.324	1.276	616.9	5.607	97.5
			1.609	0.333	1.276	529	5.553	84.6
			1.643	0.349	1.294	424	5.498	67.8
622	0.375	4	1.393	0.312	1.081	4162	5.876	624.3
			1.401	0.313	1.088	3584	5.817	541.2
			1.420	0.315	1.104	3266	5.780	496.4
			1.436	0.320	1.116	2998	5.756	458.7
			1.450	0.322	1.128	2661	5.712	409.7
			1.474	0.341	1.133	2345	5.675	365.8
			1.508	0.339	1.169	1930	5.600	304.9
			1.520	0.344	1.176	1654	5.549	264.6
			1.575	0.367	1.208	1313	5.500	210.08
630	0.375	3	1.378	0.243	1.136	2950	5.779	448.4
			1.394	0.244	1.150	2628	5.724	404.7
			1.397	0.248	1.149	2314	5.679	361.0
			1.423	0.257	1.165	1909	5.613	301.6
			1.447	0.248	1.198	1643	5.562	261.2
			1.467	0.270	1.197	1305	5.480	210.1
			1.341	0.239	1.102	4082	5.908	604.1
			1.356	0.241	1.116	3540	5.853	531.0
			1.363	0.242	1.121	3221	5.813	489.6

TABLE 1d - Continued

Run No.	Diameter (inches)	No.of Wires	$C_{D_{total}}$	$C_{D_{tare}}$	$C_{D_{net}}$	Re_∞	Mach No.	Re_2
653	0.750	4	1.111	0.0686	1.042	8047	5.910	1190.9
			1.118	0.0688	1.049	6886	5.852	1032.9
			1.122	0.0691	1.053	6414	5.821	968.5
			1.126	0.0697	1.056	5854	5.781	889.8
			1.133	0.0696	1.063	5153	5.728	793.6
			1.147	0.0737	1.073	3774	5.600	596.3
			1.160	0.0745	1.086	3230	5.552	516.8
			1.176	0.0803	1.095	2609	5.491	422.6
			1.1386	0.0709	1.067	4613	5.690	715.0
			1.159	0.0737	1.085	3787	5.615	594.6
646	0.750	3	1.110	0.0516	1.058	8143	5.908	1205.2
			1.1175	0.0518	1.065	7020	5.847	1053.0
			1.1213	0.0521	1.068	6453	5.817	980.8
			1.128	0.0524	1.075	5944	5.783	903.5
			1.133	0.0523	1.079	5254	5.721	809.1
			1.140	0.0533	1.086	4692	5.683	727.3
			1.175	0.0560	1.119	3226	5.558	512.9
			1.157	0.0554	1.101	3530	5.598	557.7
			1.195	0.0604	1.134	2661	5.504	425.8
640	1.000	3	1.068	0.0292	1.039	11192	5.921	1656.4
			1.076	0.0293	1.047	9324	5.858	1398.6
			1.085	0.0294	1.056	8528	5.827	1287.7
			1.090	0.0294	1.060	7855	5.789	1194.9

TABLE 1d - Continued

Run No.	Diameter (inches)	No.of Wires	$C_{D_{total}}$	$C_{D_{tare}}$	$C_{D_{net}}$	Re_∞	Mach No.	Re_2
640 (Continued)	1.000	3	1.094	0.0300	1.064	7095	5.744	1085.5
			1.097	0.0300	1.068	6284	5.696	974.0
			1.111	0.0293	1.082	5134	5.616	811.1
			1.113	0.0307	1.083	4366	5.557	694.2
			1.151	0.0315	1.119	3465	5.499	557.9
608	1.000	4	1.1338	0.0410	1.092	4208	5.573	669.1
			1.092	0.0393	1.052	8421	5.834	1271.6
			1.087	0.0390	1.047	10661	5.932	1577.8
			1.092	0.0390	1.052	5074	5.580	801.7
			1.189	0.0420	1.147	3451	5.471	552.2
			1.117	0.040	1.077	6105	5.471	940.2
			1.097	0.0392	1.056	7540	5.783	1146.0
			1.107	0.0400	1.067	6888	5.755	1053.9
632	0.500	3	1.194	0.115	1.079	5499	5.912	813.8
			1.206	0.115	1.091	4716	5.848	707.4
			1.2116	0.1155	1.095	4325	5.814	657.4
			1.220	0.116	1.103	3959	5.770	601.7
			1.233	0.117	1.116	3540	5.729	545.2
			1.242	0.120	1.122	3137	5.675	489.4
			1.260	0.123	1.137	2553	5.604	403.4
			1.288	0.126	1.162	2131	5.545	341.0
			1.301	0.131	1.170	1762	5.483	285.0

TABLE 1d - Continued

Run No.	Diameter (inches)	No.of Wires	$C_{D_{total}}$	$C_{D_{tare}}$	$C_{D_{net}}$	Re_{∞}	Mach No.	Re_2
619	0.500	4	1.219	0.153	1.066	5569	5.887	829.8
			1.228	0.154	1.073	4798	5.823	724.5
			1.234	0.154	1.080	3811	5.788	579.3
			1.246	0.155	1.091	4037	5.757	617.7
			1.256	0.156	1.100	3587	5.712	553.0
			1.267	0.1606	1.106	3182	5.666	496.4
			1.295	0.164	1.131	2600	5.608	410.8
			1.307	0.168	1.138	2172.5	5.540	347.5
			1.328	0.175	1.153	1766.5	5.486	286.1
			1.212	0.153	1.058	5572	5.887	830.2
			1.244	0.154	1.090	4035	5.753	617.4

TABLE 2 - TABULATED VALUES OF TIME, DISTANCE,
AND VELOCITY (MOVING MODEL TESTS)

All tables are given in the following order:

Time	Distance	Velocity
$(C\Delta t)$	$S_{ref} - S_{mod}$ (Inches)	$\dfrac{d(S_{ref} - S_{mod})}{c(C\Delta t)}$

RUN No. 2-2-A

0.1000E 01	0.1600E-01	0.9559E-03
0.7990E 01	0.2330E-01	0.1037E-02
0.1498E 02	0.3060E-01	0.1118E-02
0.2197E 02	0.3870E-01	0.1198E-02
0.3293E 02	0.5250E-01	0.1327E-02
0.3990E 02	0.6200E-01	0.1417E-02
0.4686E 02	0.7220E-01	0.1497E-02
0.5481E 02	0.8450E-01	0.1598E-02
0.6176E 02	0.9610E-01	0.1669E-02
0.6870E 02	0.1076E-00	0.1744E-02
0.7662E 02	0.1224E-00	0.1830E-02
0.8355E 02	0.1345E-00	0.1902E-02
0.9045E 02	0.1483E-00	0.1987E-02
0.9738E 02	0.1623E-00	0.2065E-02
0.1053E 03	0.1788E-00	0.2165E-02
0.1122E 03	0.1944E-00	0.2241E-02
0.1191E 03	0.2100E-00	0.2316E-02
0.1269E 03	0.2285E-00	0.2402E-02

RUN No. 2-2-B

0.1000E 01	0.3400E-02	0.8865E-03
0.7990E 01	1.0000E-02	0.9449E-03
0.1498E 02	0.1690E-01	0.1003E-02
0.2197E 02	0.2390E-01	0.1062E-02
0.3293E 02	0.3600E-01	0.1147E-02
0.3990E 02	0.4420E-01	0.1215E-02
0.4686E 02	0.5310E-01	0.1282E-02
0.5481E 02	0.6300E-01	0.1356E-02
0.6176E 02	0.7320E-01	0.1399E-02
0.6870E 02	0.8320E-01	0.1457E-02
0.7662E 02	0.9520E-01	0.1523E-02
0.8355E 02	0.1047E-00	0.1570E-02
0.9045E 02	0.1167E-00	0.1623E-02
0.9738E 02	0.1281E-00	0.1676E-02
0.1053E 03	0.1416E-00	0.1734E-02
0.1122E 03	0.1536E-00	0.1817E-02
0.1191E 03	0.1660E-00	0.1776E-02
0.1269E 03	0.1802E-00	0.1855E-02
0.1338E 03	0.1968E-00	0.1916E-02
0.1486E 03	0.2147E-00	0.2046E-02
0.1554E 03	0.2411E-00	0.2107E-02

RUN No. 2-2-C

0.1498E 02	0.3200E-02	0.7792E-03
0.2197E 02	0.8600E-02	0.8506E-03
0.3293E 02	0.1910E-01	0.9626E-03
0.3990E 02	0.2550E-01	0.1034E-02
0.4686E 02	0.3320E-01	0.1107E-02
0.5481E 02	0.4220E-01	0.1188E-02
0.6176E 02	0.5080E-01	0.1257E-02
0.6870E 02	0.5980E-01	0.1328E-02
0.7662E 02	0.7080E-01	0.1404E-02
0.8355E 02	0.8020E-01	0.1465E-02
0.9045E 02	0.9120E-01	0.1527E-02
0.9738E 02	0.1017E-00	0.1592E-02
0.1053E 03	0.1145E-00	0.1686E-02
0.1191E 03	0.1383E-00	0.1849E-02
0.1269E 03	0.1531E-00	0.1912E-02
0.1338E 03	0.1686E-00	0.2008E-02
0.1407E 03	0.1812E-00	0.2063E-02
0.1486E 03	0.1967E-00	0.2109E-02
0.1554E 03	0.2137E-00	0.2149E-02
0.1623E 03	0.2270E-00	0.2189E-02

88.

RUN No. 2-3-A

0.1000E 01	0.9750E 00	0.3157E-03
0.1200E 02	0.9810E 00	0.4857E-03
0.2994E 02	0.9926E 00	0.7144E-03
0.3690E 02	0.9986E 00	0.8045E-03
0.4788E 02	0.1001E 01	0.9202E-03
0.5876E 02	0.1019E 01	0.1027E-02
0.6967E 02	0.1030E 01	0.1147E-02
0.8055E 02	0.1042E 01	0.1240E-02
0.9141E 02	0.1056E 01	0.1264E-02
0.9836E 02	0.1065E 01	0.1314E-02
0.1091E 03	0.1079E 01	0.1388E-02
0.1160E 03	0.1089E 01	0.1436E-02
0.1269E 03	0.1105E 01	0.1512E-02
0.1376E 03	0.1122E 01	0.1595E-02
0.1484E 03	0.1139E 01	0.1677E-02
0.1563E 03	0.1153E 01	0.1740E-02
0.1607E 03	0.1172E 01	0.1823E-02

RUN No. 2-3-B

0.2994E 02	0.9814E 00	0.2083E-03
0.3690E 02	0.9831E 00	0.2286E-03
0.4788E 02	0.9856E 00	0.2603E-03
0.5876E 02	0.9889E 00	0.2922E-03
0.6967E 02	0.9921E 00	0.3192E-03
0.8055E 02	0.9954E 00	0.3450E-03
0.9141E 02	0.1000E 01	0.3707E-03
0.9836E 02	0.1002E 01	0.3900E-03
0.1091E 03	0.1006E 01	0.4124E-03
0.1160E 03	0.1009E 01	0.4233E-03
0.1269E 03	0.1014E 01	0.4602E-03
0.1376E 03	0.1019E 01	0.4894E-03
0.1484E 03	0.1025E 01	0.5195E-03
0.1563E 03	0.1029E 01	0.5425E-03
0.1670E 03	0.1035E 01	0.5764E-03
0.1798E 03	0.1041E 01	0.5983E-03
0.1855E 03	0.1046E 01	0.6096E-03
0.1964E 03	0.1053E 01	0.6431E-03
0.2031E 03	0.1057E 01	0.6597E-03
0.2108E 03	0.1062E 01	0.6793E-03
0.2215E 03	0.1070E 01	0.7057E-03

RUN No. 2-3-C

0.6967E 02	0.9642E 00	0.2603E-03
0.8055E 02	0.9672E 00	0.3113E-03
0.9141E 02	0.9711E 00	0.3629E-03
0.9836E 02	0.9735E 00	0.3956E-03
0.1091E 03	0.9781E 00	0.4409E-03
0.1161E 03	0.9814E 00	0.4685E-03
0.1269E 03	0.9868E 00	0.5187E-03
0.1376E 03	0.9923E 00	0.5605E-03
0.1484E 03	0.9986E 00	0.6076E-03
0.1563E 03	0.1004E 01	0.6486E-03
0.1670E 03	0.1011E 01	0.6877E-03
0.1778E 03	0.1019E 01	0.7436E-03
0.1856E 03	0.1025E 01	0.7805E-03
0.1964E 03	0.1033E 01	0.8345E-03
0.2031E 03	0.1039E 01	0.8598E-03
0.2108E 03	0.1046E 01	0.8922E-03
0.2215E 03	0.1056E 01	0.9451E-03
0.2322E 03	0.1066E 01	0.9872E-03
0.2467E 03	0.1081E 01	0.1039E-02
0.2573E 03	0.1092E 01	0.1076E-02
0.2727E 03	0.1109E 01	0.1132E-02

RUN No. 2-4-A

0.9999E 01	0.9950E 00	0.5094E-03
0.7992E 01	0.9987E 00	0.5443E-03
0.1497E 02	0.1002E 01	0.5796E-03
0.2294E 02	0.1007E 01	0.6186E-03
0.2990E 02	0.1012E 01	0.6552E-03
0.3685E 02	0.1017E 01	0.6981E-03
0.4378E 02	0.1021E 01	0.7470E-03
0.5071E 02	0.1026E 01	0.7843E-03
0.5861E 02	0.1033E 01	0.8256E-03
0.6550E 02	0.1040E 01	0.8719E-03
0.7241E 02	0.1045E 01	0.9041E-03
0.7929E 02	0.1051E 01	0.9351E-03
0.8713E 02	0.1059E 01	0.9756E-03
0.9399E 02	0.1066E 01	0.1029E-02
0.1008E 03	0.1073E 01	0.1054E-02
0.1086E 03	0.1081E 01	0.1085E-02
0.1154E 03	0.1089E 01	0.1119E-02
0.1222E 03	0.1097E 01	0.1157E-02
0.1300E 03	0.1106E 01	0.1202E-02
0.1368E 03	0.1114E 01	0.1237E-02
0.1436E 03	0.1123E 01	0.1304E-02
0.1513E 03	0.1133E 01	0.1353E-02
0.1619E 03	0.1147E 01	0.1401E-02
0.1725E 03	0.1165E 01	0.1429E-02
0.1830E 03	0.1178E 01	0.1454E-02
0.1936E 03	0.1194E 01	0.1479E-02

RUN No. 2-4-B

0.9999E 01	0.9910E 00	0.3687E-03
0.7992E 01	0.9943E 00	0.4183E-03
0.1497E 02	0.9971E 00	0.4679E-03
0.2294E 02	0.1000E 01	0.5249E-03
0.2990E 02	0.1005E 01	0.5654E-03
0.3685E 02	0.1009E 01	0.6127E-03
0.4378E 02	0.1013E 01	0.6559E-03
0.5071E 02	0.1018E 01	0.6714E-03
0.5861E 02	0.1023E 01	0.7119E-03
0.6550E 02	0.1029E 01	0.7494E-03
0.7241E 02	0.1034E 01	0.7818E-03
0.7929E 02	0.1039E 01	0.8190E-03
0.8713E 02	0.1046E 01	0.8637E-03
0.9399E 02	0.1052E 01	0.9026E-03
0.1008E 03	0.1058E 01	0.9329E-03
0.1086E 03	0.1066E 01	0.9663E-03
0.1154E 03	0.1072E 01	0.9904E-03
0.1222E 03	0.1079E 01	0.1033E-02
0.1300E 03	0.1087E 01	0.1073E-02
0.1368E 03	0.1095E 01	0.1108E-02
0.1436E 03	0.1103E 01	0.1147E-02
0.1513E 03	0.1111E 01	0.1187E-02
0.1619E 03	0.1124E 01	0.1233E-02
0.1725E 03	0.1138E 01	0.1279E-02
0.1830E 03	0.1152E 01	0.1325E-02
0.1936E 03	0.1166E 01	0.1370E-02

RUN No. 2-4-C

0.9999E 01	0.9873E 00	0.3447E-03
0.7992E 01	0.9899E 00	0.3761E-03
0.1497E 02	0.9925E 00	0.4076E-03
0.2294E 02	0.9958E 00	0.4437E-03
0.2990E 02	0.9991E 00	0.4750E-03
0.3685E 02	0.1003E 01	0.5182E-03
0.4378E 02	0.1006E 01	0.4930E-03
0.5071E 02	0.1010E 01	0.5681E-03
0.5861E 02	0.1015E 01	0.5979E-03
0.6550E 02	0.1019E 01	0.6409E-03
0.7241E 02	0.1023E 01	0.6672E-03
0.7929E 02	0.1028E 01	0.6952E-03
0.8713E 02	0.1034E 01	0.7287E-03
0.9390E 02	0.1039E 01	0.7605E-03
0.1008E 03	0.1044E 01	0.7866E-03
0.1086E 03	0.1050E 01	0.8116E-03
0.1154E 03	0.1056E 01	0.8479E-03
0.1222E 03	0.1062E 01	0.8832E-03
0.1300E 03	0.1069E 01	0.9145E-03
0.1368E 03	0.1075E 01	0.9568E-03
0.1436E 03	0.1082E 01	0.9871E-03
0.1513E 03	0.1089E 01	0.1021E-02
0.1619E 03	0.1101E 01	0.1052E-02
0.1725E 03	0.1112E 01	0.1084E-02
0.1830E 03	0.1123E 01	0.1117E-02
0.1936E 03	0.1136E 01	0.1141E-02

RUN No. 2-5-A

0.1000E 01	0.9816E 00	0.3992E-03
0.7990E 01	0.9845E 00	0.4266E-03
0.1498E 02	0.9873E 00	0.4540E-03
0.2593E 02	0.9928E 00	0.4970E-03
0.3289E 02	0.9964E 00	0.5274E-03
0.3984E 02	0.1000E 01	0.5605E-03
0.4678E 02	0.1004E 01	0.5888E-03
0.5371E 02	0.1008E 01	0.6216E-03
0.6063E 02	0.1013E 01	0.6591E-03
0.6754E 02	0.1017E 01	0.6927E-03
0.7838E 02	0.1025E 01	0.7450E-03
0.8919E 02	0.1033E 01	0.7921E-03
0.9606E 02	0.1039E 01	0.8245E-03
0.1039E 03	0.1046E 01	0.8533E-03
0.1107E 03	0.1051E 01	0.8824E-03
0.1176E 03	0.1058E 01	0.9127E-03
0.1244E 03	0.1064E 01	0.9406E-03
0.1322E 03	0.1071E 01	0.9848E-03
0.1497E 03	0.1089E 01	0.1065E-02
0.1565E 03	0.1097E 01	0.1099E-02
0.1642E 03	0.1106E 01	0.1153E-02
0.1710E 03	0.1113E 01	0.1168E-02
0.1777E 03	0.1121E 01	0.1188E-02
0.1854E 03	0.1131E 01	0.1211E-02
0.1922E 03	0.1138E 01	0.1232E-02

RUN No. 2-5-B

0.1000E 01	0.9773E 00	0.3639E-03
0.7990E 01	0.9797E 00	0.3897E-03
0.1498E 02	0.9829E 00	0.4154E-03
0.2593E 02	0.9875E 00	0.4558E-03
0.3289E 02	0.9906E 00	0.4808E-03
0.3984E 02	0.9942E 00	0.5064E-03
0.4678E 02	0.9978E 00	0.5399E-03
0.5371E 02	0.1001E 01	0.5697E-03
0.6063E 02	0.1006E 01	0.6006E-03
0.6754E 02	0.1010E 01	0.6362E-03
0.7838E 02	0.1017E 01	0.6884E-03
0.8919E 02	0.1025E 01	0.7267E-03
0.9606E 02	0.1030E 01	0.7543E-03
0.1039E 03	0.1036E 01	0.7836E-03
0.1107E 03	0.1041E 01	0.8097E-03
0.1176E 03	0.1047E 01	0.8391E-03
0.1244E 03	0.1053E 01	0.8762E-03
0.1322E 03	0.1060E 01	0.9164E-03
0.1497E 03	0.1077E 01	0.9882E-03
0.1565E 03	0.1083E 01	0.1010E-02
0.1642E 03	0.1092E 01	0.1069E-02
0.1710E 03	0.1098E 01	0.1080E-02
0.1777E 03	0.1106E 01	0.1106E-02
0.1854E 03	0.1116E 01	0.1135E-02
0.1922E 03	0.1122E 01	0.1160E-02

RUN No. 2-5-C

0.1000E 01	0.9744E 00	0.3416E-03
0.7990E 01	0.9766E 00	0.3597E-03
0.1498E 02	0.9790E 00	0.3779E-03
0.2593E 02	0.9835E 00	0.4062E-03
0.3289E 02	0.9866E 00	0.4376E-03
0.3984E 02	0.9898E 00	0.4740E-03
0.4678E 02	0.9923E 00	0.5018E-03
0.5371E 02	0.9965E 00	0.5349E-03
0.6063E 02	0.1001E 01	0.5735E-03
0.6754E 02	0.1004E 01	0.6170E-03
0.7838E 02	0.1011E 01	0.6497E-03
0.8919E 02	0.1019E 01	0.6908E-03
0.9606E 02	0.1024E 01	0.7199E-03
0.1039E 03	0.1029E 01	0.7533E-03
0.1107E 03	0.1034E 01	0.7802E-03
0.1176E 03	0.1040E 01	0.8124E-03
0.1322E 03	0.1052E 01	0.8846E-03
0.1497E 03	0.1068E 01	0.9588E-03
0.1565E 03	0.1075E 01	0.9885E-03
0.1642E 03	0.1083E 01	0.1040E-02
0.1710E 03	0.1090E 01	0.1056E-02
0.1777E 03	0.1097E 01	0.1083E-02
0.1854E 03	0.1106E 01	0.1114E-02
0.1922E 03	0.1113E 01	0.1141E-02

RUN No. 2-5-E

0.1000E 01	0.9722E 00	0.1625E-03
0.7990E 01	0.9733E 00	0.1734E-03
0.1498E 02	0.9747E 00	0.1844E-03
0.2593E 02	0.9768E 00	0.2015E-03
0.3289E 02	0.9784E 00	0.2167E-03
0.4678E 02	0.9807E 00	0.2568E-03
0.5371E 02	0.9833E 00	0.2791E-03
0.6063E 02	0.9852E 00	0.2985E-03
0.6754E 02	0.9874E 00	0.3312E-03
0.7838E 02	0.9911E 00	0.3451E-03
0.8919E 02	0.9949E 00	0.3664E-03
0.9606E 02	0.9975E 00	0.3793E-03
0.1039E 03	0.1001E 01	0.3991E-03
0.1107E 03	0.1003E 01	0.4188E-03
0.1176E 03	0.1006E 01	0.4395E-03
0.1244E 03	0.1009E 01	0.4614E-03
0.1322E 03	0.1013E 01	0.4894E-03
0.1497E 03	0.1022E 01	0.5303E-03
0.1565E 03	0.1026E 01	0.5538E-03
0.1642E 03	0.1030E 01	0.5819E-03
0.1710E 03	0.1034E 01	0.5875E-03
0.1777E 03	0.1038E 01	0.6014E-03
0.1854E 03	0.1043E 01	0.6172E-03
0.1922E 03	0.1047E 01	0.6310E-03

RUN No. 2-6-A

0.1000E 01	0.1780E-01	0.3050E-03
0.9000E 01	0.2010E-01	0.3360E-03
0.1994E 02	0.2420E-01	0.3783E-03
0.3490E 02	0.3040E-01	0.4362E-03
0.4680E 02	0.3560E-01	0.4855E-03
0.5773E 02	0.4130E-01	0.5240E-03
0.6567E 02	0.4550E-01	0.5499E-03
0.7654E 02	0.5200E-01	0.5694E-03
0.8443E 02	0.5650E-01	0.6012E-03
0.9626E 02	0.6390E-01	0.6552E-03
0.1071E 03	0.6940E-01	0.7181E-03
0.1149E 03	0.7700E-01	0.7540E-03
0.1257E 03	0.8540E-01	0.8127E-03
0.1372E 03	0.9570E-01	0.8695E-03
0.1490E 03	0.1050E-00	0.8374E-03
0.1626E 03	0.1179E-00	0.8980E-03
0.1742E 03	0.1289E-00	0.9658E-03
0.1820E 03	0.1306E-00	0.1006E-02
0.1926E 03	0.1474E-00	0.1085E-02
0.2004E 03	0.1552E-00	0.1143E-02
0.2119E 03	0.1679E-00	0.1229E-02

RUN No. 2-6-B

0.3490E 02	0.3910E-01	0.4552E-03
0.4680E 02	0.4470E-01	0.5058E-03
0.5773E 02	0.5070E-01	0.5522E-03
0.6567E 02	0.5510E-01	0.5859E-03
0.7654E 02	0.6160E-01	0.6123E-03
0.8443E 02	0.6690E-01	0.6481E-03
0.9626E 02	0.7500E-01	0.7086E-03
0.1071E 03	0.8110E-01	0.7707E-03
0.1149E 03	0.8890E-01	0.8083E-03
0.1257E 03	0.9800E-01	0.8747E-03
0.1372E 03	0.1086E-00	0.9440E-03
0.1490E 03	0.1193E-00	0.9785E-03
0.1626E 03	0.1337E-00	0.1036E-02
0.1742E 03	0.1458E-00	0.1081E-02
0.1820E 03	0.1542E-00	0.1112E-02
0.1926E 03	0.1664E-00	0.1147E-02
0.2004E 03	0.1753E-00	0.1138E-02
0.2119E 03	0.1892E-00	0.1115E-02
0.2197E 03	0.1987E-00	0.1099E-02
0.2274E 03	0.2047E-00	0.1084E-02

RUN No. 2-6-C

0.3490E 02	0.3200E-01	0.3927E-03
0.4680E 02	0.3670E-01	0.4563E-03
0.5773E 02	0.4240E-01	0.5147E-03
0.6567E 02	0.4640E-01	0.5571E-03
0.7654E 02	0.5300E-01	0.5985E-03
0.8443E 02	0.5790E-01	0.6430E-03
0.9626E 02	0.6600E-01	0.7091E-03
0.1071E 03	0.7240E-01	0.7772E-03
0.1149E 03	0.8050E-01	0.8230E-03
0.1257E 03	0.8910E-01	0.8955E-03
0.1372E 03	0.1003E-00	0.9706E-03
0.1490E 03	0.1114E-00	0.1020E-02
0.1626E 03	0.1265E-00	0.1092E-02
0.1742E 03	0.1391E-00	0.1137E-02
0.1820E 03	0.1485E-00	0.1169E-02
0.1926E 03	0.1611E-00	0.1204E-02
0.2004E 03	0.1702E-00	0.1275E-02
0.2119E 03	0.1849E-00	0.1378E-02
0.2197E 03	0.1948E-00	0.1447E-02
0.2274E 03	0.2088E-00	0.1516E-02

RUN No. 2-7-A

0.1000E 01	0.1011E 01	0.7359F-03
0.7990E 01	0.1017E 01	0.7896E-03
0.1498E 02	0.1022E 01	0.8432E-03
0.2296E 02	0.1029E 01	0.9045E-03
0.2992E 02	0.1036E 01	0.9586E-03
0.3689E 02	0.1043E 01	0.1017E-02
0.4384E 02	0.1050E 01	0.1068E-02
0.5078E 02	0.1058E 01	0.1125E-02
0.5870E 02	0.1067E 01	0.1198F-02
0.6564E 02	0.1075E 01	0.1256E-02
0.7256E 02	0.1084E 01	0.1302E-02
0.7947E 02	0.1094E 01	0.1358E-02
0.8736E 02	0.1104E 01	0.1416E-02
0.9425E 02	0.1114E 01	0.1465E-02
0.1011E 03	0.1125E 01	0.1557E-02
0.1080E 03	0.1135E 01	0.1601E-02
0.1159E 03	0.1148E 01	0.1645E-02
0.1227E 03	0.1162E 01	0.1676E-02
0.1296E 03	0.1171E 01	0.1713E-02
0.1374E 03	0.1185E 01	0.1753E-02
0.1442E 03	0.1197E 01	0.1796E-02
0.1511E 03	0.1210E 01	0.1840E-02
0.1588E 03	0.1224E 01	0.1890E-02

RUN No. 2-7-B

0.1000E 01	0.9849E 00	0.6101E-03
0.7990E 01	0.9894E 00	0.6682E-03
0.1498E 02	0.9941E 00	0.7262E-03
0.2296E 02	0.1000E 01	0.7925E-03
0.2992E 02	0.1006E 01	0.8467E-03
0.3689E 02	0.1012E 01	0.9010E-03
0.4384E 02	0.1019E 01	0.9560E-03
0.5078E 02	0.1025E 01	0.1011E-02
0.5870E 02	0.1033E 01	0.1086E-02
0.6564E 02	0.1041E 01	0.1146F-02
0.7256E 02	0.1049E 01	0.1205E-02
0.7947E 02	0.1058E 01	0.1267E-02
0.8736E 02	0.1068E 01	0.1331E-02
0.9425E 02	0.1077E 01	0.1389E-02
0.1011E 03	0.1088E 01	0.1446E-02
0.1080E 03	0.1098E 01	0.1502E-02
0.1159E 03	0.1110E 01	0.1557E-02
0.1227E 03	0.1121E 01	0.1613E-02
0.1296E 03	0.1132E 01	0.1668E-02
0.1374E 03	0.1145E 01	0.1733E-02
0.1442E 03	0.1157E 01	0.1793E-02
0.1511E 03	0.1169E 01	0.1855F-02
0.1588E 03	0.1184E 01	0.1926F-02
0.1657E 03	0.1197E 01	0.1989F-02

RUN No. 2-7-C

0.2992E 02	0.9840E 00	0.3460E-03
0.4384E 02	0.9895E 00	0.4230E-03
0.5078E 02	0.9926E 00	0.4614E-03
0.5870E 02	0.9961E 00	0.5052E-03
0.6564E 02	0.9999E 00	0.5431E-03
0.7256E 02	0.1004E 01	0.5774E-03
0.7947E 02	0.1008E 01	0.6157E-03
0.8736E 02	0.1013E 01	0.6482E-03
0.9425E 02	0.1017E 01	0.6864E-03
0.1011E 03	0.1022E 01	0.7192F-03
0.1080E 03	0.1027E 01	0.7652E-03
0.1159E 03	0.1034E 01	0.7949E-03
0.1227E 03	0.1039E 01	0.8222E-03
0.1296E 03	0.1046E 01	0.8500E-03
0.1374E 03	0.1051E 01	0.8841E-03
0.1442E 03	0.1058E 01	0.8989E-03
0.1511E 03	0.1064E 01	0.9409E-03
0.1588E 03	0.1072E 01	0.1003E-02
0.1657E 03	0.1077E 01	0.1038E-02
0.1763E 03	0.1091E 01	0.1103E-02
0.1841E 03	0.1099E 01	0.1147E-02
0.1946E 03	0.1111E 01	0.1203E-02
0.2052E 03	0.1124E 01	0.1234E-02
0.2158E 03	0.1137E 01	0.1265E-02
0.2264E 03	0.1151E 01	0.1297E-02

RUN No. 2-8-A

0.1000E 01	0.9842E 00	0.8571E-03
0.7995E 01	0.9904E 00	0.9089E-03
0.1498E 02	0.9970E 00	0.9607E-03
0.2495E 02	0.1007E 01	0.1035E-02
0.3291E 02	0.1016E 01	0.1100E-02
0.3987E 02	0.1023E 01	0.1154E-02
0.4781E 02	0.1033E 01	0.1204E-02
0.5475E 02	0.1041E 01	0.1255E-02
0.6168E 02	0.1050E 01	0.1320E-02
0.6861E 02	0.1059E 01	0.1362E-02
0.7651E 02	0.1070E 01	0.1433E-02
0.8342E 02	0.1081E 01	0.1494E-02
0.9032E 02	0.1091E 01	0.1548E-02
0.9820E 02	0.1104E 01	0.1593E-02
0.1051E 03	0.1115E 01	0.1639E-02
0.1119E 03	0.1126E 01	0.1676E-02
0.1198E 03	0.1139E 01	0.1729E-02
0.1267E 03	0.1152E 01	0.1796E-02
0.1345E 03	0.1165E 01	0.1876E-02
0.1413E 03	0.1179E 01	0.1946E-02
0.1481E 03	0.1192E 01	0.2016E-02

RUN No. 2-8-B

0.1498E 02	0.9578E 00	0.5440E-03
0.2495E 02	0.9631E 00	0.7188E-03
0.3291E 02	0.9699E 00	0.8583E-03
0.3987E 02	0.9767E 00	0.9804E-03
0.4781E 02	0.9851E 00	0.1098E-02
0.5475E 02	0.9929E 00	0.1177E-02
0.6168E 02	0.1002E 01	0.1255E-02
0.6861E 02	0.1010E 01	0.1327E-02
0.7651E 02	0.1021E 01	0.1404E-02
0.8342E 02	0.1031E 01	0.1480E-02
0.9032E 02	0.1042E 01	0.1562E-02
0.9820E 02	0.1054E 01	0.1650E-02
0.1051E 03	0.1066E 01	0.1721E-02
0.1119E 03	0.1078E 01	0.1796E-02
0.1198E 03	0.1093E 01	0.1881E-02
0.1267E 03	0.1105E 01	0.1952E-02
0.1345E 03	0.1121E 01	0.2037E-02
0.1413E 03	0.1135E 01	0.2111E-02
0.1481E 03	0.1150E 01	0.2190E-02
0.1559E 03	0.1167E 01	0.2280E-02
0.1628E 03	0.1183E 01	0.2358E-02

RUN No. 2-8-C

0.6168E 02	0.9454E 00	0.6744E-03
0.6861E 02	0.9498E 00	0.7539E-03
0.7651E 02	0.9565E 00	0.8445E-03
0.8342E 02	0.9620E 00	0.9238E-03
0.9032E 02	0.9695E 00	0.1000E-02
0.9820E 02	0.9780E 00	0.1079E-02
0.1051E 03	0.9848E 00	0.1144E-02
0.1119E 03	0.9930E 00	0.1195E-02
0.1198E 03	0.1003E 01	0.1277E-02
0.1267E 03	0.1012E 01	0.1356E-02
0.1345E 03	0.1022E 01	0.1439E-02
0.1413E 03	0.1033E 01	0.1511E-02
0.1481E 03	0.1043E 01	0.1578E-02
0.1559E 03	0.1056E 01	0.1649E-02
0.1628E 03	0.1068E 01	0.1708E-02
0.1705E 03	0.1081E 01	0.1782E-02
0.1773E 03	0.1093E 01	0.1842E-02
0.1851E 03	0.1108E 01	0.1922E-02
0.1957E 03	0.1129E 01	0.2032E-02
0.2025E 03	0.1143E 01	0.2093E-02
0.2131E 03	0.1166E 01	0.2190E-02
0.2208E 03	0.1183E 01	0.2260E-02

RUN No. 14-1-A

0.1000E 01	0.9117E 00	0.1353E-02
0.8000E 01	0.9216E 00	0.1417E-02
0.1498E 02	0.9308E 00	0.1482E-02
0.2295E 02	0.9432E 00	0.1557E-02
0.2894E 02	0.9534E 00	0.1643E-02
0.3639E 02	0.9669E 00	0.1793E-02
0.4390E 02	0.9776E 00	0.1911E-02
0.5080E 02	0.9925E 00	0.2030E-02
0.5770E 02	0.1008E 01	0.2154E-02
0.6470E 02	0.1023E 01	0.2276E-02
0.7160E 02	0.1039E 01	0.2370E-02
0.7950E 02	0.1058E 01	0.2436E-02
0.8640E 02	0.1075E 01	0.2543E-02
0.9330E 02	0.1093E 01	0.2636E-02
0.1002E 03	0.1111E 01	0.2726E-02
0.1080E 03	0.1134E 01	0.2830E-02
0.1149E 03	0.1153E 01	0.2920E-02
0.1218E 03	0.1173E 01	0.3011E-02

RUN No. 14-1-B

0.1000E 01	0.9049E 00	0.1001E-02
0.8000E 01	0.9133E 00	0.1060E-02
0.1498E 02	0.9199E 00	0.1119E-02
0.2295E 02	0.9294E 00	0.1188E-02
0.2894E 02	0.9362E 00	0.1231E-02
0.3689E 02	0.9469E 00	0.1325E-02
0.4390E 02	0.9561E 00	0.1387E-02
0.5080E 02	0.9658E 00	0.1452E-02
0.5770E 02	0.9766E 00	0.1507E-02
0.6470E 02	0.9870E 00	0.1570E-02
0.7160E 02	0.9980E 00	0.1624E-02
0.7950E 02	0.1011E 01	0.1677E-02

RUN No. 14-1-C

0.1000E 01	0.8659E 00	0.5085E-03	0.8000E 01	0.8594E 00	0.3860E-03
0.8000E 01	0.8699E 00	0.5611E-03	0.1498E 02	0.8615E 00	0.4287E-03
0.1498E 02	0.8739E 00	0.6138E-03	0.2295E 02	0.8658E 00	0.4780E-03
0.2295E 02	0.8791E 00	0.6179E-03	0.2894E 02	0.8685E 00	0.5147E-03
0.2894E 02	0.8829E 00	0.7240E-03	0.3689E 02	0.8730E 00	0.5737E-03
0.3689E 02	0.8892E 00	0.8064E-03	0.4390E 02	0.8770E 00	0.6126E-03
0.4390E 02	0.8948E 00	0.8693E-03	0.5080E 02	0.8812E 00	0.6490E-03
0.5080E 02	0.9012E 00	0.9397E-03	0.5770E 02	0.8863E 00	0.6846E-03
0.5770E 02	0.9084E 00	0.9964E-03	0.6470E 02	0.8913E 00	0.7296E-03
0.6470E 02	0.9150E 00	0.1058E-02	0.7160E 02	0.8958E 00	0.7630E-03
0.7160E 02	0.9228E 00	0.1112E-02	0.7950E 02	0.9022E 00	0.8051E-03
0.7950E 02	0.9316E 00	0.1177E-02	0.8640E 02	0.9084E 00	0.8518E-03
0.8640E 02	0.9401E 00	0.1251E-02	0.9330E 02	0.9138E 00	0.8928E-03
0.9330E 02	0.9489E 00	0.1309E-02	0.1002E 03	0.9204E 00	0.9212E-03
0.1002E 03	0.9580E 00	0.1361E-02	0.1080E 03	0.9281E 00	0.9656E-03
0.1080E 03	0.9696E 00	0.1430E-02	0.1149E 03	0.9344E 00	0.1007E-02
0.1149E 03	0.9793E 00	0.1490E-02	0.1218E 03	0.9413E 00	0.1039E-02
0.1218E 03	0.9890E 00	0.1547E-02	0.1287E 03	0.9491E 00	0.1087E-02
0.1287E 03	0.1001E 01	0.1621E-02	0.1356E 03	0.9564E 00	0.1031E-02
0.1360E 03	0.1012E 01	0.1675E-02	0.1133E 03	0.9653E 00	0.1141E-02
0.1433E 03	0.1025E 01	0.1728E-02	0.1502E 03	0.9741E 00	0.1167E-02
0.1502E 03	0.1038E 01	0.1766E-02	0.1609E 03	0.9855E 00	0.1204E-02
0.1609E 03	0.1056E 01	0.1830E-02	0.1678E 03	0.9939E 00	0.1231E-02
0.1678E 03	0.1068E 01	0.1866E-02	0.1785E 03	0.1008E 01	0.1283E-02
0.1785E 03	0.1090E 01	0.1955E-02	0.1901E 03	0.1022E 01	0.1421E-02
0.1901E 03	0.1112E 01	0.2093E-02	0.2086E 03	0.1049E 01	0.1718E-02
0.1979E 03	0.1128E 01	0.2172E-02	0.2153E 03	0.1060E 01	0.1828E-02
0.2086E 03	0.1153E 01	0.2299E-02	0.2259E 03	0.1085E 01	0.2011E-02
0.2153E 03	0.1169E 01	0.2380E-02			
0.2258E 03	0.1194E 01	0.2506E-02			

RUN No. 14-2-B

0.8000E 01	0.8629E 00	0.4200E-03
0.1500E 02	0.8658E 00	0.4614E-03
0.2294E 02	0.8702E 00	0.5090E-03
0.2991E 02	0.8732E 00	0.5505E-03
0.3686E 02	0.8776E 00	0.6010E-03
0.4380E 02	0.8817E 00	0.6494E-03
0.5173E 02	0.8870E 00	0.7213E-03
0.5860E 02	0.8924E 00	0.9643E-03
0.6556E 02	0.8979E 00	0.9643E-03
0.6556E 02	0.8979E 00	0.8254E-03
0.7640E 02	0.9075E 00	0.9201E-03
0.8329E 02	0.9131E 00	0.9723E-03
0.9115E 02	0.9217E 00	0.1038E-02
0.1019E 03	0.9338E 00	0.1130E-02
0.1088E 03	0.9412E 00	0.1101E-02
0.1164E 03	0.9508E 00	0.1190E-02
0.1234E 03	0.9596E 00	0.1265E-02
0.1302E 03	0.9635E 00	0.1344E-02
0.1380E 03	0.9791E 00	0.1436E-02
0.1448E 03	0.9890E 00	0.1516E-02
0.1526E 03	0.1001E 01	0.1625E-02
0.1632E 03	0.1018E 01	0.1614E-02
0.1738E 03	0.1035E 01	0.1689E-02
0.1845E 03	0.1053E 01	0.1770E-02
0.1950E 03	0.1072E 01	0.1857E-02
0.2055E 03	0.1093E 01	0.1942E-02
0.2170E 03	0.1116E 01	0.2034E-02

RUN No. 14-2-C

0.1000E 01	0.8567E 00	0.4902E-03
0.8000E 01	0.8608E 00	0.5126E-03
0.2229E 02	0.8686E 00	0.5606E-03
0.2991E 02	0.8720E 00	0.5827E-03
0.3686E 02	0.8768E 00	0.6199E-03
0.4380E 02	0.8808E 00	0.6599E-03
0.5173E 02	0.8860E 00	0.7090E-03
0.5860E 02	0.8915E 00	0.7434E-03
0.6556E 02	0.8968E 00	0.7865E-03
0.7640E 02	0.9055E 00	0.8417E-03
0.8329E 02	0.9115E 00	0.8696E-03
0.9115E 02	0.9182E 00	0.9140E-03
0.1019E 03	0.9287E 00	0.8665E-03
0.1088E 03	0.9352E 00	0.1015E-02
0.1164E 03	0.9436E 00	0.1054E-02
0.1234E 03	0.9508E 00	0.1085E-02
0.1302E 03	0.9585E 00	0.1124E-02
0.1380E 03	0.9672E 00	0.1161E-02
0.1448E 03	0.9751E 00	0.1198E-02
0.1526E 03	0.9849E 00	0.1243E-02
0.1632E 03	0.9983E 00	0.1304E-02
0.1738E 03	0.1013E 01	0.1360E-02
0.1845E 03	0.1027E 01	0.1414E-02
0.1950E 03	0.1042E 01	0.1471E-02
0.2055E 03	0.1059E 01	0.1527E-02
0.2170E 03	0.1076E 01	0.1589E-02

96.

RUN No. 14-3-A

0.1794E 02	0.8546E 00	0.1008E-03
0.2591E 02	0.8555E 00	0.1005E-03
0.3285E 02	0.8564E 00	0.1003E-03
0.4375E 02	0.8572E 00	0.1000E-03
0.5066E 02	0.8580E 00	0.1118E-03
0.5755E 02	0.8584E 00	0.1206E-03
0.6543E 02	0.8596E 00	0.1363E-03
0.7229E 02	0.8609E 00	0.1528E-03
0.8012E 02	0.8619E 00	0.1695E-03
0.8697E 02	0.8630E 00	0.1759E-03
0.9380E 02	0.8645E 00	0.1864E-03
0.1006E 03	0.8657E 00	0.1990E-03
0.1113E 03	0.8678E 00	0.2124E-03
0.1119E 03	0.8698E 00	0.2215E-03
0.1258E 03	0.8709E 00	0.2192E-03
0.1335E 03	0.8730E 00	0.2223E-03
0.1402E 03	0.8746E 00	0.2201E-03
0.1518E 03	0.8766E 00	0.2364E-03
0.1595E 03	0.8786E 00	0.2524E-03
0.1661E 03	0.8802E 00	0.2657E-03
0.1737E 03	0.8826E 00	0.2947E-03
0.1804E 03	0.8846E 00	0.3076E-03
0.1909E 03	0.8877E 00	0.3252E-03
0.1984E 03	0.8907E 00	0.3384E-03
0.2089E 03	0.8939E 00	0.3566E-03

RUN No. 14-3-B

0.1794E 02	0.8213E 00	0.7515E-04
0.2591E 02	0.8225E 00	0.1107E-03
0.3285E 02	0.8230E 00	0.1419E-03
0.4375E 02	0.8248E 00	0.1913E-03
0.5066E 02	0.8264E 00	0.2308E-03
0.5755E 02	0.8302E 00	0.2757E-03
0.6543E 02	0.8328E 00	0.3225E-03
0.7229E 02	0.8358E 00	0.3686E-03
0.8012E 02	0.8387E 00	0.4184E-03
0.8697E 02	0.8422E 00	0.4629E-03
0.9380E 02	0.8455E 00	0.5051E-03
0.1006E 03	0.8520E 00	0.5486E-03
0.1113E 03	0.8570E 00	0.6160E-03
0.1190E 03	0.8613E 00	0.6661E-03
0.1258E 03	0.8672E 00	0.6578E-03
0.1335E 03	0.8725E 00	0.6793E-03
0.1402E 03	0.8781E 00	0.6943E-03
0.1518E 03	0.8851E 00	0.7620E-03
0.1595E 03	0.8906E 00	0.8344E-03
0.1661E 03	0.8985E 00	0.8959E-03
0.1737E 03	0.9053E 00	0.9993E-03
0.1804E 03	0.9165E 00	0.1047E-03
0.1909E 03	0.9253E 00	0.1123E-02
0.2089E 03	0.9253E 00	0.1180E-02

RUN No. 14-3-C

0.1794E 02	0.8567E 00	0.2923E-03
0.2591E 02	0.8596E 00	0.3633E-03
0.3285E 02	0.8622E 00	0.3736E-03
0.4375E 02	0.8669E 00	0.4936E-03
0.5066E 02	0.8709E 00	0.5506E-03
0.5755E 02	0.8742E 00	0.6059E-03
0.6543E 02	0.8797E 00	0.6776E-03
0.7229E 02	0.8846E 00	0.7327E-03
0.8012E 02	0.8903E 00	0.7945E-03
0.8697E 02	0.8964E 00	0.8396E-03
0.9380E 02	0.9021E 00	0.9044E-03
0.1006E 03	0.9084E 00	0.9695E-03
0.1113E 03	0.9184E 00	0.1063E-02
0.1190E 03	0.9284E 00	0.1149E-02
0.1258E 03	0.9360E 00	0.1123E-02
0.1335E 03	0.9450E 00	0.1152E-02
0.1402E 03	0.9546E 00	0.1147E-02
0.1518E 03	0.9635E 00	0.1249E-02
0.1595E 03	0.9745E 00	0.1350E-02
0.1661E 03	0.9844E 00	0.1433E-02
0.1737E 03	0.9966E 00	0.1598E-02
0.1804E 03	0.1007E 01	0.1659E-02
0.1909E 03	0.1025E 01	0.1761E-02
0.1984E 03	0.1039E 01	0.1836E-02
0.2089E 03	0.1058E 01	0.1940E-02

RUN No. 14-4-A

0.1000E 01	0.8705E 00	0.3142E-03
0.9000E 01	0.8738E 00	0.3861E-03
0.1600E 02	0.8765E 00	0.4490E-03
0.2700E 02	0.8817E 00	0.5468E-03
0.3690E 02	0.8878E 00	0.6370E-03
0.4781E 02	0.8951E 00	0.7403E-03
0.5570E 02	0.9015E 00	0.8096E-03
0.6270E 02	0.9074E 00	0.8713E-03
0.6960E 02	0.9135E 00	0.9378E-03
0.7650E 02	0.9201E 00	0.9910E-03
0.8440E 02	0.9283E 00	0.1081E-02
0.9130E 02	0.9361E 00	0.1150E-02
0.9820E 02	0.9436E 00	0.1215E-02
0.1060E 03	0.9547E 00	0.1290E-02
0.1129E 03	0.9631E 00	0.1354E-02
0.1198E 03	0.9725E 00	0.1427E-02
0.1276E 03	0.9840E 00	0.1495E-02
0.1345E 03	0.9945E 00	0.1575E-02
0.1423E 03	0.1007E 01	0.1643E-02
0.1491E 03	0.1019E 01	0.1714E-02
0.1559E 03	0.1031E 01	0.1777E-02
0.1637E 03	0.1044E 01	0.1851E-02
0.1705E 03	0.1058E 01	0.1915E-02
0.1812E 03	0.1079E 01	0.2018E-02

RUN No. 14-4-C

0.1000E 01	0.8401E 00	0.7894E-05
0.9000E 01	0.8410E 00	0.1290E-04
0.1600E 02	0.8405E 00	0.3119E-04
0.2700E 02	0.8412E 00	0.5988E-04
0.3690E 02	0.8416E 00	0.8809E-04
0.4781E 02	0.8428E 00	0.1295E-03
0.5570E 02	0.8441E 00	0.1556E-03
0.6270E 02	0.8454E 00	0.1633E-03
0.6960E 02	0.8465E 00	0.1793E-03
0.7650E 02	0.8480E 00	0.1940E-03
0.8440E 02	0.8489E 00	0.2227E-03
0.9130E 02	0.8508E 00	0.2370E-03
0.9820E 02	0.8527E 00	0.2525E-03
0.1060E 03	0.8553E 00	0.2815E-03
0.1129E 03	0.8564E 00	0.2669E-03
0.1198E 03	0.8585E 00	0.2814E-03
0.1276E 03	0.8614E 00	0.3170E-03
0.1345E 03	0.8619E 00	0.3699E-03
0.1423E 03	0.8658E 00	0.3999E-03
0.1491E 03	0.8693E 00	0.4285E-03
0.1559E 03	0.8727E 00	0.4683E-03
0.1637E 03	0.8754E 00	0.4673E-03
0.1705E 03	0.8788E 00	0.4643E-03
0.1812E 03	0.8841E 00	0.4852E-03
0.1890E 03	0.8882E 00	0.5128E-03
0.1996E 03	0.8928E 00	0.5343E-03
0.2064E 03	0.8971E 00	0.5478E-03
0.2141E 03	0.9016E 00	0.5633E-03

RUN No. 14-4-D

0.7650E 02	0.8471E 00	0.2897E-03
0.8440E 02	0.8493E 00	0.3414E-03
0.9130E 02	0.8517E 00	0.3872E-03
0.9821E 02	0.8549E 00	0.4327E-03
0.1060E 03	0.8588E 00	0.4924E-03
0.1129E 03	0.8616E 00	0.5245E-03
0.1198E 03	0.8657E 00	0.5690E-03
0.1276E 03	0.8707E 00	0.6239E-03
0.1345E 03	0.9742E 00	0.6841E-03
0.1423E 03	0.8805E 00	0.7378E-03
0.1491E 03	0.8855E 00	0.7901E-03
0.1559E 03	0.8913E 00	0.8503E-03
0.1637E 03	0.8979E 00	0.8962E-03
0.1705E 03	0.9042E 00	0.9455E-03
0.1812E 03	0.9148E 00	0.1018E-02
0.1890E 03	0.9230E 00	0.1087E-02
0.1996E 03	0.9345E 00	0.1176E-02
0.2064E 03	0.9427E 00	0.1217E-02
0.2141E 03	0.9532E 00	0.1275E-02
0.2208E 03	0.9617E 00	0.1325E-02
0.2324E 03	0.9770E 00	0.1416E-02

RUN No. 14-5-A

0.1000E 01	0.8593E 00	0.1497E-03
0.8000E 01	0.8604E 00	0.2004E-03
0.1600E 02	0.8613E 00	0.2581E-03
0.2700E 02	0.8659E 00	0.3381E-03
0.3700E 02	0.8693E 00	0.3964E-03
0.4490E 02	0.8727E 00	0.4056E-03
0.5180E 02	0.8759E 00	0.4339E-03
0.5873E 02	0.8790E 00	0.5144E-03
0.6660E 02	0.8815E 00	0.4952E-03
0.7350E 02	0.8863E 00	0.5046E-03
0.8050E 02	0.8897E 00	0.5559E-03
0.8836E 02	0.8945E 00	0.5788E-03
0.1021E 03	0.9026E 00	0.6246E-03
0.1100E 03	0.9067E 00	0.6603E-03
0.1169E 03	0.9121E 00	0.7238E-03
0.1247E 03	0.9179E 00	0.7394E-03
0.1316E 03	0.9230E 00	0.7694E-03
0.1384E 03	0.9282E 00	0.7815E-03
0.1462E 03	0.9347E 00	0.7935E-03
0.1531E 03	0.9399E 00	0.8269E-03
0.1608E 03	0.9466E 00	0.8866E-03
0.1676E 03	0.9517E 00	0.9123E-03
0.1754E 03	0.9599E 00	0.9515E-03
0.1890E 03	0.9752E 00	0.9706E-03
0.1967E 03	0.9805E 00	0.9814E-03
0.2035E 03	0.9871E 00	0.8701E-03

RUN No. 14-6-A

0.1000E 01	0.8656E 00	0.3613E-03
0.7992E 01	0.8693E 00	0.4810E-03
0.1497E 02	0.8730E 00	0.6011E-03
0.2294E 02	0.8796E 00	0.7387E-03
0.2990E 02	0.8809E 00	0.8392E-03
0.3684E 02	0.8910E 00	0.9264E-03
0.4476E 02	0.8985E 00	0.9937E-03
0.5167E 02	0.9057E 00	0.1076E-02
0.5858E 02	0.9126E 00	0.1050E-02
0.6646E 02	0.9213E 00	0.1113E-02
0.7334E 02	0.9291E 00	0.1162E-02
0.8021E 02	0.9362E 00	0.1224E-02
0.8804E 02	0.9474E 00	0.1306E-02
0.9489E 02	0.9560E 00	0.1364E-02
0.1027E 03	0.9670E 00	0.1415E-02
0.1095E 03	0.9777E 00	0.1449E-02
0.1163E 03	0.9870E 00	0.1508E-02
0.1240E 03	0.9983E 00	0.1553E-02
0.1308E 03	0.1010E 01	0.1602E-02
0.1386E 03	0.1023E 01	0.1680E-02
0.1453E 03	0.1034E 01	0.1736E-02
0.1544E 03	0.1048E 01	0.1802E-02
0.1597E 03	0.1060E 01	0.1857E-02

RUN No. 14-6-B

0.1000E 01	0.8613E 00	0.2169E-03
0.7992E 01	0.8628E 00	0.2280E-03
0.1497E 02	0.8643E 00	0.2391E-03
0.2294E 02	0.8663E 00	0.2517E-03
0.2990E 02	0.8682E 00	0.2760E-03
0.3684E 02	0.8703E 00	0.3015E-03
0.4476E 02	0.8721E 00	0.3525E-03
0.5167E 02	0.8751E 00	0.3666E-03
0.5858E 02	0.8776E 00	0.3659E-03
0.6646E 02	0.8822E 00	0.3846E-03
0.7334E 02	0.8833E 00	0.3877E-03
0.8021E 02	0.8851E 00	0.4002E-03
0.8804E 02	0.8894E 00	0.4111E-03
0.9489E 02	0.8924E 00	0.4606E-03
0.1027E 03	0.8961E 00	0.4876E-03
0.1095E 03	0.8990E 00	0.4916E-03
0.1163E 03	0.9029E 00	0.5136E-03
0.1240E 03	0.9069E 00	0.5331E-03
0.1308E 03	0.9104E 00	0.5504E-03
0.1386E 03	0.9150E 00	0.5794E-03
0.1453E 03	0.9187E 00	0.6075E-03
0.1544E 03	0.9232E 00	0.6310E-03
0.1597E 03	0.9285E 00	0.6392E-03
0.1674E 03	0.9334E 00	0.6457E-03
0.1741E 03	0.9375E 00	0.6512E-03
0.1818E 03	0.9423E 00	0.6572E-03

RUN No. 14-6-C

0.1000E 01	0.8611E 00	0.2213E-03
0.7992E 01	0.8624E 00	0.2439E-03
0.1497E 02	0.8640E 00	0.2666E-03
0.2294E 02	0.8666E 00	0.2927E-03
0.2990E 02	0.8690E 00	0.3247E-03
0.3684E 02	0.8709E 00	0.3532E-03
0.4476E 02	0.8736E 00	0.3694E-03
0.5167E 02	0.8767E 00	0.3957E-03
0.5858E 02	0.8797E 00	0.4116E-03
0.6646E 02	0.8825E 00	0.4470E-03
0.7334E 02	0.8861E 00	0.4683E-03
0.8021E 02	0.8884E 00	0.4981E-03
0.8804E 02	0.8937E 00	0.5340E-03
0.9489E 02	0.8970E 00	0.5594E-03
0.1027E 03	0.9016E 00	0.5930E-03
0.1095E 03	0.9054E 00	0.5974E-03
0.1163E 03	0.9099E 00	0.6276E-03
0.1240E 03	0.9149E 00	0.6453E-03
0.1308E 03	0.9190E 00	0.6700E-03
0.1386E 03	0.9247E 00	0.7018E-03
0.1453E 03	0.9290E 00	0.7328E-03
0.1544E 03	0.9350E 00	0.7643E-03
0.1597E 03	0.9407E 00	0.7881E-03
0.1674E 03	0.9468E 00	0.8175E-03
0.1741E 03	0.9520E 00	0.8427E-03
0.1818E 03	0.9588E 00	0.8715E-03

RUN No. 14-7-A

0.1000E 01	0.8983E 00	0.1119E-02
0.8000E 01	0.9067E 00	0.1222E-02
0.1497E 02	0.9161E 00	0.1323E-02
0.2294E 02	0.9266E 00	0.1439E-02
0.2991E 02	0.9369E 00	0.1508E-02
0.3686E 02	0.9473E 00	0.1574E-02
0.4380E 02	0.9603E 00	0.1646E-02
0.5070E 02	0.9704E 00	0.1699E-02
0.5865E 02	0.9843E 00	0.1766E-02
0.6556E 02	0.9969E 00	0.1824E-02
0.7247E 02	0.1009E 01	0.1909E-02
0.7936E 02	0.1023E 01	0.1976E-02
0.8624E 02	0.1037E 01	0.2049E-02
0.9410E 02	0.1053E 01	0.2125E-02
0.1009E 03	0.1068E 01	0.2183E-02
0.1078E 03	0.1083E 01	0.2254E-02
0.1146E 03	0.1099E 01	0.2313E-02
0.1224E 03	0.1117E 01	0.2391E-02
0.1292E 03	0.1134E 01	0.2459E-02
0.1370E 03	0.1153E 01	0.2533E-02

RUN No. 14-7-B

0.1000E 01	0.8603E 00	0.4487E-03
0.8000E 01	0.8704E 00	0.5152E-03
0.1497E 02	0.9745E 00	0.5813E-03
0.2294E 02	0.8795E 00	0.6574E-03
0.2991E 02	0.8847E 00	0.7233E-03
0.3686E 02	0.8855E 00	0.7436E-03
0.4380E 02	0.8966E 00	0.8303E-03
0.5070E 02	0.9014E 00	0.9136E-03
0.5865E 02	0.9057E 00	0.1013E-02
0.6556E 02	0.9158E 00	0.1018E-02
0.7247E 02	0.9228E 00	0.1104E-02
0.7936E 02	0.9305E 00	0.1166E-02
0.8624E 02	0.9384E 00	0.1162E-02
0.9410E 02	0.9480E 00	0.1225E-02
0.1009E 03	0.9559E 00	0.1279E-02
0.1078E 03	0.9650E 00	0.1332E-02
0.1146E 03	0.9747E 00	0.1385E-02
0.1224E 03	0.9859E 00	0.1442E-02
0.1292E 03	0.9958E 00	0.1482E-02
0.1370E 03	0.1007E 01	0.1533E-02
0.1438E 03	0.1018E 01	0.1587E-02
0.1506E 03	0.1029E 01	0.1644E-02
0.1584E 03	0.1042E 01	0.1709E-02
0.1651E 03	0.1054E 01	0.1763E-02
0.1719E 03	0.1066E 01	0.1808E-02
0.1796E 03	0.1080E 01	0.1859E-02
0.1863E 03	0.1093E 01	0.1906E-02
0.1931E 03	0.1106E 01	0.1957E-02
0.2007E 03	0.1121E 01	0.2013E-02
0.2075E 03	0.1135E 01	0.2057E-02
0.2151E 03	0.1151E 01	0.2111E-02
0.2218E 03	0.1165E 01	0.2157E-02

RUN No. 14-8-A

0.1000E 01	0.9610E-01	0.1025E-02
0.8990E 01	0.1046E-00	0.1137E-02
0.1598E 02	0.1124E-00	0.1235E-02
0.2494E 02	0.1243E-00	0.1361E-02
0.2693E 02	0.1280E-00	0.1396E-02
0.3489E 02	0.1387E-00	0.1506E-02
0.4283E 02	0.1510E-00	0.1618E-02
0.4680E 02	0.1578E-00	0.1676E-02
0.5175E 02	0.1661E-00	0.1767E-02
0.5967E 02	0.1807E-00	0.1892E-02
0.6362E 02	0.1883E-00	0.1944E-02
0.6856E 02	0.1982E-00	0.2019E-02
0.7546E 02	0.2125E-00	0.2105E-02
0.8137E 02	0.2250E-00	0.2183E-02
0.8925E 02	0.2428E-00	0.2292E-02
0.9416E 02	0.2537E-00	0.2363E-02
0.1000E 03	0.2683E-00	0.2448E-02
0.1079E 03	0.2879E-00	0.2561E-02

RUN No. 14-8-B

0.1000E 01	0.5730E-01	0.3565E-03
0.8990E 01	0.6030E-01	0.4197E-03
0.1598E 02	0.6380E-01	0.4749E-03
0.2494E 02	0.6800E-01	0.5458E-03
0.2693E 02	0.6900E-01	0.5525E-03
0.3489E 02	0.7410E-01	0.5992E-03
0.4283E 02	0.7910E-01	0.6431E-03
0.4680E 02	0.8120E-01	0.6584E-03
0.5175E 02	0.8480E-01	0.6831E-03
0.5967E 02	0.9030E-01	0.7314E-03
0.6362E 02	0.9310E-01	0.7520E-03
0.6856E 02	0.9730E-01	0.7729E-03
0.7546E 02	0.1026E-00	0.8081E-03
0.8137E 02	0.1072E-00	0.8363E-03
0.8925E 02	0.1141E-00	0.8747E-03
0.9416E 02	0.1184E-00	0.9065E-03
0.1000E 03	0.1239E-00	0.9411E-03
0.1079E 03	0.1314E-00	0.9783E-03
0.1147E 03	0.1384E-00	0.1018E-02
0.1216E 03	0.1453E-00	0.1062E-02
0.1284E 03	0.1525E-00	0.1102E-02
0.1362E 03	0.1615E-00	0.1147E-02
0.1440E 03	0.1709E-00	0.1188E-02
0.1518E 03	0.1801E-00	0.1227E-02
0.1586E 03	0.1885E-00	0.1252E-02
0.1654E 03	0.1970E-00	0.1279E-02
0.1729E 03	0.2070E-00	0.1310E-02
0.1818E 03	0.2187E-00	0.1346E-02

RUN No. 14-8-C

0.3489E 02	0.5960E-01	0.3435E-03
0.4283E 02	0.6260E-01	0.4032E-03
0.4680E 02	0.6430E-01	0.4331E-03
0.5175E 02	0.6610E-01	0.4703E-03
0.5967E 02	0.7050E-01	0.5273E-03
0.6362E 02	0.7290E-01	0.5547E-03
0.6856E 02	0.7520E-01	0.5911E-03
0.7546E 02	0.7960E-01	0.6334E-03
0.8137E 02	0.8340E-01	0.6873E-03
0.8925E 02	0.8880E-01	0.7477E-03
0.9416E 02	0.9320E-01	0.7899E-03
0.1000E 03	0.9800E-01	0.8345E-03
0.1079E 03	0.1041E-00	0.8812E-03
0.1147E 03	0.1110E-00	0.9179E-03
0.1216E 03	0.1172E-00	0.9769E-03
0.1284E 03	0.1236E-00	0.1036E-02
0.1362E 03	0.1320E-00	0.1093E-02
0.1440E 03	0.1413E-00	0.1161E-02
0.1518E 03	0.1504E-00	0.1221E-02
0.1586E 03	0.1588E-00	0.1263E-02
0.1654E 03	0.1675E-00	0.1292E-02
0.1729E 03	0.1776E-00	0.1335E-02
0.1818E 03	0.1898E-00	0.1393E-02
0.1915E 03	0.2028E-00	0.1484E-02
0.1982E 03	0.2129E-00	0.1535E-02
0.2078E 03	0.2284E-00	0.1619E-02
0.2126E 03	0.2372E-00	0.1663E-02
0.2203E 03	0.2493E-00	0.1707E-02
0.2279E 03	0.2627E-00	0.1750E-02
0.2356E 03	0.2763E-00	0.1793E-02

RUN No. 1A

0.1000E 01	0.4240E-01	0.1156E-02
0.1099E 02	0.5500E-01	0.1354E-02
0.2096E 02	0.6950E-01	0.1551E-02
0.3190E 02	0.8760E-01	0.1767E-02
0.4183E 02	0.1060E-00	0.1977E-02
0.5174E 02	0.1266E-00	0.2188E-02
0.6262E 02	0.1512E-00	0.2413E-02
0.7249E 02	0.1770E-00	0.2610E-02
0.8332E 02	0.2065E-00	0.2865E-02
0.9315E 02	0.2348E-00	0.3089E-02
0.1039E 03	0.2681E-00	0.3336E-02
0.1127E 03	0.3012E-00	0.3537E-02

RUN No. 1B

0.1000E 01	0.3310E-01	0.6306E-03
0.1099E 02	0.4030E-01	0.8733E-03
0.2096E 02	0.5100E-01	0.1116E-02
0.3190E 02	0.6400E-01	0.1381E-02
0.4183E 02	0.7890E-01	0.1630E-02
0.5174E 02	0.9640E-01	0.1870E-02
0.6262E 02	0.1181E-00	0.2138E-02
0.7249E 02	0.1409E-00	0.2373E-02
0.8332E 02	0.1679E-00	0.2675E-02
0.9315E 02	0.1945E-00	0.2891E-02
0.1039E 03	0.2268E-00	0.3144E-02
0.1127E 03	0.2594E-00	0.3350E-02
0.1245E 03	0.2962E-00	0.3625E-02

RUN No. 1C

0.1000E 01	0.1100E-02	0.6459E-03
0.1099E 02	0.8900E-02	0.8831E-03
0.2096E 02	0.1910E-01	0.1120E-02
0.3190E 02	0.3230E-01	0.1380E-02
0.4183E 02	0.4740E-01	0.1625E-02
0.5174E 02	0.6440E-01	0.1862E-02
0.6262E 02	0.8620E-01	0.2129E-02
0.7249E 02	0.1091E-00	0.2363E-02
0.8332E 02	0.1354E-00	0.2660E-02
0.9315E 02	0.1625E-00	0.2873E-02
0.1039E 03	0.1945E-00	0.3123E-02
0.1127E 03	0.2264E-00	0.3326E-02
0.1245E 03	0.2633E-00	0.3598E-02

RUN No. 1D

0.1099E 02	0.1450E-01	-0.1140E-04
0.2096E 02	0.1510E-01	0.5300E-04
0.3190E 02	0.1610E-01	0.1237E-03
0.4183E 02	0.1730E-01	0.1878E-03
0.5174E 02	0.1950E-01	0.2492E-03
0.6262E 02	0.2250E-01	0.3180E-03
0.7249E 02	0.2640E-01	0.3847E-03
0.8332E 02	0.3080E-01	0.4691E-03
0.9315E 02	0.3520E-01	0.5372E-03
0.1039E 03	0.4140E-01	0.6109E-03
0.1127E 03	0.4820E-01	0.6785E-03
0.1245E 03	0.5590E-01	0.7627E-03
0.1342E 03	0.6350E-01	0.8232E-03
0.1449E 03	0.7300E-01	0.8814E-03
0.1556E 03	0.8290E-01	0.9440E-03
0.1653E 03	0.9240E-01	0.9862E-03
0.1759E 03	0.1031E-00	0.1014E-02
0.1856E 03	0.1131E-00	0.1026E-02
0.1962E 03	0.1245E-00	0.1030E-02
0.2067E 03	0.1353E-00	0.1034E-02
0.2173E 03	0.1457E-00	0.1038E-02

RUN No. 2A

```
0.1198E 02   0.1010E 01   0.5569E-03
0.1894E 02   0.1014E 01   0.5850E-03
0.2593E 02   0.1018E 01   0.6133E-03
0.3388E 02   0.1023E 01   0.6454E-03
0.4083E 02   0.1028E 01   0.6783E-03
0.4777E 02   0.1033E 01   0.7136E-03
0.5569E 02   0.1038E 01   0.7511E-03
0.6260E 02   0.1044E 01   0.7862E-03
0.7345E 02   0.1053E 01   0.8488E-03
0.8722E 02   0.1065E 01   0.9276E-03
0.9410E 02   0.1071E 01   0.9670E-03
0.1010E 03   0.1078E 01   0.9990E-03
0.1088E 03   0.1086E 01   0.1035E-02
0.1156E 03   0.1094E 01   0.1058E-02
0.1225E 03   0.1101E 01   0.1090E-02
0.1303E 03   0.1109E 01   0.1127E-02
0.1372E 03   0.1117E 01   0.1161E-02
0.1439E 03   0.1125E 01   0.1192E-02
0.1516E 03   0.1135E 01   0.1219E-02
0.1584E 03   0.1143E 01   0.1245E-02
0.1661E 03   0.1153E 01   0.1261E-02
0.1768E 03   0.1166E 01   0.1298E-02
0.1873E 03   0.1180E 01   0.1335E-02
0.1979E 03   0.1194E 01   0.1371E-02
```

RUN No. 2B

```
0.1000E 01   0.9967E 00   0.4157E-03
0.1198E 02   0.1001E 01   0.4626E-03
0.1894E 02   0.1005E 01   0.4922E-03
0.2593E 02   0.1008E 01   0.5221E-03
0.4083E 02   0.1017E 01   0.5879E-03
0.4777E 02   0.1021E 01   0.6136E-03
0.5569E 02   0.1026E 01   0.6468E-03
0.6260E 02   0.1030E 01   0.6740E-03
0.7345E 02   0.1038E 01   0.7312E-03
0.8034E 02   0.1043E 01   0.7688E-03
0.8722E 02   0.1048E 01   0.7978E-03
0.9410E 02   0.1054E 01   0.8308E-03
0.1010E 03   0.1060E 01   0.9296E-03
0.1088E 03   0.1067E 01   0.9292E-03
0.1156E 03   0.1073E 01   0.8950E-03
0.1225E 03   0.1084E 01   0.8933E-03
0.1303E 03   0.1086E 01   0.9098E-03
0.1372E 03   0.1091E 01   0.8966E-03
0.1439E 03   0.1099E 01   0.8677E-03
0.1584E 03   0.1114E 01   0.1026E-02
0.1661E 03   0.1121E 01   0.1050E-02
0.1768E 03   0.1133E 01   0.1058E-02
0.1873E 03   0.1144E 01   0.1065E-02
0.1979E 03   0.1155E 01   0.1072E-02
```

RUN No. 2C

```
0.1000E 01   0.9823E 00   0.1336E-03
0.1198E 02   0.9838E 00   0.1566E-03
0.1894E 02   0.9849E 00   0.1712E-03
0.2593E 02   0.9862E 00   0.1858E-03
0.3388E 02   0.9879E 00   0.2006E-03
0.4083E 02   0.9893E 00   0.2105E-03
0.4777E 02   0.9907E 00   0.2189E-03
0.5569E 02   0.9925E 00   0.2280E-03
0.6260E 02   0.9941E 00   0.2404E-03
0.7345E 02   0.9968E 00   0.2591E-03
0.8034E 02   0.9986E 00   0.2728E-03
0.8722E 02   0.1001E 01   0.2849E-03
0.9410E 02   0.1002E 01   0.2965E-03
0.1010E 03   0.1005E 01   0.3048E-03
0.1088E 03   0.1007E 01   0.3108E-03
0.1156E 03   0.1009E 01   0.3166E-03
0.1225E 03   0.1011E 01   0.3236E-03
0.1303E 03   0.1014E 01   0.3348E-03
0.1372E 03   0.1016E 01   0.3437E-03
0.1439E 03   0.1019E 01   0.3481E-03
0.1516E 03   0.1021E 01   0.3567E-03
0.1584E 03   0.1024E 01   0.3638E-03
0.1661E 03   0.1026E 01   0.3661E-03
0.1768E 03   0.1031E 01   0.3736E-03
0.1873E 03   0.1035E 01   0.3810E-03
0.1979E 03   0.1038E 01   0.3884E-03
```

RUN No. 3B

```
0.1000E 01    0.2000E-03    0.3025E-03
0.1099E 02    0.3600E-02    0.4087E-03
0.2196E 02    0.8400E-02    0.5254E-03
0.5569E 02    0.3270E-01    0.8840E-03
0.6663E 02    0.4290E-01    0.9895E-03
0.7739E 02    0.5410E-01    0.1092E-02
0.8821E 02    0.6680E-01    0.1187E-02
0.9801E 02    0.7870E-01    0.1260E-02
0.1088E 03    0.9310E-01    0.1324E-02
0.1195E 03    0.1079E-00    0.1375E-02
0.1302E 03    0.1228E-00    0.1410E-02
0.1409E 03    0.1380E-00    0.1421E-02
0.1516E 03    0.1538E-00    0.1432E-02
0.1623E 03    0.1691E-00    0.1453E-02
0.1739E 03    0.1851E-00    0.1467E-02
0.1845E 03    0.2008E-00    0.1486E-02
0.1950E 03    0.2176E-00    0.1505E-02
0.2056E 03    0.2329E-00    0.1525E-02
```

RUN No. 4A

```
0.1000E 01    0.9904E 00    0.6434E-03
0.1199E 02    0.9984E 00    0.7905E-03
0.2196E 02    0.1007E 01    0.9239E-03
0.3290E 02    0.1018E 01    0.1070E-02
0.4387E 02    0.1030E 01    0.1218E-02
0.5375E 02    0.1043E 01    0.1361E-02
0.6463E 02    0.1059E 01    0.1526E-02
0.7549E 02    0.1076E 01    0.1681E-02
0.8536E 02    0.1093E 01    0.1812E-02
0.9613E 02    0.1114E 01    0.1949E-02
0.1070E 03    0.1136E 01    0.2075E-02
0.1177E 03    0.1159E 01    0.2187E-02
0.1285E 03    0.1183E 01    0.2302E-02
0.1392E 03    0.1208E 01    0.2416E-02
0.1529E 03    0.1242E 01    0.2561E-02
```

RUN No. 4B

```
0.1000E 01    0.9791E 00    0.6502E-03
0.1199E 02    0.9872E 00    0.8250E-03
0.2196E 02    0.9961E 00    0.9835E-03
0.3290E 02    0.1008E 01    0.1158E-02
0.4387E 02    0.1022E 01    0.1367E-02
0.5375E 02    0.1036E 01    0.1495E-02
0.6463E 02    0.1052E 01    0.1633E-02
0.7549E 02    0.1075E 01    0.1741E-02
0.8536E 02    0.1089E 01    0.1832E-02
0.9613E 02    0.1110E 01    0.1932E-02
0.1070E 03    0.1131E 01    0.2030E-02
0.1177E 03    0.1153E 01    0.2178E-02
0.1285E 03    0.1178E 01    0.2292E-02
0.1392E 03    0.1204E 01    0.2405E-02
0.1529E 03    0.1237E 01    0.2550E-02
```

RUN No. 4D

```
0.1000E 01    0.9629E 00    0.7921E-04
0.1199E 02    0.9641E 00    0.1107E-03
0.2196E 02    0.9655E 00    0.1393E-03
0.3290E 02    0.9668E 00    0.1706E-03
0.4387E 02    0.9690E 00    0.1973E-03
0.5375E 02    0.9711E 00    0.2256E-03
0.6463E 02    0.9739E 00    0.2573E-03
0.7549E 02    0.9765E 00    0.2848E-03
0.8536E 02    0.9797E 00    0.3090E-03
0.9613E 02    0.9831E 00    0.3386E-03
0.1070E 03    0.9870E 00    0.3674E-03
0.1177E 03    0.9909E 00    0.3951E-03
0.1285E 03    0.9956E 00    0.4241E-03
0.1392E 03    0.1000E 01    0.4499E-03
0.1529E 03    0.1007E 01    0.4811E-03
0.1636E 03    0.1012E 01    0.4998E-03
0.1742E 03    0.1017E 01    0.5125E-03
0.1849E 03    0.1023E 01    0.5206E-03
0.1955E 03    0.1029E 01    0.5292E-03
0.2066E 03    0.1034E 01    0.5347E-03
0.2205E 03    0.1042E 01    0.5417E-03
0.2340E 03    0.1049E 01    0.5483E-03
```

RUN No. 6A

0.1000E 01	0.2980E-01	0.1911E-03
0.9990E 01	0.3150E-01	0.2446E-03
0.1697E 02	0.3360E-01	0.2861E-03
0.2693E 02	0.3660E-01	0.3454E-03
0.3390E 02	0.3940E-01	0.3917E-03
0.4680E 02	0.4460E-01	0.4763E-03
0.5473E 02	0.4860E-01	0.5289E-03
0.6561E 02	0.5490E-01	0.6048E-03
0.7745E 02	0.6270E-01	0.6916E-03
0.8435E 02	0.6730E-01	0.7504E-03
0.9124E 02	0.7270E-01	0.7809E-03
0.9714E 02	0.7760E-01	0.8295E-03
0.1010E 03	0.8130E-01	0.8595E-03
0.1118E 03	0.9000E-01	0.9249E-03
0.1187E 03	0.9730E-01	0.9725E-03
0.1246E 03	0.1025E-00	0.1013E-02
0.1314E 03	0.1100E-00	0.1071E-02
0.1402E 03	0.1196E-00	0.1116E-02
0.1470E 03	0.1274E-00	0.1163E-02
0.1538E 03	0.1355E-00	0.1197E-02
0.1606E 03	0.1435E-00	0.1231E-02
0.1684E 03	0.1535E-00	0.1270E-02

RUN No. 6B

0.1000E 01	0.1550E-01	0.3861E-04
0.9990E 01	0.1580E-01	0.5736E-04
0.1697E 02	0.1620E-01	0.7192E-04
0.2693E 02	0.1730E-01	0.9270E-04
0.3390E 02	0.1780E-01	0.1110E-03
0.4680E 02	0.1940E-01	0.1346E-03
0.5473E 02	0.2050E-01	0.1509E-03
0.6561E 02	0.2260E-01	0.1816E-03
0.7745E 02	0.2430E-01	0.2060E-03
0.8435E 02	0.2610E-01	0.2323E-03
0.9124E 02	0.2800E-01	0.2409E-03
0.9714E 02	0.2900E-01	0.2659E-03
0.1010E 03	0.3060E-01	0.2697E-03
0.1118E 03	0.3310E-01	0.3013E-03
0.1187E 03	0.3560E-01	0.3236E-03
0.1246E 03	0.3750E-01	0.3424E-03
0.1314E 03	0.3990E-01	0.3684E-03
0.1402E 03	0.4310E-01	0.3824E-03
0.1470E 03	0.4620E-01	0.3918E-03
0.1538E 03	0.4870E-01	0.4090E-03
0.1606E 03	0.5140E-01	0.4241E-03
0.1684E 03	0.5450E-01	0.4340E-03
0.1761E 03	0.5840E-01	0.4556E-03
0.1829E 03	0.6160E-01	0.4744E-03
0.1906E 03	0.6490E-01	0.4959E-03

RUN No. 6C

0.1000E 01	0.5100E-02	0.3026E-03
0.9990E 01	0.8300E-02	0.4122E-03
0.1697E 02	0.1120E-01	0.4974E-03
0.2693E 02	0.1720E-01	0.6189E-03
0.3390E 02	0.2160E-01	0.7047E-03
0.4680E 02	0.3170E-01	0.8606E-03
0.5473E 02	0.3890E-01	0.9550E-03
0.6561E 02	0.5000E-01	0.1096E-02
0.7745E 02	0.6370E-01	0.1244E-02
0.8435E 02	0.7270E-01	0.1381E-02
0.9124E 02	0.8240E-01	0.1443E-02
0.9714E 02	0.9070E-01	0.1522E-02
0.1010E 03	0.9890E-01	0.1574E-02
0.1118E 03	0.1145E-00	0.1699E-02
0.1187E 03	0.1268E-00	0.1788E-02
0.1246E 03	0.1374E-00	0.1842E-02
0.1314E 03	0.1509E-00	0.1959E-02
0.1402E 03	0.1686E-00	0.2054E-02
0.1470E 03	0.1822E-00	0.2127E-02
0.1538E 03	0.1975E-00	0.2201E-02

RUN No. 7A			RUN No. 7B		
0.	0.9275E 00	0.1279E-03	0.	0.9178E 00	0.2985E-04
0.1398E 02	0.9296E 00	0.1776E-03	0.1398E 02	0.9189E 00	0.9014E-04
0.2493E 02	0.9321E 00	0.2167E-03	0.2493E 02	0.9200E 00	0.1374E-03
0.3586E 02	0.9343E 00	0.2556E-03	0.3586E 02	0.9217E 00	0.1845E-03
0.4676E 02	0.9372E 00	0.3003E-03	0.4676E 02	0.9239E 00	0.2327E-03
0.5664E 02	0.9406E 00	0.3378E-03	0.5664E 02	0.9265E 00	0.2799E-03
0.6754E 02	0.9443E 00	0.3876E-03	0.6754E 02	0.9298E 00	0.3414E-03
0.7438E 02	0.9474E 00	0.4069E-03	0.7438E 02	0.9322E 00	0.3746E-03
0.8518E 02	0.9518E 00	0.4338E-03	0.8518E 02	0.9364E 00	0.4245E-03
0.9496E 02	0.9567E 00	0.4600E-03	0.9496E 02	0.9414E 00	0.4728E-03
0.1067E 03	0.9617E 00	0.4980E-03	0.1067E 03	0.9470E 00	0.5325E-03
0.1135E 03	0.9650E 00	0.5151E-03	0.1135E 03	0.9503E 00	0.5585E-03
0.1204E 03	0.9688E 00	0.5328E-03	0.1204E 03	0.9546E 00	0.5930E-03
0.1281E 03	0.9735E 00	0.5612E-03	0.1281E 03	0.9596E 00	0.6409E-03
0.1349E 03	0.9769E 00	0.5757E-03	0.1349E 03	0.9635E 00	0.6812E-03
0.1456E 03	0.9834E 00	0.5884E-03	0.1456E 03	0.9714E 00	0.7333E-03
0.1562E 03	0.9895E 00	0.6014E-03	0.1562E 03	0.9796E 00	0.7853E-03
0.1669E 03	0.9961E 00	0.6288E-03	0.1669E 03	0.9881E 00	0.8372E-03
0.1775E 03	0.1003E 01	0.6923E-03	0.1775E 03	0.9976E 00	0.8742E-03
0.1851E 03	0.1007E 01	0.7572E-03	0.1851E 03	0.1004E 01	0.9093E-03
0.1956E 03	0.1015E 01	0.8545E-03	0.1956E 03	0.1014E 01	0.9525E-03
0.2061E 03	0.1026E 01	0.9843E-03	0.2061E 03	0.1024E 01	0.9999E-03
0.2175E 03	0.1038E 01	0.1128E-02	0.2175E 03	0.1036E 01	0.1051E-02
0.2243E 03	0.1045E 01	0.1223E-02	0.2243E 03	0.1043E 01	0.1086E-02
0.2346E 03	0.1059E 01	0.1344E-02	0.2346E 03	0.1055E 01	0.1138E-02
0.2418E 03	0.1068E 01	0.1439E-02	0.2418E 03	0.1062E 01	0.1172E-02
0.2488E 03	0.1080E 01	0.1531E-02	0.2488E 03	0.1071E 01	0.1203E-02
0.2554E 03	0.1089E 01	0.1619E-02	0.2554E 03	0.1079E 01	0.1234E-02

RUN No. 8A

0.1000E 01	0.1870E-01	0.1410E-02
0.1897E 02	0.4800E-01	0.1820E-02
0.2992E 02	0.6890E-01	0.2070E-02
0.4381E 02	0.1002E-00	0.2386E-02
0.5070E 02	0.1170E-00	0.2534E-02
0.6164E 02	0.1459E-00	0.2760E-02
0.6856E 02	0.1663E-00	0.2901E-02
0.7549E 02	0.1864E-00	0.3048E-02
0.8236E 02	0.2075E-00	0.3185E-02
0.8924E 02	0.2301E-00	0.3323E-02
0.9318E 02	0.2437E-00	0.3402E-02

RUN No. 8B

0.2992E 02	0.7320E-01	0.3259E-03
0.4381E 02	0.7830E-01	0.3913E-03
0.5070E 02	0.8080E-01	0.4238E-03
0.6164E 02	0.8580E-01	0.4753E-03
0.6856E 02	0.8970E-01	0.5130E-03
0.7549E 02	0.9270E-01	0.5633E-03
0.8236E 02	0.9680E-01	0.6058E-03
0.8924E 02	0.1011E-00	0.6472E-03
0.9318E 02	0.1042E-00	0.6862E-03
0.1040E 03	0.1117E-00	0.7352E-03
0.1147E 03	0.1200E-00	0.7738E-03
0.1255E 03	0.1284E-00	0.8089E-03
0.1363E 03	0.1374E-00	0.8384E-03
0.1469E 03	0.1465E-00	0.8589E-03
0.1576E 03	0.1563E-00	0.8760E-03
0.1683E 03	0.1653E-00	0.8832E-03
0.1789E 03	0.1748E-00	0.8859E-03
0.1895E 03	0.1844E-00	0.8900E-03
0.2040E 03	0.1971E-00	0.9023E-03
0.2145E 03	0.2065E-00	0.9113E-03
0.2212E 03	0.2130E-00	0.9170E-03

RUN No. 8C

0.6856E 02	0.7090E-01	0.5713E-03
0.8236E 02	0.8040E-01	0.8195E-03
0.8924E 02	0.8640E-01	0.9432E-03
0.9318E 02	0.9030E-01	0.1014E-02
0.1040E 03	0.1024E-00	0.1211E-02
0.1147E 03	0.1166E-00	0.1405E-02
0.1255E 03	0.1324E-00	0.1593E-02
0.1363E 03	0.1509E-00	0.1769E-02
0.1469E 03	0.1711E-00	0.1934E-02
0.1576E 03	0.1927E-00	0.2079E-02
0.1683E 03	0.2155E-00	0.2203E-02
0.1789E 03	0.2401E-00	0.2303E-02
0.1895E 03	0.2650E-00	0.2399E-02
0.2040E 03	0.3011E-00	0.2510E-02
0.2145E 03	0.3271E-00	0.2591E-02
0.2212E 03	0.3451E-00	0.2642E-02

RUN No. 9A

```
0.1000E 01    0.9843E 00    0.5106E-03
0.7995E 01    0.9885E 00    0.5430E-03
0.1498E 02    0.9921E 00    0.5754E-03
0.2594E 02    0.9987E 00    0.6262E-03
0.3689E 02    0.1006E 01    0.6693E-03
0.4781E 02    0.1014E 01    0.7250E-03
0.6564E 02    0.1027E 01    0.8177E-03
0.7552E 02    0.1035E 01    0.8707E-03
0.8637E 02    0.1045E 01    0.9217E-03
0.9720E 02    0.1056E 01    0.9807E-03
0.1051E 03    0.1063E 01    0.1024E-02
0.1159E 03    0.1074E 01    0.1066E-02
0.1227E 03    0.1082E 01    0.1096E-02
0.1296E 03    0.1090E 01    0.1131E-02
0.1374E 03    0.1098E 01    0.1167E-02
0.1442E 03    0.1107E 01    0.1195E-02
0.1520E 03    0.1116E 01    0.1231E-02
0.1588E 03    0.1125E 01    0.1269E-02
0.1666E 03    0.1135E 01    0.1303E-02
0.1773E 03    0.1149E 01    0.1349E-02
0.1841E 03    0.1158E 01    0.1379E-02
```

RUN No. 9B

```
0.1000E 01    0.9812E 00    0.4829E-03
0.7995E 01    0.9852E 00    0.5217E-03
0.1498E 02    0.9887E 00    0.5604E-03
0.2594E 02    0.9952E 00    0.6211E-03
0.3689E 02    0.1002E 01    0.6835E-03
0.4781E 02    0.1010E 01    0.7582E-03
0.5772E 02    0.1018E 01    0.8282E-03
0.6564E 02    0.1025E 01    0.8799E-03
0.7552E 02    0.1034E 01    0.9450E-03
0.8637E 02    0.1045E 01    0.1010E-02
0.9720E 02    0.1056E 01    0.1075E-02
0.1051E 03    0.1064E 01    0.1126E-02
0.1159E 03    0.1077E 01    0.1190E-02
0.1227E 03    0.1085E 01    0.1238E-02
0.1296E 03    0.1094E 01    0.1297E-02
0.1374E 03    0.1104E 01    0.1325E-02
0.1442E 03    0.1113E 01    0.1328E-02
0.1520E 03    0.1125E 01    0.1357E-02
0.1588E 03    0.1133E 01    0.1371E-02
0.1666E 03    0.1143E 01    0.1380E-02
0.1773E 03    0.1159E 01    0.1393E-02
0.1841E 03    0.1168E 01    0.1401E-02
```

RUN No. 10A

0.1000E 01	0.5500E-01	0.4748E-03
0.7994E 01	0.5800E-01	0.5219E-03
0.1298E 02	0.6140E-01	0.5556E-03
0.1996E 02	0.6540E-01	0.6026E-03
0.2992E 02	0.7120E-01	0.6430E-03
0.3489E 02	0.7480E-01	0.6488E-03
0.4283E 02	0.8080E-01	0.6748E-03
0.4977E 02	0.8460E-01	0.6975E-03
0.5869E 02	0.9090E-01	0.7332E-03
0.6660E 02	0.9690E-01	0.7771E-03
0.7055E 02	1.0000E-01	0.7949E-03
0.7942E 02	0.1076E-00	0.8266E-03
0.8730E 02	0.1145E-00	0.8646E-03
0.9615E 02	0.1213E-00	0.8827E-03
0.1030E 03	0.1275E-00	0.9128E-03
0.1109E 03	0.1361E-00	0.9367E-03
0.1197E 03	0.1430E-00	0.9748E-03
0.1304E 03	0.1550E-00	0.1001E-02
0.1373E 03	0.1607E-00	0.1018E-02
0.1460E 03	0.1702E-00	0.1058E-02
0.1548E 03	0.1796E-00	0.1097E-02
0.1645E 03	0.1904E-00	0.1141E-02

RUN No. 10B

0.1000E 01	0.3050E-01	0.3173E-03
0.7994E 01	0.3250E-01	0.3654E-03
0.1298E 02	0.3510E-01	0.3997E-03
0.1996E 02	0.3800E-01	0.4477E-03
0.2992E 02	0.4240E-01	0.4864E-03
0.3489E 02	0.4480E-01	0.4930E-03
0.4283E 02	0.5000E-01	0.5214E-03
0.4977E 02	0.5250E-01	0.5397E-03
0.5869E 02	0.5750E-01	0.5766E-03
0.6660E 02	0.6240E-01	0.6056E-03
0.7055E 02	0.6440E-01	0.6346E-03
0.7942E 02	0.7090E-01	0.6661E-03
0.8730E 02	0.7590E-01	0.7027E-03
0.9615E 02	0.8230E-01	0.7347E-03
0.1030E 03	0.8700E-01	0.7608E-03
0.1109E 03	0.9400E-01	0.7904E-03
0.1197E 03	0.1004E-00	0.8209E-03
0.1304E 03	0.1102E-00	0.8516E-03
0.1373E 03	0.1151E-00	0.8704E-03
0.1460E 03	0.1234E-00	0.9069E-03
0.1548E 03	0.1312E-00	0.9372E-03
0.1645E 03	0.1407E-00	0.9709E-03
0.1761E 03	0.1522E-00	0.1011E-02

RUN No. 10C

0.1000E 01	0.2420E-01	0.2972E-03
0.7994E 01	0.2610E-01	0.3509E-03
0.1298E 02	0.2860E-01	0.3892E-03
0.1996E 02	0.3150E-01	0.4428E-03
0.2992E 02	0.3590E-01	0.4953E-03
0.3489E 02	0.3820E-01	0.5020E-03
0.4283E 02	0.4360E-01	0.5286E-03
0.4977E 02	0.4650E-01	0.5526E-03
0.5869E 02	0.5130E-01	0.5858E-03
0.6660E 02	0.5600E-01	0.6169E-03
0.7055E 02	0.5860E-01	0.6393E-03
0.7942E 02	0.6480E-01	0.6784E-03
0.8730E 02	0.7020E-01	0.7217E-03
0.9615E 02	0.7630E-01	0.7497E-03
0.1030E 03	0.8140E-01	0.7834E-03
0.1109E 03	0.8890E-01	0.8143E-03
0.1197E 03	0.9500E-01	0.8468E-03
0.1304E 03	0.1054E-00	0.8748E-03
0.1373E 03	0.1105E-00	0.8851E-03
0.1460E 03	0.1186E-00	0.9267E-03
0.1548E 03	0.1270E-00	0.9534E-03
0.1645E 03	0.1360E-00	0.9831E-03
0.1761E 03	0.1482E-00	0.1019E-02

RUN No. 10D

0.1000E 01	0.2140E-01	0.2509E-03
0.7994E 01	0.2360E-01	0.2968E-03
0.1298E 02	0.2540E-01	0.3296E-03
0.1996E 02	0.2800E-01	0.3754E-03
0.2992E 02	0.3170E-01	0.4288E-03
0.3489E 02	0.3280E-01	0.4412E-03
0.4283E 02	0.3850E-01	0.4689E-03
0.4977E 02	0.4120E-01	0.4943E-03
0.5869E 02	0.4540E-01	0.5285E-03
0.6660E 02	0.4940E-01	0.5303E-03
0.7055E 02	0.5140E-01	0.5557E-03
0.7942E 02	0.5750E-01	0.5981E-03
0.8730E 02	0.6120E-01	0.6327E-03
0.9615E 02	0.6750E-01	0.6667E-03
0.1030E 03	0.7210E-01	0.6853E-03
0.1373E 03	0.9820E-01	0.8148E-03
0.1460E 03	0.1054E-00	0.8504E-03
0.1548E 03	0.1129E-00	0.9013E-03
0.1645E 03	0.1216E-00	0.9387E-03
0.1761E 03	0.1327E-00	0.1003E-02
0.1848E 03	0.1425E-00	0.1051E-02
0.1954E 03	0.1532E-00	0.1110E-02

RUN No. 10E

0.1298E 02	0.1840E-01	0.3043E-03
0.1996E 02	0.2050E-01	0.3279E-03
0.2992E 02	0.2370E-01	0.3616E-03
0.3489E 02	0.2560E-01	0.3785E-03
0.4283E 02	0.2950E-01	0.4011E-03
0.4977E 02	0.3160E-01	0.4261E-03
0.5869E 02	0.3570E-01	0.4748E-03
0.6660E 02	0.3900E-01	0.5026E-03
0.7055E 02	0.4140E-01	0.5288E-03
0.7942E 02	0.4710E-01	0.5712E-03
0.8730E 02	0.5080E-01	0.6262E-03
0.9615E 02	0.5650E-01	0.6595E-03
0.1030E 03	0.6110E-01	0.6944E-03
0.1109E 03	0.6790E-01	0.7399E-03
0.1197E 03	0.7340E-01	0.7763E-03
0.1304E 03	0.8280E-01	0.8150E-03
0.1373E 03	0.8750E-01	0.8390E-03
0.1460E 03	0.9570E-01	0.8837E-03
0.1548E 03	0.1034E-00	0.9256E-03
0.1645E 03	0.1127E-00	0.9961E-03
0.1761E 03	0.1237E-00	0.1055E-02
0.1848E 03	0.1344E-00	0.1107E-02
0.1954E 03	0.1467E-00	0.1172E-02
0.2070E 03	0.1596E-00	0.1243E-02

RUN No. 11A

```
0.1000E 01   0.7910E-01   0.4200E-03
0.7990E 01   0.8240E-01   0.4941E-03
0.1498E 02   0.8610E-01   0.5682E-03
0.2196E 02   0.9020E-01   0.6423E-03
0.2892E 02   0.9490E-01   0.7237E-03
0.3689E 02   0.1012E-00   0.8152E-03
0.4383E 02   0.1068E-00   0.8925E-03
0.5077E 02   0.1138E-00   0.9677E-03
0.5770E 02   0.1205E-00   0.1039E-02
0.6462E 02   0.1279E-00   0.1120E-02
0.7154E 02   0.1359E-00   0.1190E-02
0.7943E 02   0.1455E-00   0.1287E-02
0.8632E 02   0.1550E-00   0.1363E-02
0.9321E 02   0.1644E-00   0.1419E-02
0.1001E 03   0.1748E-00   0.1483E-02
0.1079E 03   0.1868E-00   0.1549E-02
0.1158E 03   0.1983E-00   0.1639E-02
0.1226E 03   0.2101E-00   0.1719E-02
0.1295E 03   0.2220E-00   0.1826E-02
0.1373E 03   0.2370E-00   0.1919E-02
0.1441E 03   0.2502E-00   0.1988E-02
0.1502E 03   0.2637E-00   0.2040E-02
0.1587E 03   0.2800E-00   0.2114E-02
0.1694E 03   0.3035E-00   0.2206E-02
```

RUN No. 12B

0.	0.1785E-00	-0.6042E-04
0.6994E 01	0.1781E-00	-0.9669E-04
0.1398E 02	0.1771E-00	-0.1329E-03
0.2096E 02	0.1761E-00	-0.1691E-03
0.2793E 02	0.1749E-00	-0.2062E-03
0.3588E 02	0.1730E-00	-0.2488E-03
0.4283E 02	0.1712E-00	-0.2906E-03
0.4977E 02	0.1691E-00	-0.3308E-03
0.5769E 02	0.1662E-00	-0.3749E-03
0.6856E 02	0.1617E-00	-0.4344E-03
0.7547E 02	0.1587E-00	-0.4744E-03
0.8631E 02	0.1532E-00	-0.5342E-03
0.9712E 02	0.1473E-00	-0.5877E-03
0.1078E 03	0.1403E-00	-0.6407E-03
0.1148E 03	0.1357E-00	-0.6821E-03
0.1226E 03	0.1307E-00	-0.7213E-03
0.1333E 03	0.1226E-00	-0.7470E-03
0.1401E 03	0.1167E-00	-0.8103E-03
0.1470E 03	0.1114E-00	-0.8608E-03
0.1567E 03	0.1045E-00	-0.9218E-03
0.1615E 03	0.9740E-01	-0.9450E-03
0.1693E 03	0.9050E-01	-0.1006E-02
0.1760E 03	0.8390E-01	-0.1047E-02
0.1828E 03	0.7690E-01	-0.1034E-02
0.1905E 03	0.6800E-01	-0.1056E-02
0.1973E 03	0.6110E-01	-0.1080E-02
0.2050E 03	0.5290E-01	-0.1091E-02
0.2117E 03	0.4620E-01	-0.1100E-02
0.2194E 03	0.3660E-01	-0.1111E-02

RUN No. 12C

0.	0.2672E-00	-0.1783E-03
0.6994E 01	0.2655E-00	-0.2799E-03
0.1398E 02	0.2648E-00	-0.3814E-03
0.2096E 02	0.2599E-00	-0.4827E-03
0.2793E 02	0.2565E-00	-0.5780E-03
0.3588E 02	0.2513E-00	-0.6829E-03
0.4283E 02	0.2468E-00	-0.7360E-03
0.4977E 02	0.2413E-00	-0.8190E-03
0.5769E 02	0.2342E-00	-0.9028E-03
0.6856E 02	0.2240E-00	-0.1029E-02
0.7547E 02	0.2164E-00	-0.1113E-02
0.8631E 02	0.2042E-00	-0.1243E-02
0.9712E 02	0.1898E-00	-0.1381E-02
0.1078E 03	0.1738E-00	-0.1510E-02
0.1148E 03	0.1635E-00	-0.1594E-02
0.1226E 03	0.1505E-00	-0.1671E-02
0.1333E 03	0.1318E-00	-0.1735E-02
0.1401E 03	0.1193E-00	-0.1854E-02
0.1470E 03	0.1070E-00	-0.1955E-02
0.1567E 03	0.9020E-01	-0.2103E-02
0.1615E 03	0.7560E-01	-0.2197E-02
0.1693E 03	0.5910E-01	-0.2349E-02
0.1760E 03	0.4390E-01	-0.2482E-02

RUN No. 12D

0.	0.2706E-00	-0.8861E-04
0.6994E 01	0.2697E-00	-0.1210E-03
0.1398E 02	0.2685E-00	-0.1534E-03
0.2096E 02	0.2678E-00	-0.1858E-03
0.2793E 02	0.2662E-00	-0.2215E-03
0.3588E 02	0.2645E-00	-0.2706E-03
0.4283E 02	0.2623E-00	-0.3216E-03
0.4977E 02	0.2599E-00	-0.3717E-03
0.5769E 02	0.2568E-00	-0.4453E-03
0.6856E 02	0.2518E-00	-0.5603E-03
0.7547E 02	0.2477E-00	-0.6438E-03
0.8631E 02	0.2398E-00	-0.7841E-03
0.9712E 02	0.2307E-00	-0.9178E-03
0.1078E 03	0.2198E-00	-0.1041E-02
0.1148E 03	0.2123E-00	-0.1118E-02
0.1226E 03	0.2035E-00	-0.1208E-02
0.1333E 03	0.1898E-00	-0.1293E-02
0.1401E 03	0.1806E-00	-0.1399E-02
0.1470E 03	0.1705E-00	-0.1498E-02
0.1567E 03	0.1576E-00	-0.1627E-02
0.1615E 03	0.1468E-00	-0.1688E-02
0.1693E 03	0.1337E-00	-0.1793E-02
0.1760E 03	0.1219E-00	-0.1883E-02
0.1828E 03	0.1089E-00	-0.1920E-02
0.1905E 03	0.9330E-01	-0.2023E-02
0.1973E 03	0.7990E-01	-0.2108E-02
0.2050E 03	0.6330E-01	-0.2206E-02
0.2117E 03	0.4790E-01	-0.2292E-02

RUN No. 12E

0.4977E 02	0.7780E-01	-0.1867E-04
0.5769E 02	0.7770E-01	-0.3709E-04
0.6856E 02	0.7690E-01	-0.6237E-04
0.7547E 02	0.7650E-01	-0.7844E-04
0.8631E 02	0.7560E-01	-0.1006E-03
0.9712E 02	0.7450E-01	-0.1212E-03
0.1078E 03	0.7270E-01	-0.1458E-03
0.1148E 03	0.7200E-01	-0.1651E-03
0.1226E 03	0.7060E-01	-0.1842E-03
0.1333E 03	0.6850E-01	-0.2016E-03
0.1401E 03	0.6680E-01	-0.2426E-03
0.1470E 03	0.6530E-01	-0.2629E-03
0.1567E 03	0.6330E-01	-0.2827E-03
0.1615E 03	0.6030E-01	-0.3000E-03
0.1693E 03	0.5860E-01	-0.3283E-03
0.1760E 03	0.5690E-01	-0.3406E-03
0.1828E 03	0.5400E-01	-0.3397E-03
0.1905E 03	0.5100E-01	-0.3679E-03
0.1973E 03	0.4900E-01	-0.3859E-03
0.2050E 03	0.4580E-01	-0.3952E-03
0.2117E 03	0.4320E-01	-0.4104E-03
0.2194E 03	0.3980E-01	-0.4364E-03
0.2337E 03	0.3330E-01	-0.4600E-03
0.2404E 03	0.3020E-01	-0.4679E-03
0.2481E 03	0.2650E-01	-0.4716E-03
0.2547E 03	0.2340E-01	-0.4771E-03
0.2623E 03	0.1970E-01	-0.4807E-03
0.2737E 03	0.1430E-01	-0.4860E-03
0.2804E 03	0.1100E-01	-0.4691E-03
0.2917E 03	0.5400E-02	-0.4943E-03

RUN No. 13A

0.1000E 01	0.9400E-01	0.3567E-03
0.3990E 01	0.9440E-01	0.3876E-03
0.1099E 02	0.9770E-01	0.4599E-03
0.1797E 02	0.1013E-00	0.5319E-03
0.2494E 02	0.1052E-00	0.6188E-03
0.3190E 02	0.1097E-00	0.6744E-03
0.3885E 02	0.1145E-00	0.7944E-03
0.4578E 02	0.1206E-00	0.9246E-03
0.5262E 02	0.1254E-00	0.1061E-02
0.6063E 02	0.1367E-00	0.1232E-02
0.6753E 02	0.1455E-00	0.1370E-02
0.7444E 02	0.1552E-00	0.1495E-02
0.8133E 02	0.1659E-00	0.1583E-02
0.8821E 02	0.1774E-00	0.1690E-02
0.9508E 02	0.1890E-00	0.1788E-02
0.1019E 03	0.2020E-00	0.1881E-02
0.1088E 03	0.2150E-00	0.1973E-02
0.1166E 03	0.2308E-00	0.2087E-02
0.1234E 03	0.2454E-00	0.2174E-02
0.1303E 03	0.2605E-00	0.2264E-02
0.1371E 03	0.2766E-00	0.2349E-02
0.1439E 03	0.2926E-00	0.2435E-02
0.1516E 03	0.3118E-00	0.2532E-02

RUN No. 13B

0.1797E 02	0.8230E-01	0.3462E-04
0.2494E 02	0.8280E-01	0.8267E-04
0.3190E 02	0.8300E-01	0.1306E-03
0.3885E 02	0.8460E-01	0.1786E-03
0.4578E 02	0.8600E-01	0.2268E-03
0.5262E 02	0.8770E-01	0.2788E-03
0.6063E 02	0.8990E-01	0.3296E-03
0.6753E 02	0.9240E-01	0.3899E-03
0.7444E 02	0.9530E-01	0.4503E-03
0.8133E 02	0.9850E-01	0.5107E-03
0.8821E 02	0.1025E-00	0.5638E-03
0.9508E 02	0.1065E-00	0.6166E-03
0.1019E 03	0.1109E-00	0.6692E-03
0.1088E 03	0.1155E-00	0.7284E-03
0.1166E 03	0.1214E-00	0.7918E-03
0.1234E 03	0.1270E-00	0.8412E-03
0.1303E 03	0.1336E-00	0.9034E-03
0.1371E 03	0.1393E-00	0.9652E-03
0.1439E 03	0.1457E-00	0.1018E-02
0.1516E 03	0.1544E-00	0.1080E-02
0.1574E 03	0.1611E-00	0.1136E-02
0.1652E 03	0.1697E-00	0.1203E-02
0.1719E 03	0.1780E-00	0.1253E-02
0.1796E 03	0.1878E-00	0.1426E-02
0.1864E 03	0.1973E-00	0.1441E-02
0.1931E 03	0.2066E-00	0.1461E-02
0.1998E 03	0.2226E-00	0.1482E-02
0.2075E 03	0.2280E-00	0.1477E-02
0.2142E 03	0.2383E-00	0.1501E-02
0.2209E 03	0.2490E-00	0.1556E-02
0.2295E 03	0.2620E-00	0.1628E-02
0.2390E 03	0.2794E-00	0.1706E-02

RUN No. 13C

0.8133E 02	0.8900E-01	0.4219E-03
0.8821E 02	0.9220E-01	0.4569E-03
0.9508E 02	0.9530E-01	0.4919E-03
0.1019E 03	0.9900E-01	0.5268E-03
0.1088E 03	0.1024E-00	0.5628E-03
0.1166E 03	0.1071E-00	0.6105E-03
0.1234E 03	0.1114E-00	0.6540E-03
0.1303E 03	0.1160E-00	0.7050E-03
0.1371E 03	0.1209E-00	0.7474E-03
0.1439E 03	0.1262E-00	0.7874E-03
0.1516E 03	0.1327E-00	0.8229E-03
0.1574E 03	0.1375E-00	0.8565E-03
0.1652E 03	0.1442E-00	0.8680E-03
0.1719E 03	0.1500E-00	0.9163E-03
0.1796E 03	0.1578E-00	0.9790E-03
0.1864E 03	0.1626E-00	0.1026E-02
0.1931E 03	0.1717E-00	0.1071E-02
0.1998E 03	0.1789E-00	0.1110E-02
0.2075E 03	0.1873E-00	0.1135E-02
0.2142E 03	0.1949E-00	0.1134E-02
0.2209E 03	0.2029E-00	0.1160E-02
0.2295E 03	0.2119E-00	0.1193E-02
0.2390E 03	0.2244E-00	0.1230E-02

RUN No. 14A

0.1000E 01	0.1004E 01	0.9020E-03
0.7990E 01	0.1010E 01	0.1076E-02
0.1598E 02	0.1021E 01	0.1274E-02
0.2296E 02	0.1029E 01	0.1448E-02
0.2993E 02	0.1040E 01	0.1610E-02
0.3689E 02	0.1052E 01	0.1755E-02
0.4384E 02	0.1065E 01	0.1917E-02
0.5178E 02	0.1080E 01	0.2072E-02
0.5871E 02	0.1095E 01	0.2228E-02
0.6564E 02	0.1111E 01	0.2350E-02
0.7256E 02	0.1128E 01	0.2521E-02
0.8046E 02	0.1149E 01	0.2712E-02
0.8836E 02	0.1169E 01	0.2919E-02
0.9426E 02	0.1189E 01	0.3074E-02
0.1011E 03	0.1210E 01	0.3254E-02

RUN No. 14B

0.1000E 01	0.9960E 00	0.4674E-03
0.7990E 01	0.9987E 00	0.6444E-03
0.1598E 02	0.1006E 01	0.8467E-03
0.2296E 02	0.1011E 01	0.1023E-02
0.2993E 02	0.1020E 01	0.1195E-02
0.3689E 02	0.1029E 01	0.1341E-02
0.4384E 02	0.1038E 01	0.1502E-02
0.5178E 02	0.1051E 01	0.1652E-02
0.5871E 02	0.1063E 01	0.1814E-02
0.6564E 02	0.1076E 01	0.1931E-02
0.7256E 02	0.1090E 01	0.2087E-02
0.8046E 02	0.1108E 01	0.2267E-02
0.8836E 02	0.1124E 01	0.2445E-02
0.9426E 02	0.1141E 01	0.2583E-02
0.1011E 03	0.1159E 01	0.2754E-02
0.1090E 03	0.1181E 01	0.2949E-02
0.1159E 03	0.1202E 01	0.3119E-02

RUN No. 14C

0.1000E 01	0.9836E 00	0.5361E-03
0.7990E 01	0.9867E 00	0.6936E-03
0.1598E 02	0.9940E 00	0.8737E-03
0.2296E 02	0.1000E 01	0.1031E-02
0.2993E 02	0.1008E 01	0.1192E-02
0.3689E 02	0.1017E 01	0.1334E-02
0.4384E 02	0.1026E 01	0.1491E-02
0.5178E 02	0.1039E 01	0.1635E-02
0.5871E 02	0.1051E 01	0.1803E-02
0.6564E 02	0.1064E 01	0.1929E-02
0.7256E 02	0.1077E 01	0.2085E-02
0.8046E 02	0.1096E 01	0.2270E-02
0.8836E 02	0.1112E 01	0.2466E-02
0.9426E 02	0.1129E 01	0.2609E-02
0.1011E 03	0.1147E 01	0.2750E-02
0.1090E 03	0.1170E 01	0.2933E-02
0.1159E 03	0.1190E 01	0.3094E-02
0.1227E 03	0.1212E 01	0.3254E-02

RUN No. 14D

0.1000E 01	0.9866E 00	0.1408E-03
0.7990E 01	0.9873E 00	0.2140E-03
0.1598E 02	0.9900E 00	0.2977E-03
0.2296E 02	0.9917E 00	0.3708E-03
0.2993E 02	0.9952E 00	0.4400E-03
0.3689E 02	0.9982E 00	0.5018E-03
0.4384E 02	0.1002E 01	0.5798E-03
0.5178E 02	0.1007E 01	0.6557E-03
0.5871E 02	0.1011E 01	0.7427E-03
0.6564E 02	0.1017E 01	0.8007E-03
0.7256E 02	0.1023E 01	0.8783E-03
0.8046E 02	0.1031E 01	0.9562E-03
0.8836E 02	0.1037E 01	0.1041E-02
0.9426E 02	0.1044E 01	0.1112E-02
0.1011E 03	0.1052E 01	0.1187E-02
0.1090E 03	0.1062E 01	0.1279E-02
0.1159E 03	0.1071E 01	0.1339E-02
0.1227E 03	0.1080E 01	0.1414E-02
0.1306E 03	0.1091E 01	0.1470E-02
0.1374E 03	0.1102E 01	0.1551E-02
0.1442E 03	0.1113E 01	0.1638E-02
0.1520E 03	0.1125E 01	0.1735E-02
0.1589E 03	0.1138E 01	0.1820E-02
0.1666E 03	0.1153E 01	0.1917E-02
0.1773E 03	0.1174E 01	0.2051E-02

RUN No. 15A

0.1000E 01	0.5470E-01	0.7283E-04
0.7994E 01	0.5530E-01	0.7782E-04
0.1897E 02	0.5610E-01	0.8566E-04
0.2594E 02	0.5680E-01	0.9063E-04
0.3688E 02	0.5810E-01	0.1008E-03
0.4789E 02	0.5850E-01	0.1145E-03
0.5869E 02	0.6030E-01	0.1389E-03
0.7055E 02	0.6190E-01	0.1707E-03
0.8139E 02	0.6360E-01	0.2049E-03
0.9223E 02	0.6650E-01	0.2338E-03
0.1030E 03	0.6910E-01	0.2720E-03
0.1148E 03	0.7230E-01	0.3105E-03
0.1226E 03	0.7480E-01	0.3394E-03
0.1285E 03	0.7710E-01	0.3616E-03
0.1363E 03	0.7990E-01	0.3953E-03
0.1431E 03	0.8270E-01	0.4163E-03
0.1577E 03	0.8920E-01	0.4619E-03
0.1655E 03	0.9310E-01	0.4881E-03
0.1732E 03	0.9590E-01	0.5047E-03
0.1800E 03	0.1006E-00	0.5252E-03
0.1906E 03	0.1061E-00	0.5542E-03
0.2012E 03	0.1117E-00	0.5752E-03
0.2089E 03	0.1167E-00	0.5798E-03
0.2166E 03	0.1211E-00	0.5845E-03
0.2233E 03	0.1250E-00	0.5885E-03

RUN No. 16A

0.1000E 01	0.3850E-01	0.1838E-04
0.8990E 01	0.3860E-01	0.1711E-04
0.1597E 02	0.3870E-01	0.1599E-04
0.2295E 02	0.3890E-01	0.1488E-04
0.2892E 02	0.3870E-01	0.5111E-05
0.3488E 02	0.3930E-01	0.1334E-04
0.4281E 02	0.3900E-01	0.4423E-04
0.4777E 02	0.3860E-01	0.5476E-04
0.5272E 02	0.3960E-01	0.5140E-04
0.6063E 02	0.4070E-01	0.5761E-04
0.6556E 02	0.4060E-01	0.6887E-04
0.7050E 02	0.4040E-01	0.6061E-04
0.7739E 02	0.4070E-01	0.7629E-04
0.8723E 02	0.4180E-01	0.1376E-03
0.9410E 02	0.4320E-01	0.1461E-03
0.9802E 02	0.4460E-01	0.1400E-03
0.1039E 03	0.4460E-01	0.1404E-03
0.1100E 03	0.4550E-01	0.1302E-03
0.1166E 03	0.4600E-01	0.1380E-03
0.1215E 03	0.4700E-01	0.1626E-03
0.1293E 03	0.4850E-01	0.1710E-03
0.1332E 03	0.4900E-01	0.1886E-03
0.1409E 03	0.5080E-01	0.1974E-03
0.1487E 03	0.5170E-01	0.2119E-03
0.1584E 03	0.5440E-01	0.2406E-03
0.1719E 03	0.5780E-01	0.2706E-03
0.1816E 03	0.6040E-01	0.2698E-03
0.1893E 03	0.6320E-01	0.3251E-03
0.1960E 03	0.6470E-01	0.3197E-03
0.2037E 03	0.6630E-01	0.3234E-03
0.2104E 03	0.7140E-01	0.3006E-03
0.2180E 03	0.7180E-01	0.2975E-03
0.2218E 03	0.7320E-01	0.3114E-03
0.2285E 03	0.7440E-01	0.2995E-03
0.2333E 03	0.7670E-01	0.3395E-03
0.2390E 03	0.7880E-01	0.3539E-03
0.2456E 03	0.8130E-01	0.3706E-03
0.2551E 03	0.8450E-01	0.3944E-03

RUN No. 17A

0.1000E 01	0.7190E-01	0.2578E-03
0.8990E 01	0.7450E-01	0.3366E-03
0.1598E 02	0.7730E-01	0.4055E-03
0.2396E 02	0.7940E-01	0.4842E-03
0.3292E 02	0.8560E-01	0.5915E-03
0.4187E 02	0.9120E-01	0.6629E-03
0.5180E 02	0.9750E-01	0.7328E-03
0.6172E 02	0.1080E-00	0.7632E-03
0.7162E 02	0.1129E-00	0.8126E-03
0.8151E 02	0.1217E-00	0.8728E-03
0.8743E 02	0.1267E-00	0.8920E-03
0.9730E 02	0.1363E-00	0.1008E-02
0.1062E 03	0.1456E-00	0.1072E-02
0.1180E 03	0.1588E-00	0.1164E-02
0.1248E 03	0.1671E-00	0.1216E-02
0.1337E 03	0.1779E-00	0.1266E-02
0.1395E 03	0.1857E-00	0.1305E-02
0.1474E 03	0.1963E-00	0.1349E-02
0.1552E 03	0.2065E-00	0.1393E-02
0.1620E 03	0.2165E-00	0.1432E-02

RUN No. 17B

0.1000E 01	0.6640E-01	0.2532E-03
0.8990E 01	0.6900E-01	0.3192E-03
0.1598E 02	0.7110E-01	0.3769E-03
0.2396E 02	0.7450E-01	0.4427E-03
0.3292E 02	0.7870E-01	0.5110E-03
0.4187E 02	0.8380E-01	0.5822E-03
0.5180E 02	0.9000E-01	0.6600E-03
0.6172E 02	0.9670E-01	0.7311E-03
0.7162E 02	0.1042E-00	0.8037E-03
0.8151E 02	0.1131E-00	0.8731E-03
0.8743E 02	0.1178E-00	0.9171E-03
0.9730E 02	0.1275E-00	0.9883E-03
0.1062E 03	0.1363E-00	0.1051E-02
0.1180E 03	0.1492E-00	0.1146E-02
0.1248E 03	0.1575E-00	0.1195E-02
0.1337E 03	0.1684E-00	0.1261E-02
0.1395E 03	0.1758E-00	0.1304E-02
0.1474E 03	0.1862E-00	0.1356E-02
0.1552E 03	0.1971E-00	0.1409E-02
0.1620E 03	0.2069E-00	0.1454E-02

RUN No. 17C

0.1000E 01	0.5530E-01	0.7097E-04
0.8990E 01	0.5590E-01	0.1135E-03
0.1598E 02	0.5660E-01	0.1508E-03
0.2396E 02	0.5870E-01	0.1933E-03
0.3292E 02	0.6000E-01	0.2414E-03
0.4187E 02	0.6260E-01	0.2863E-03
0.5180E 02	0.6570E-01	0.3374E-03
0.6172E 02	0.6920E-01	0.3907E-03
0.7162E 02	0.7330E-01	0.4398E-03
0.8151E 02	0.7840E-01	0.4807E-03
0.8743E 02	0.8070E-01	0.5116E-03
0.9730E 02	0.8640E-01	0.5553E-03
0.1062E 03	0.9100E-01	0.5955E-03
0.1180E 03	0.9870E-01	0.6608E-03
0.1248E 03	0.1033E-00	0.6965E-03
0.1337E 03	0.1097E-00	0.7417E-03
0.1395E 03	0.1141E-00	0.7709E-03
0.1474E 03	0.1204E-00	0.8049E-03
0.1552E 03	0.1267E-00	0.8492E-03
0.1620E 03	0.1328E-00	0.8769E-03
0.1689E 03	0.1385E-00	0.9120E-03
0.1766E 03	0.1464E-00	0.9531E-03
0.1844E 03	0.1533E-00	0.9944E-03
0.1932E 03	0.1626E-00	0.1041E-02

RUN No. 18A

```
0.1000E 01    0.8635E 00    0.5275E-04
0.1199E 02    0.8640E 00    0.7612E-04
0.2396E 02    0.8654E 00    0.1016E-03
0.3391E 02    0.8666E 00    0.1227E-03
0.4186E 02    0.8672E 00    0.1393E-03
0.5179E 02    0.8687E 00    0.1646E-03
0.6269E 02    0.8709E 00    0.2000E-03
0.7357E 02    0.8728E 00    0.2401E-03
0.8444E 02    0.8762E 00    0.2750E-03
0.1061E 03    0.8828E 00    0.3535E-03
0.1169E 03    0.8865E 00    0.3998E-03
0.1277E 03    0.8908E 00    0.4406E-03
0.1385E 03    0.8963E 00    0.4812E-03
0.1453E 03    0.8998E 00    0.5101E-03
0.1521E 03    0.9030E 00    0.5357E-03
0.1667E 03    0.9112E 00    0.5785E-03
0.1746E 03    0.9159E 00    0.6102E-03
0.1814E 03    0.9201E 00    0.6295E-03
0.1882E 03    0.9244E 00    0.5122E-03
0.1959E 03    0.9298E 00    0.5618E-03
0.2027E 03    0.9341E 00    0.5664E-03
0.2104E 03    0.9298E 00    0.5717E-03
0.2172E 03    0.9439E 00    0.5763E-03
```

RUN No. 18B

```
0.1000E 01    0.8563E 00    0.6655E-04
0.1199E 02    0.8568E 00    0.9597E-04
0.2396E 02    0.8588E 00    0.1280E-03
0.3391E 02    0.8600E 00    0.1546E-03
0.4186E 02    0.8609E 00    0.1764E-03
0.5179E 02    0.8630E 00    0.1997E-03
0.6269E 02    0.8655E 00    0.2418E-03
0.7357E 02    0.8680E 00    0.2828E-03
0.8444E 02    0.8714E 00    0.3188E-03
0.1061E 03    0.8795E 00    0.4000E-03
0.1169E 03    0.8836E 00    0.4447E-03
0.1277E 03    0.8886E 00    0.4860E-03
0.1385E 03    0.8942E 00    0.5274E-03
0.1453E 03    0.8981E 00    0.5556E-03
0.1521E 03    0.9018E 00    0.5826E-03
0.1667E 03    0.9107E 00    0.6339E-03
0.1746E 03    0.9156E 00    0.6559E-03
0.1814E 03    0.9205E 00    0.6787E-03
0.1882E 03    0.9251E 00    0.6982E-03
0.1959E 03    0.9304E 00    0.7116E-03
0.2027E 03    0.9355E 00    0.7190E-03
0.2104E 03    0.9412E 00    0.7276E-03
0.2172E 03    0.9459E 00    0.7350E-03
```

TABLE 3a - RESULTS, MOVING MODEL STUDIES - M ~ 4

Run No.	Diameter (inches)	w_{mod} #/cu.in.	Mach No.	q_∞ (psia)	A cm/marks	Magnification ft/in	Re_∞	T_w/T_o	C_D	Re_2
14-1 A	1/32	0.285	4.028	0.02394	10.88	1.616	77.1	1	1.792	20.97
B	3/32	0.1005					231	1	1.202	62.80
C	1/4	0.0415					617	1	1.236	167.8
D	1/16	0.285					154	1	1.420	41.9
14-2 B	1/8	0.1005	4.028	0.02394	11.02	1.616	308	1	1.464	83.77
C	1/16	0.285					154.3	1	1.399	41.96
14-3 A	1/4	0.1005	3.512	0.01269	10.92	1.616	285	1	1.315	94.6
B	1/32	0.285					35.6	1	1.923	11.82
C	3/32	0.1005					106	1	1.598	35.2
15) A	1/16	0.285	3.510	0.012304	11.08	1.616	67.6	1	1.642	22.8
16) A	1/16	0.285	3.129	0.00680	11.00	1.616	36.7	1	1.707	14.72
14-5 A	1/4	0.0415	3.659	0.01098	11.02	1.605	251	0.26	1.320	78.96
14-6 A	1/16	0.1005	3.659	0.01098	11.04	1.616	64.4	0.26	1.578	20.26
B	1/16	0.285					64.4	0.26	1.499	20.26
C	1/8	0.1005					128	0.26	1.458	40.40
14-7 A	3/32	0.1005	4.026	0.02395	10.87	1.616	238	0.26	1.236	64.73
B	1/4	0.0415					637	0.26	1.098	173.3
14-8 A	1/16	0.1005	4.026	0.02395	10.80	1.616	159	0.26	1.293	43.25
B	1/16	0.285					159	0.26	1.360	43.25
C	1/8	0.1005					318.5	0.26	1.309	86.63
17) A	1/32	0.285	3.531	0.012057	10.95	1.616	33.5	0.26	1.824	11.2
B	1/32	0.285					33.5	0.26	1.778	11.2
C	3/32	0.1005					100.5	0.26	1.405	33.5
18) A	1/32	0.285	3.083	0.006916	10.88	1.609	16.71	0.26	1.722	6.78
B	1/32	0.285					16.71	0.26	1.681	6.78
14-4 A	1/16	0.1005	3.512	0.01269	11.00	1.616	71.2	1	1.666	23.6
C	1/16	0.285					71.2	1	1.437	23.6
D	1/32	0.285					35.6	1	1.797	11.82

TABLE 3b - RESULTS, MOVING MODEL STUDIES - M ~ 6

Run No.	Diameter (inches)	w_{mod} #/cu.in.	Mach No.	q_∞ (psia)	A cm/4 marks	Magnification ft/in	Re_∞	T_w/T_o	C_D	Re_2
1) A	3/32	0.1005	5.832	0.05632	10.50	1.632	940.2	1	1.175	142
B	1/32	0.285					313.4	1	1.314	47.3
C	1/32	0.285					313.4	1	1.314	47.3
D	1/4	0.1005					2507	1	1.010	378.8
2) A	1/32	0.285	5.832	0.05632	10.69	1.632	313.4	1	1.420	47.3
B	1/16	0.285					627	1	1.303	94.7
C	1/8	0.285					1253	1	1.133	189.3
3) B	3/32	0.1005	5.498	0.02655	10.72	1.632	408	1	1.240	66.87
4) A	1/32	0.285	5.498	0.02655	10.76	1.632	136	1	1.575	22.3
B	1/32	0.285					136	1	1.607	22.3
D	1/8	0.285					545	1	1.269	89.32
11) A	1/16	0.285	5.905	0.05490	10.78	1.632	631	1	1.222	92.9
12) B	1/16	0.285	5.482	0.02719	10.92	1.632	276	1	1.298	45.73
C	1/32	0.285					138	1	1.497	22.9
D	1/32	0.285					138	1	1.612	22.9
E	1/8	0.285					555	1	1.280	91.9
6) A	1/16	0.285	5.498	0.02655	10.69	1.632	272	0.26	1.496	44.6
B	1/8	0.285					545	0.26	1.139	89.3
C	1/32	0.285					136	0.26	1.446	22.3
7) A	1/16	0.285	5.843	0.05680	10.78	1.632	627	0.26	1.308	94.0
B	1/8	0.285					1354	0.26	1.061	203.0
8) A	1/32	0.285	5.843	0.05680	10.80	1.632	314	0.26	1.266	47.1
B	1/4	0.1005					2708	0.26	1.032	406.0
C	3/32	0.1005					942	0.26	1.148	141.3
13) A	1/32	0.285	5.482	0.02719	10.69	1.632	138	0.26	1.399	22.9
B	1/4	0.1005					1104	0.26	1.002	182.9
C	1/16	0.285					276	0.26	1.278	45.73
14) A	1/32	0.285	5.898	0.05462	10.92	1.632	314	0.26	1.288	46.2
B	1/32	0.285					314	0.26	1.288	46.2
C	1/32	0.285					314	0.26	1.277	46.2
D	1/16	0.285					628	0.26	1.213	92.4

TABLE 3c - RESULTS, MOVING MODEL STUDIES - M ~ 2

Run No.		Diameter (inches)	w_{mod} #/cu.in.	Mach No.	q_∞ (psia)	A cm/4 marks	Magnification ft/in	Re_∞	T_w/T_o	C_D	Re_2
2-2	A	1/8	0.0415	2.093	0.01351	10.99	1.605	102.5	1	1.533	62.9
	B	1/32	0.285					25.6	1	1.914	15.7
	C	1/16	0.1005					51.2	1	1.607	31.4
2-3	A	3/32	0.0415	1.931	0.00599	10.96	1.600	33.2	1	1.622	21.98
	B	1/32	0.0285					11.2	1	2.246	7.41
	C	1/4	0.0415					9.0	1	1.521	5.96
2-4	A	1/8	0.0415	1.931	0.00599	10.88	1.605	45.1	1	1.556	29.86
	B	1/16	0.1005					22.5	1	1.737	14.89
	C	1/32	0.285					11.2	1	2.187	7.41
9)	A	1/8	0.1005	2.079	0.0131	10.95	1.608	100.0	1	1.592	62.5
	B	3/32	0.1005					75.0	1	1.605	46.8
2-5	A	1/32	0.285	1.931	0.00599	10.78	1.607	11.3	0.26	2.184	7.48
	B	1/32	0.285					11.3	0.26	2.205	7.48
	C	1/32	0.285					11.3	0.26	2.176	7.48
	E	1/4	0.0415					90.2	0.26	1.479	59.7
2-6	A	1/32	0.285	1.931	0.00599	11.20	1.613	11.3	0.26	2.275	7.48
	B	1/16	0.1005					22.6	0.26	1.767	14.96
	C	1/8	0.0415					45.2	0.25	1.703	29.92
2-7	A	1/32	0.285	2.117	0.01315	10.92	1.607	24.53	0.26	1.860	15.1
	B	1/32	0.285					24.53	0.26	1.888	15.1
	C	1/4	0.0415					196.3	0.26	1.368	121
2-8	A	1/32	0.285	2.117	0.01315	10.98	1.600	24.6	0.26	1.743	15.2
	B	1/8	0.0415					98.2	0.26	1.503	60.69
	C	1/16	0.1005					49.1	0.26	1.557	30.34
10)	A	1/32	0.285	2.098	0.00524	10.94	1.613	9.92	0.26	2.219	6.22
	B	1/32	0.285					9.92	0.26	2.190	6.22
	C	1/32	0.285					9.92	0.26	2.296	6.22
	D	1/32	0.285					9.92	0.26	2.279	6.22
	F	1/16	0.1005					19.9	0.26	2.013	12.44

TABLE 4 - MOVING MODEL STUDIES

Regression of C_D on Re_2

$M \sim 4$, $T_w/T_o = 1$, QUADRATIC FIT VALID

Linear Fit $\qquad C_D = 0.999 + \dfrac{2.99}{\sqrt{Re_2}}$

Quadratic Fit $\qquad C_D = 1.029 + \dfrac{2.63}{\sqrt{Re_2}} + \dfrac{0.989}{Re_2}$

$M \sim 4$, $T_w/T_o = 0.26$, LINEAR FIT VALID

Linear Fit $\qquad C_D = 1.066 + \dfrac{1.97}{\sqrt{Re_2}}$

Quadratic Fit $\qquad C_D = 0.725 + \dfrac{5.52}{\sqrt{Re_2}} - \dfrac{7.51}{Re_2}$

$M \sim 2$, $T_w/T_o = 1$, LINEAR FIT VALID

Linear Fit $\qquad C_D = 1.143 + \dfrac{2.792}{\sqrt{Re_2}}$

Quadratic Fit $\qquad C_D = 1.594 - \dfrac{1.47}{\sqrt{Re_2}} + \dfrac{8.71}{Re_2}$

$M \sim 2$, $T_w/T_o = 0.26$, LINEAR FIT VALID

Linear Fit $\qquad C_D = 1.100 + \dfrac{2.92}{\sqrt{Re_2}}$

Quadratic Fit $\qquad C_D = 1.104 + \dfrac{2.89}{\sqrt{Re_2}} + \dfrac{0.052}{Re_2}$

$\underline{M \sim 6, \; T_w/T_o = 1,}$ LINEAR FIT VALID

Linear Fit $\qquad C_D = 0.897 + \dfrac{3.18}{\sqrt{Re_2}}$

Quadratic Fit $\qquad C_D = 0.893 + \dfrac{3.25}{\sqrt{Re_2}} - \dfrac{0.22}{Re_2}$

$\underline{M \sim 6, \; T_w/T_o = 0.26,}$ LINEAR FIT VALID

Linear Fit $\qquad C_D = 0.914 + \dfrac{2.52}{\sqrt{Re_2}}$

Quadratic Fit $\qquad C_D = 0.790 + \dfrac{4.63}{\sqrt{Re_2}} - \dfrac{7}{Re_2}$
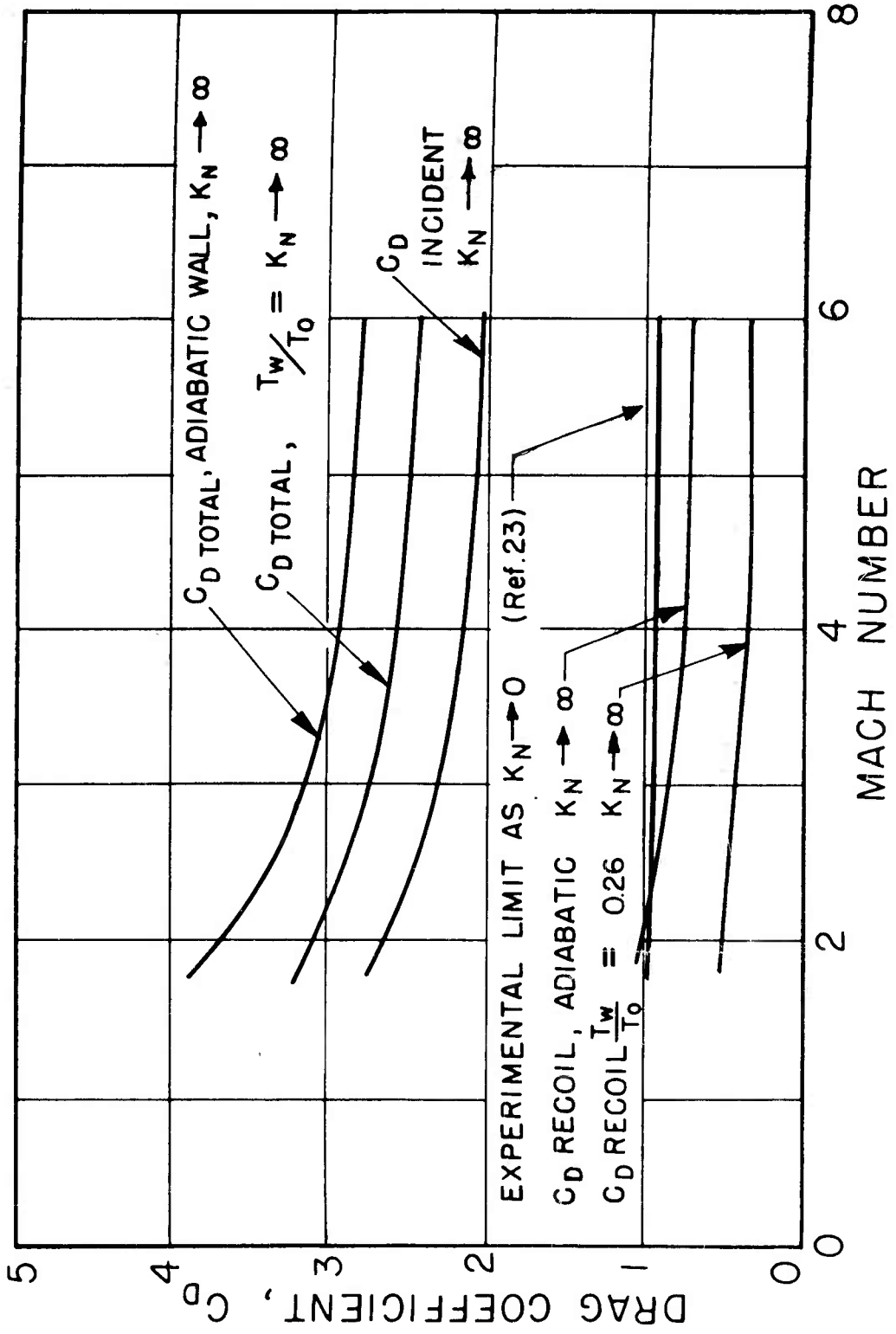
FIG. I SPHERE DRAG COEFFICIENTS IN FREE MOLECULE ($K_N \rightarrow \infty$) AND CONTINUUM LIMIT ($K_N \rightarrow 0$) FOR VALUES OF M AND T_W/T_0 INVESTIGATED DURING PRESENT TESTS (COMPLETELY DIFFUSE REFLECTION)
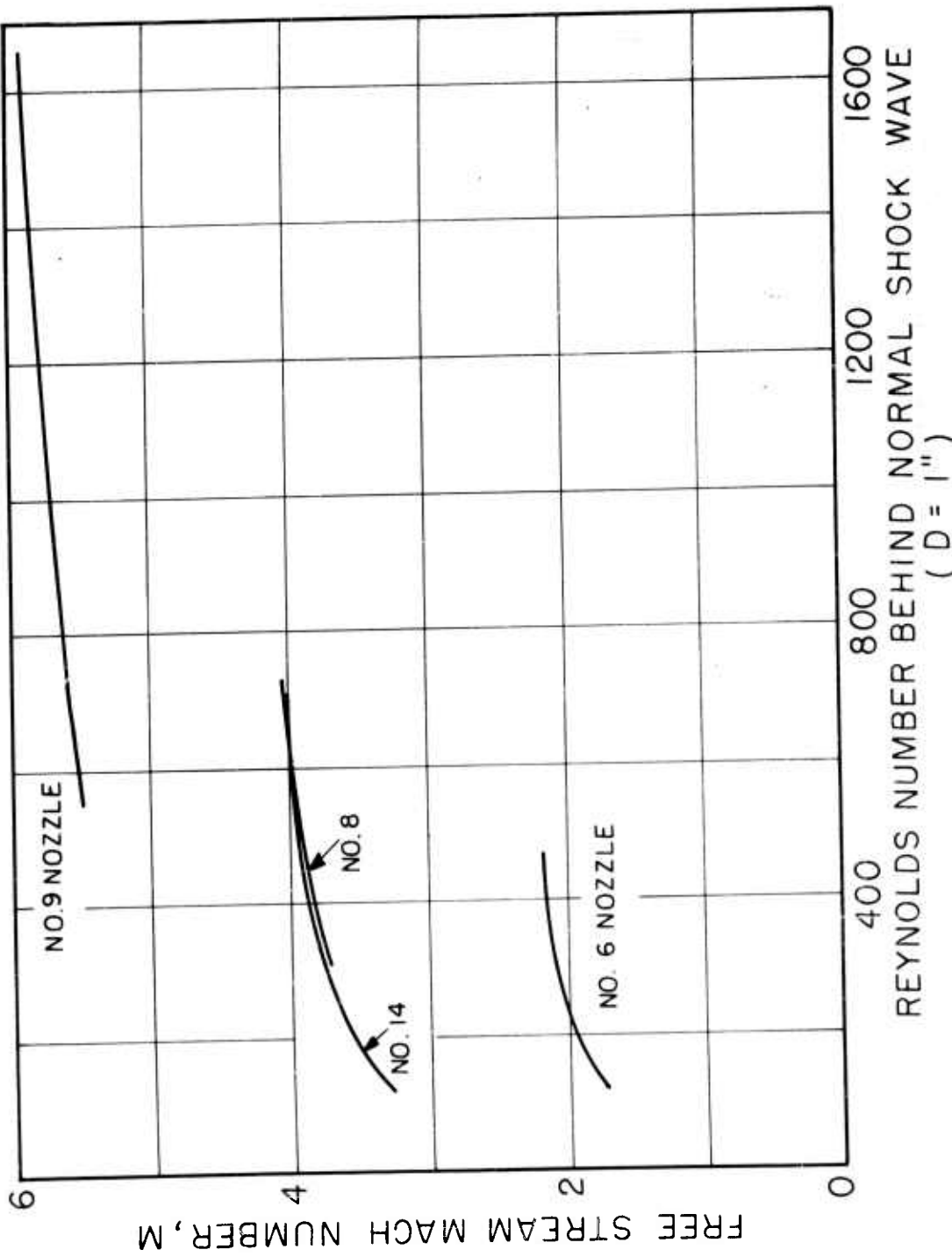
HYD 7621

FIG 2 VARIATION OF FREE STREAM MACH NUMBER WITH Re_2 FOR THE WINDTUNNEL NOZZLES UTILIZED DURING THE PRESENT TESTS

SPHERE MOUNTED ON YOKE

YOKE

LINEAR VARIABLE DIFFERENTIAL TRANSFORMER

BASE

FIXTURE PIVOT

QUARTZ SPRING

PAN TO CALIBRATE SPRINGS

SPRING EXTENSION ARM

DAMPING VANE

MAGNET
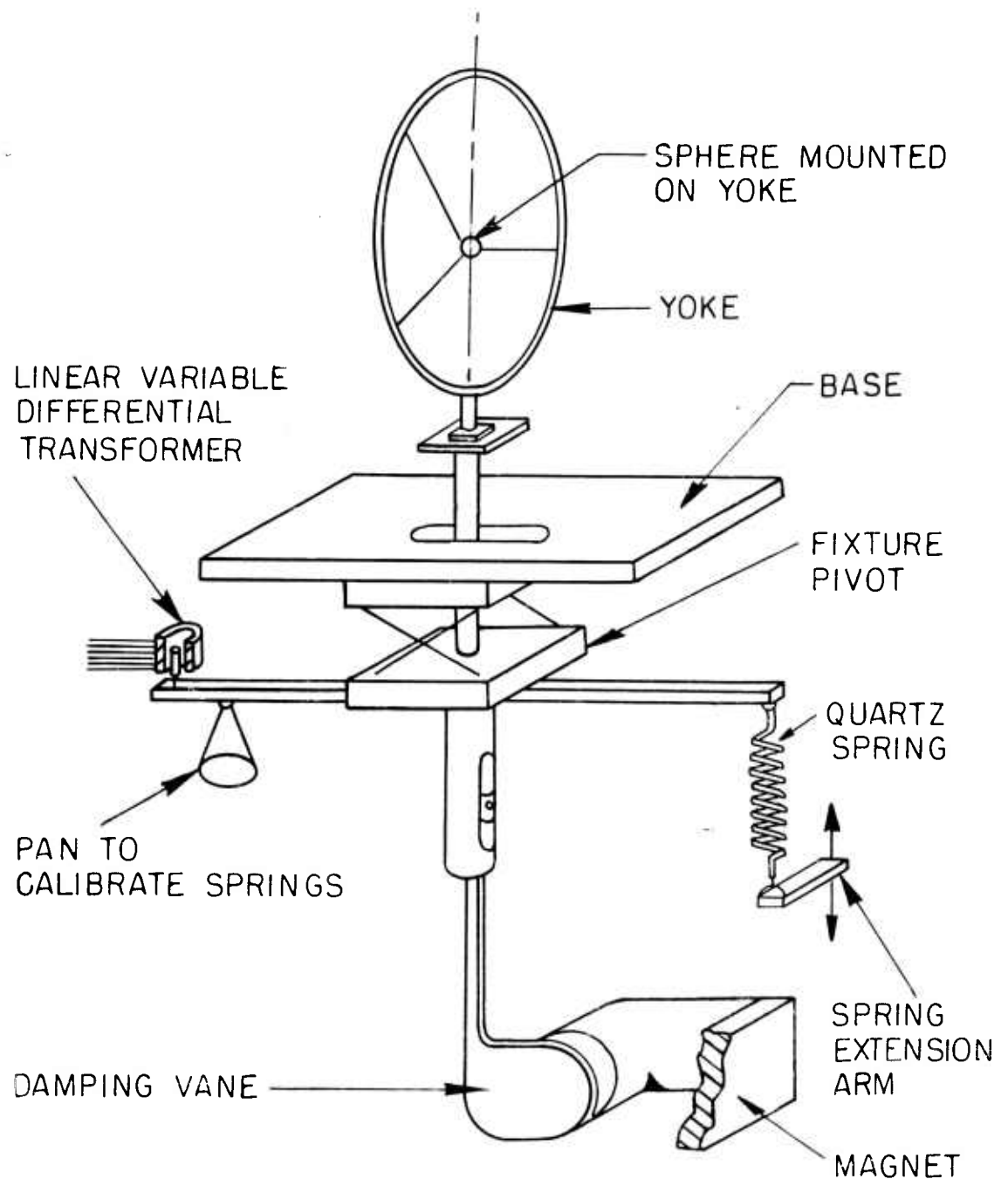
FIG. 3   SCHEMATIC DIAGRAM OF BALANCE

HYD 7623

FIG. 4 MODEL MOUNTED ON YOKE [SHIELDS OFF]
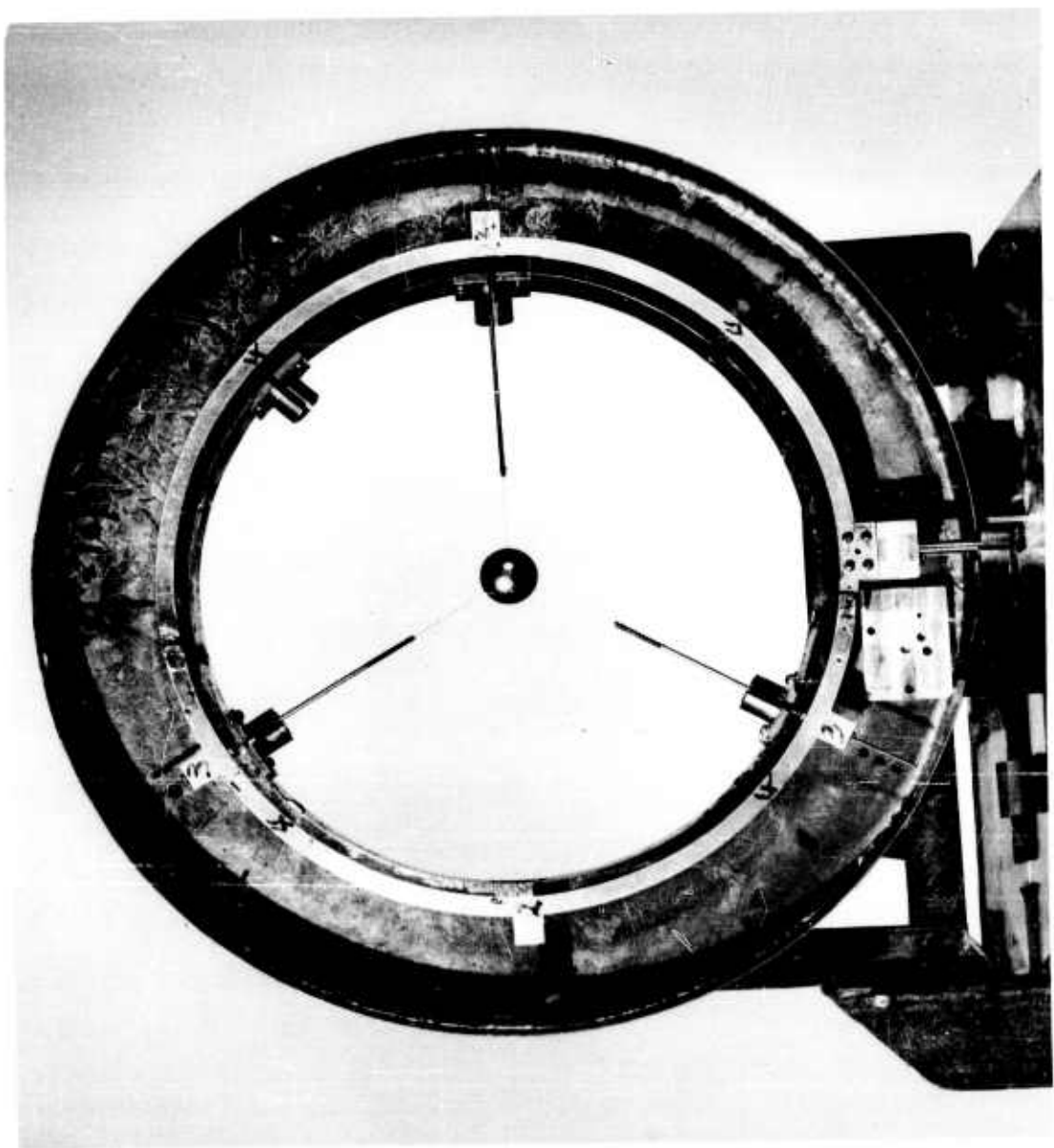
FIG. 5 MODEL MOUNTED ON YOKE [SHIELDS ON]
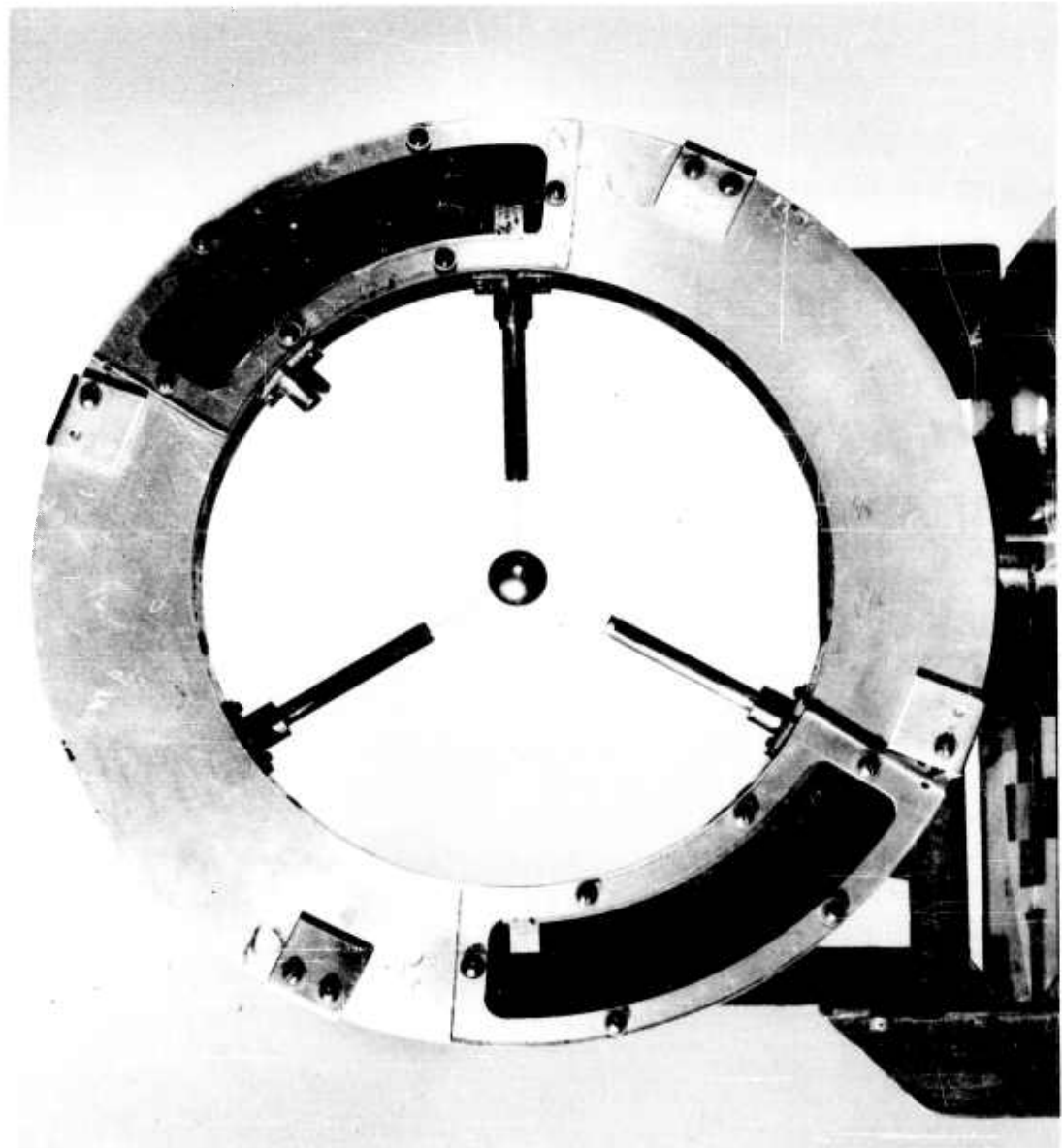
HYD 7625
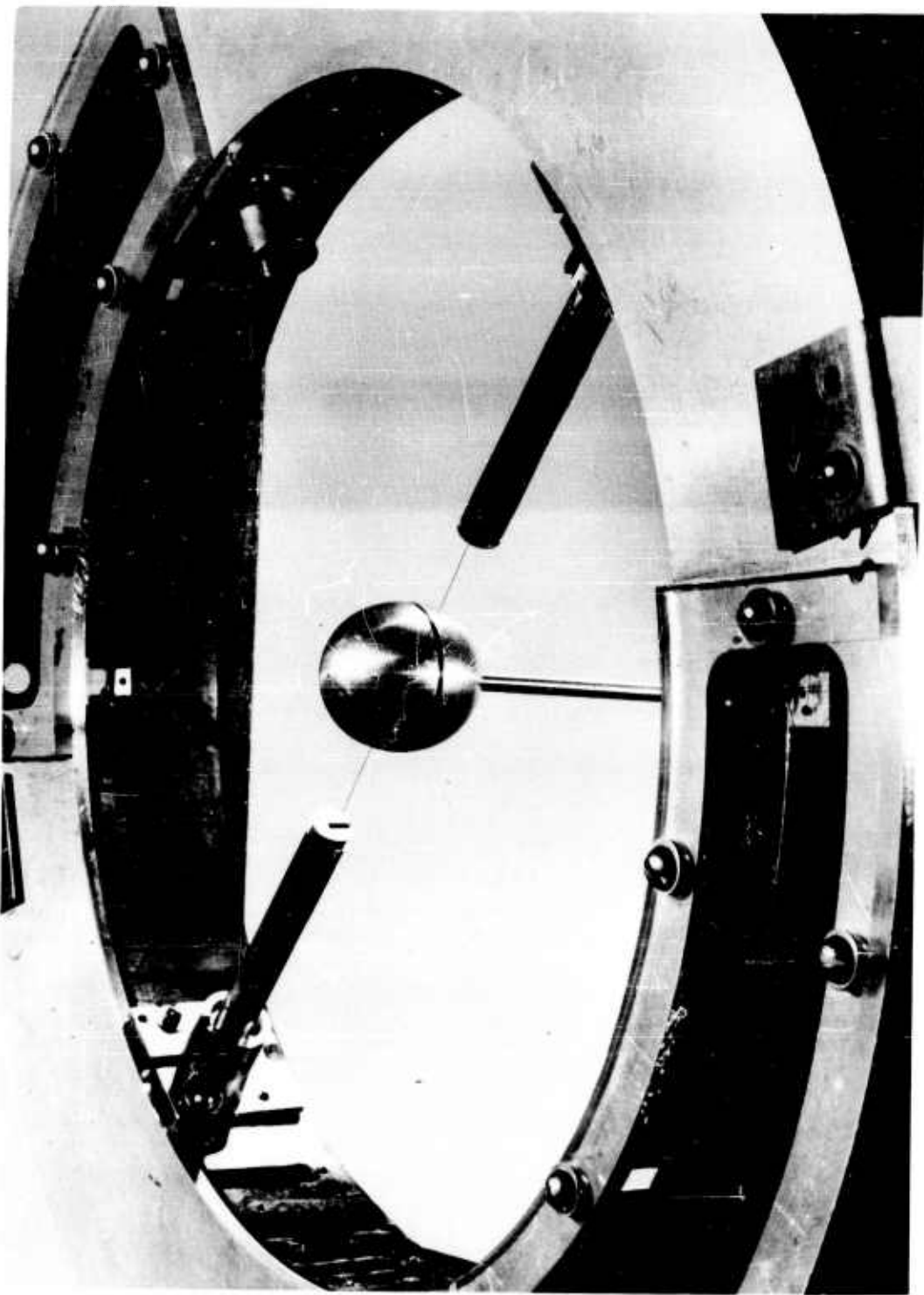
FIG.6 TESTING ARRANGEMENT FOR WIRE
TAPE FORCE MEASUREMENTS

6 LAMPS

SPHERE DISPENSER

COOLANT TUBING

WIND TUNNEL NOZZLE

TRANSLUCENT SCREEN BEHIND JET

WINDOW TUNNEL WINDOW

FASTAX CAMERA
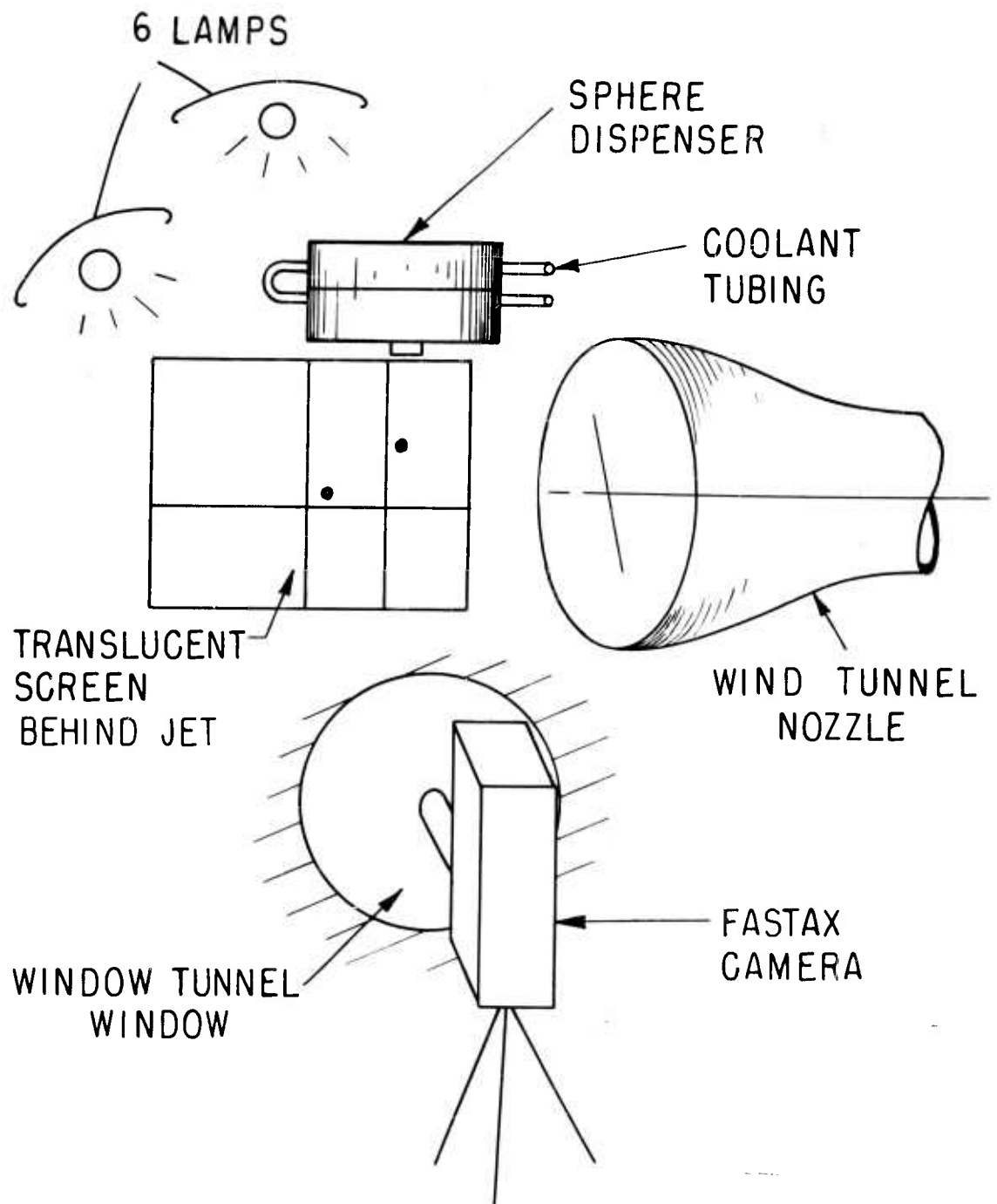
FIG. 7 SCHEMATIC OF TEST APPARATUS FOR MOVING MODEL TESTS

HYD 7627

FIG.8 DETAILS OF CONSTANT TEMPERATURE SPHERE DISPENSER
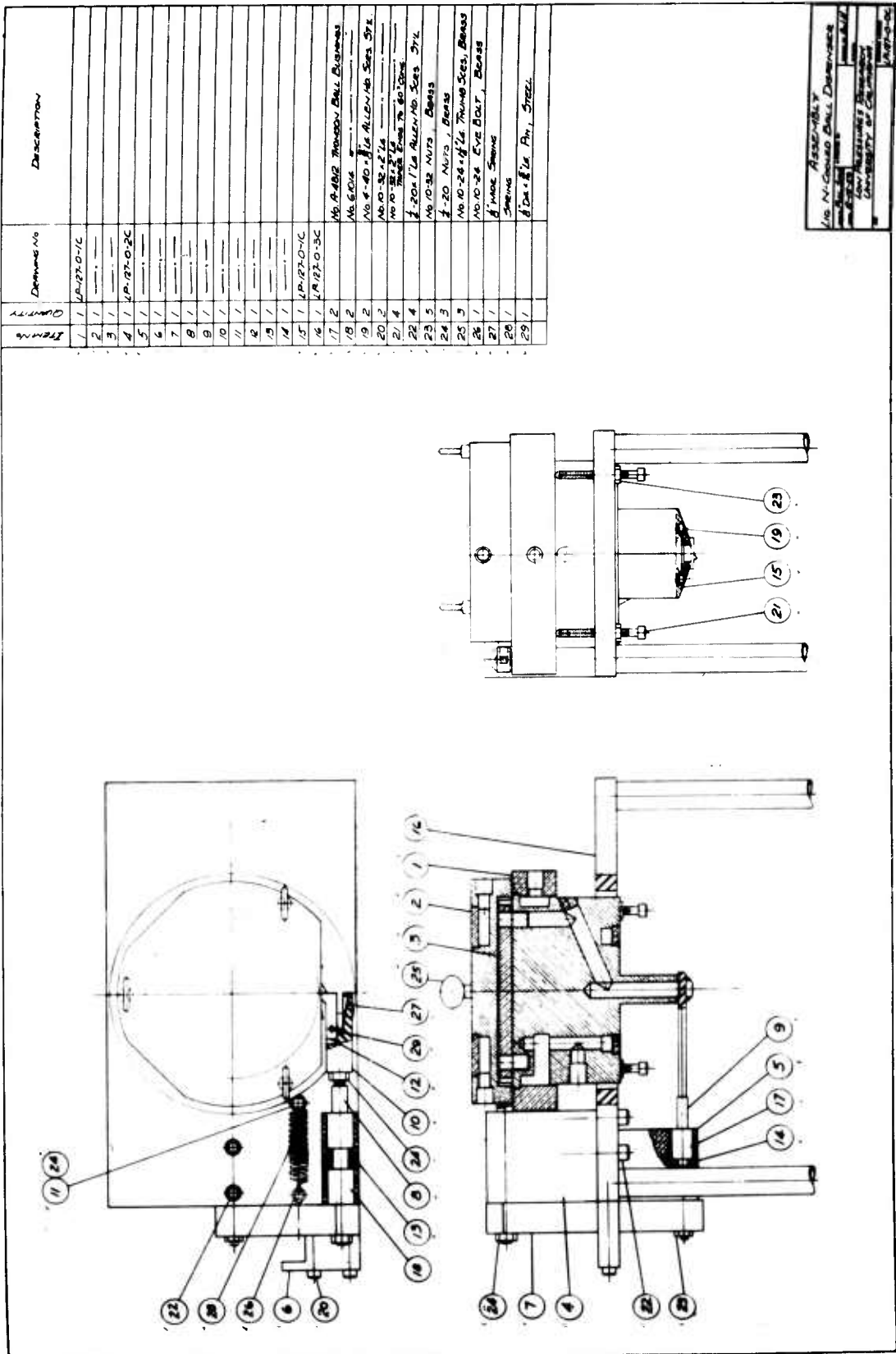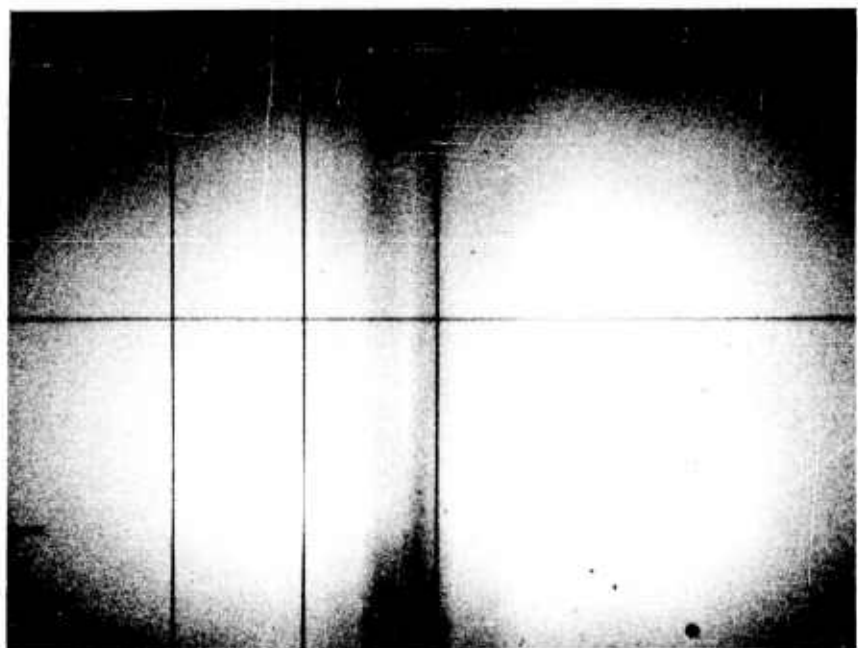
HYD 7628

FIG. 9 ENLARGED PHOTOGRAPH , TYPICAL FRAME
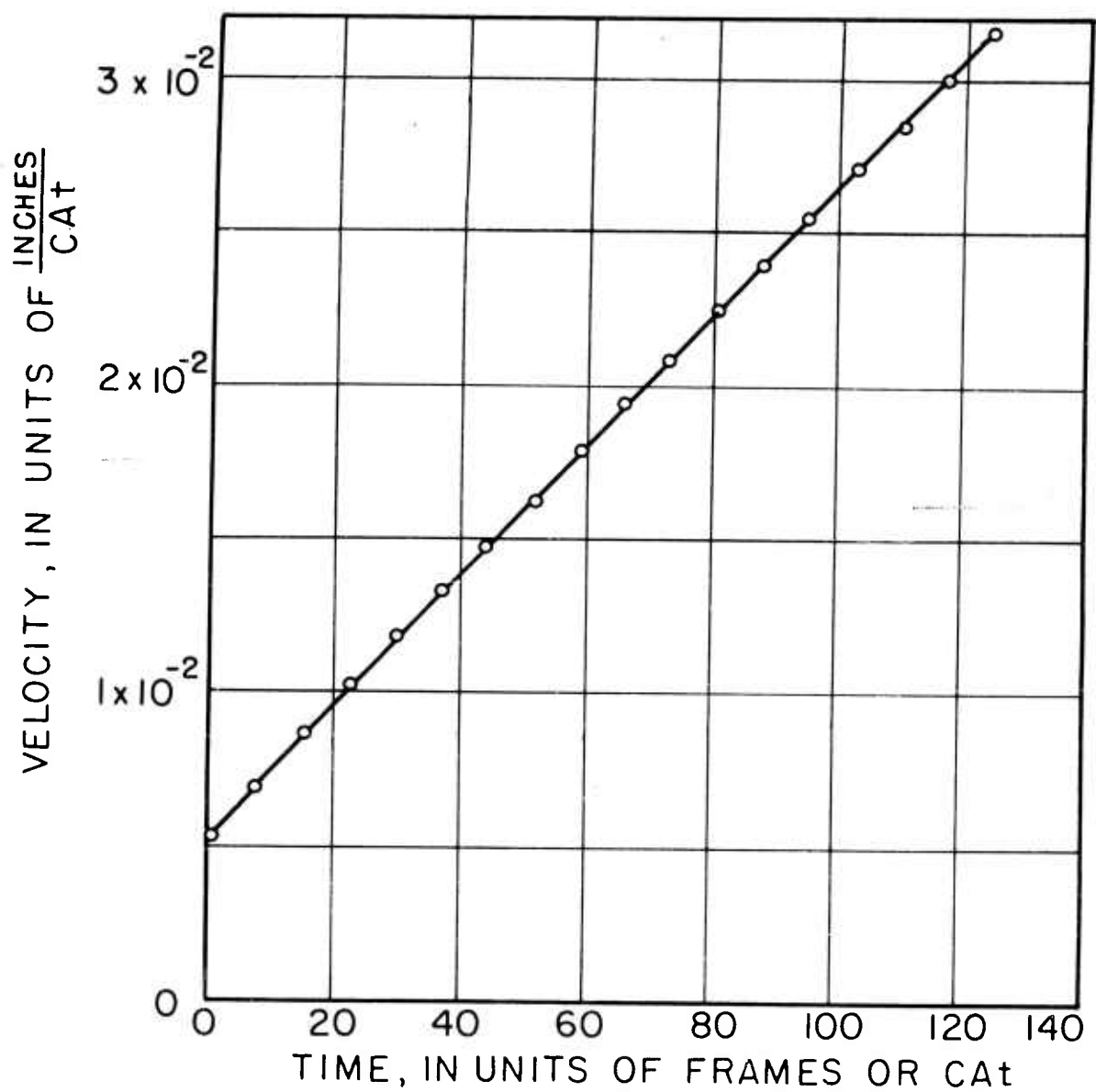
FIG. 10 TYPICAL PLOT OF MODEL VELOCITY vs TIME
RUN 14C
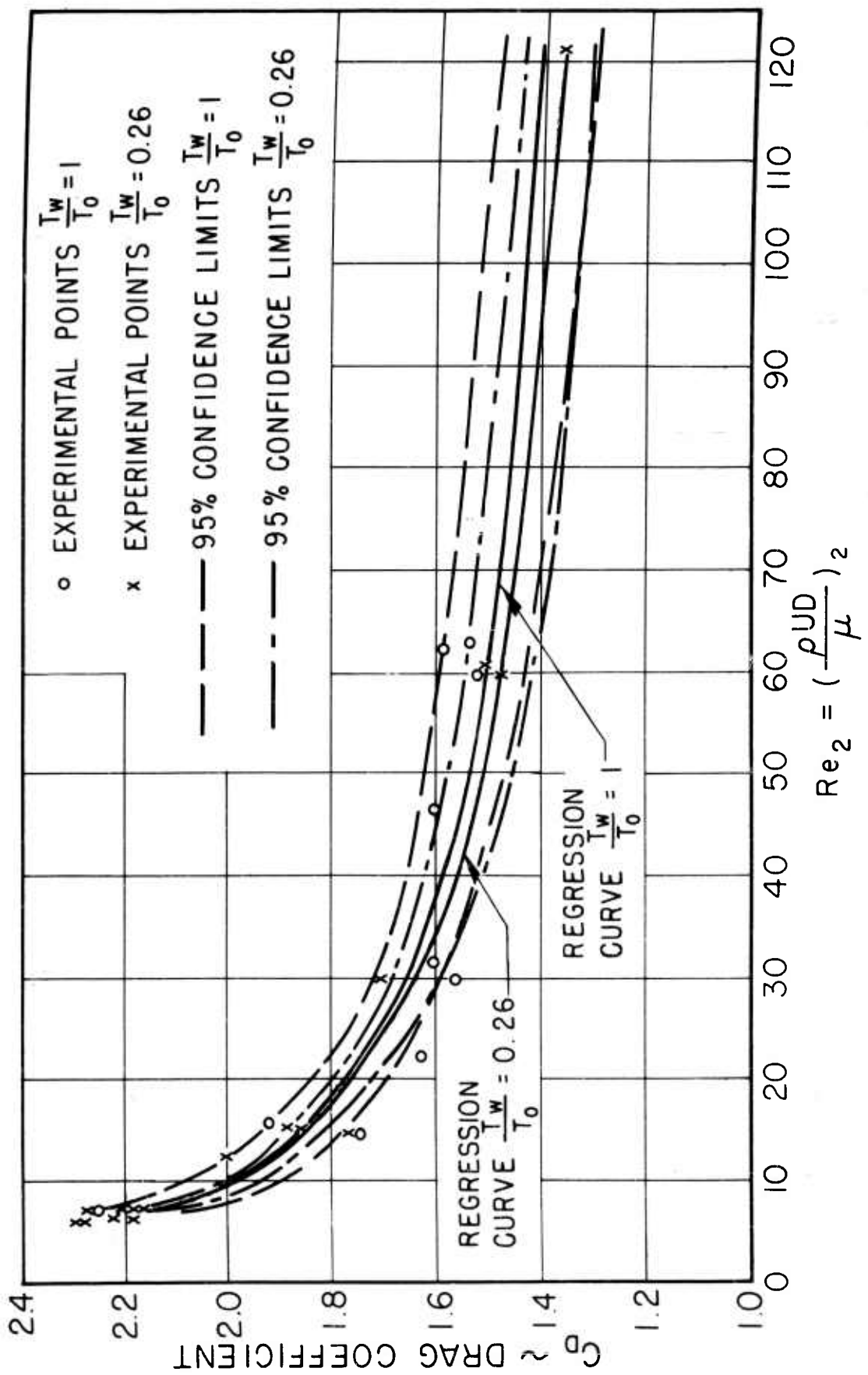
FIG. II SPHERE DRAG COEFFICIENTS AT M~2 AS A FUNCTION OF Re_2 AND $\frac{T_w}{T_o}$ (MOVING MODEL TESTS)

HYD 7631
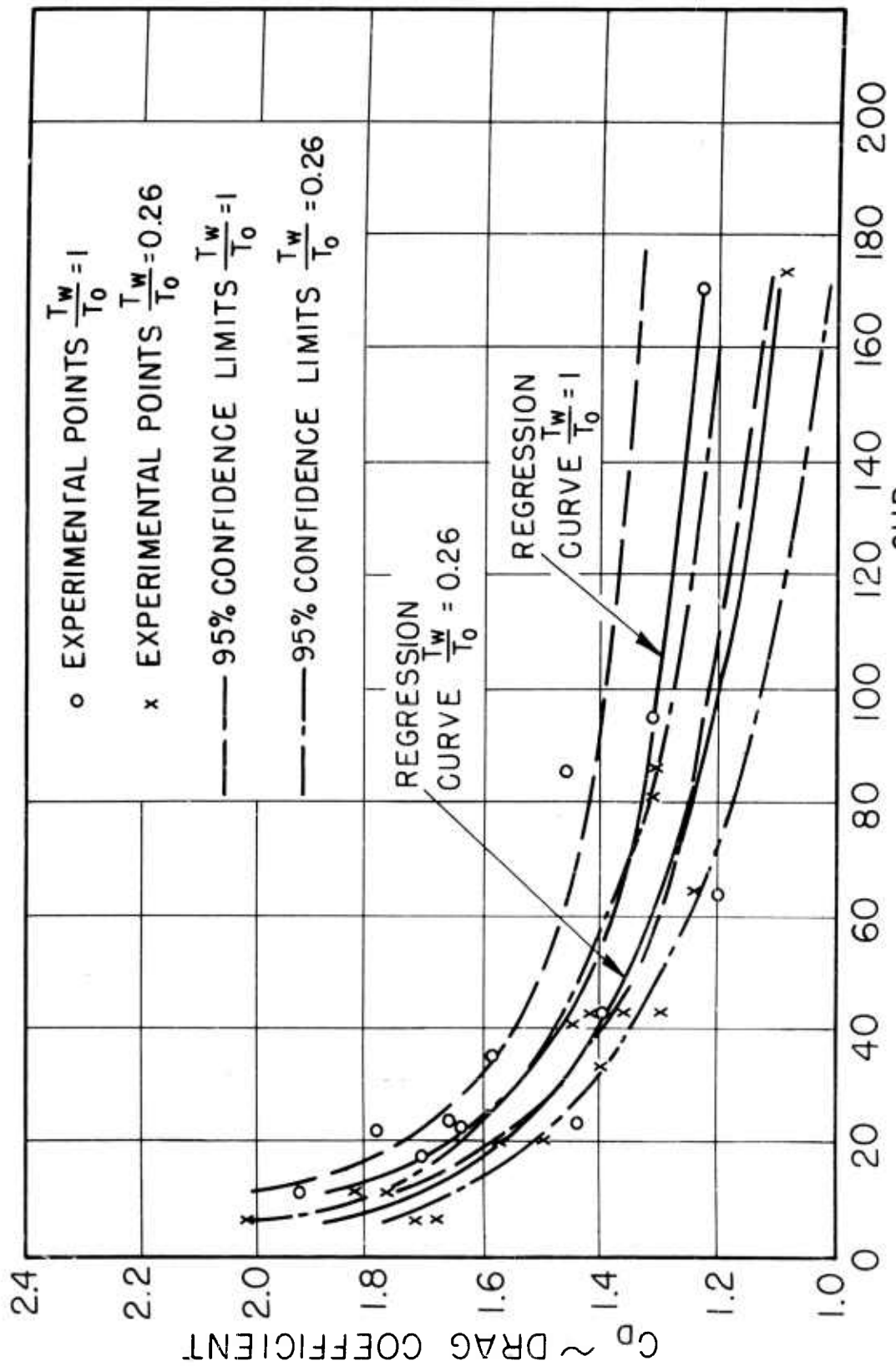
FIG. 12 SPHERE DRAG COEFFICIENTS AT M~4 AS A FUNCTION OF Re_2 AND $\frac{T_w}{T_o}$ (MOVING MODEL TESTS)
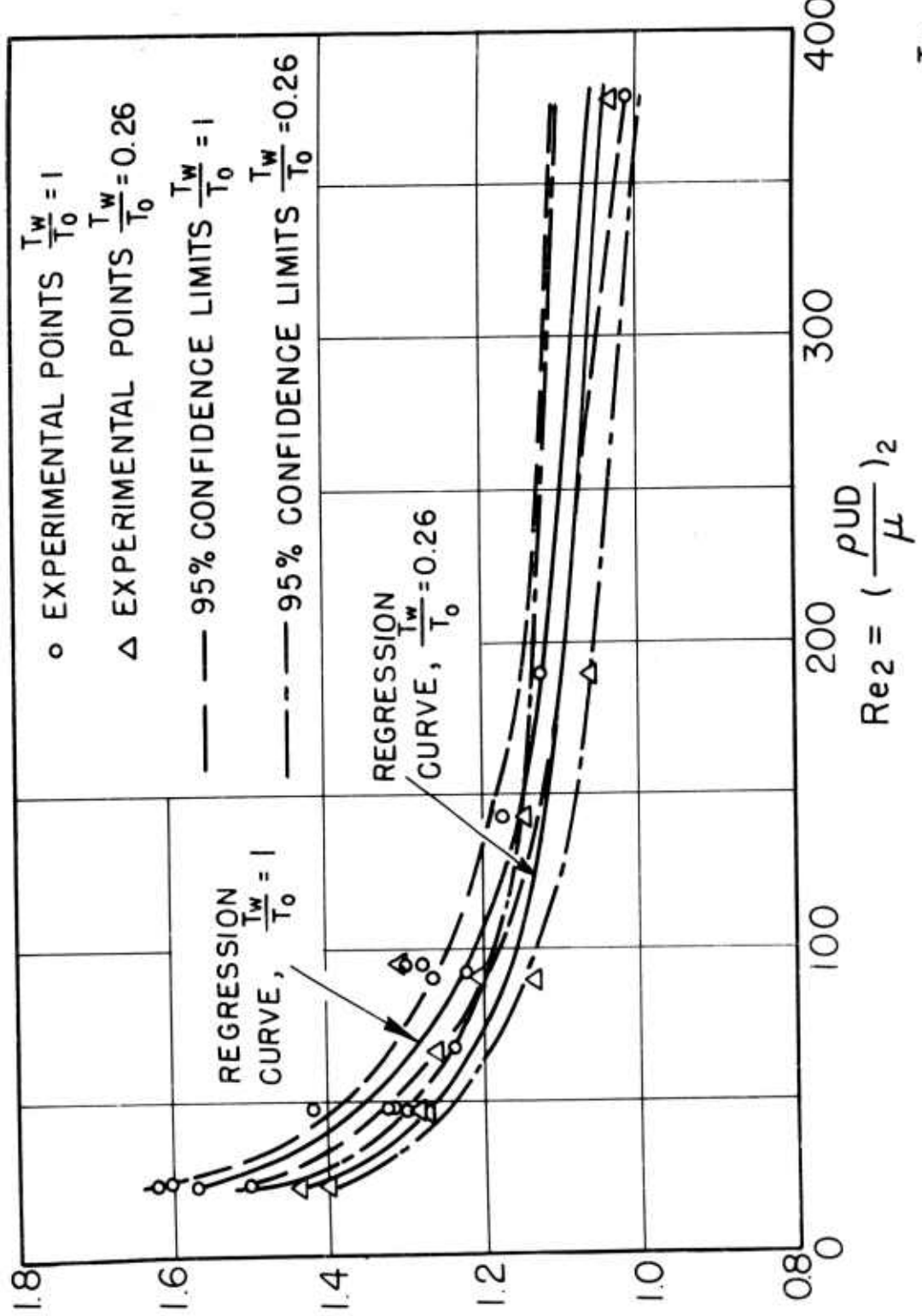
FIG. 13 SPHERE DRAG COEFFICIENTS AT $M \sim 6$ AS A FUNCTION OF Re_2 AND $\frac{T_w}{T_o}$

(MOVING MODEL TESTS)

HYD 7633
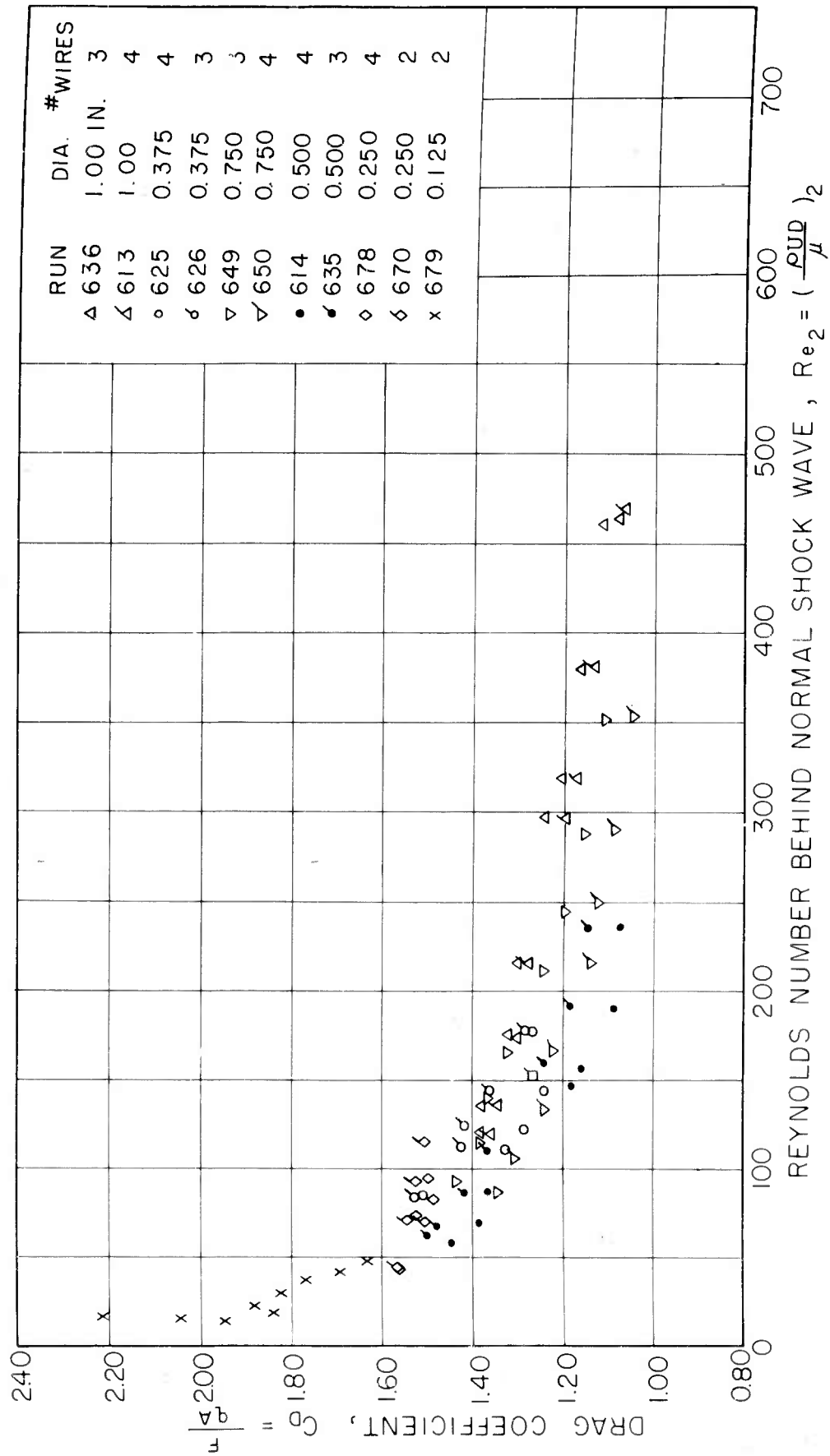
FIG 14 SPHERE DRAG COEFFICIENTS AT M~2 IN AIR [DRAG BALANCE STUDIES]
$\frac{T_w}{T_o} = 1$, No. 6 M~2 NOZZLE

RUN	DIA.	#WIRES
◁ 636	1.00 IN.	3
◁ 613	1.00	4
○ 625	0.375	4
◊ 626	0.375	3
▽ 649	0.750	3
▽ 650	0.750	4
● 614	0.500	4
● 635	0.500	3
◊ 678	0.250	4
◊ 670	0.250	2
× 679	0.125	2

HYD 7634
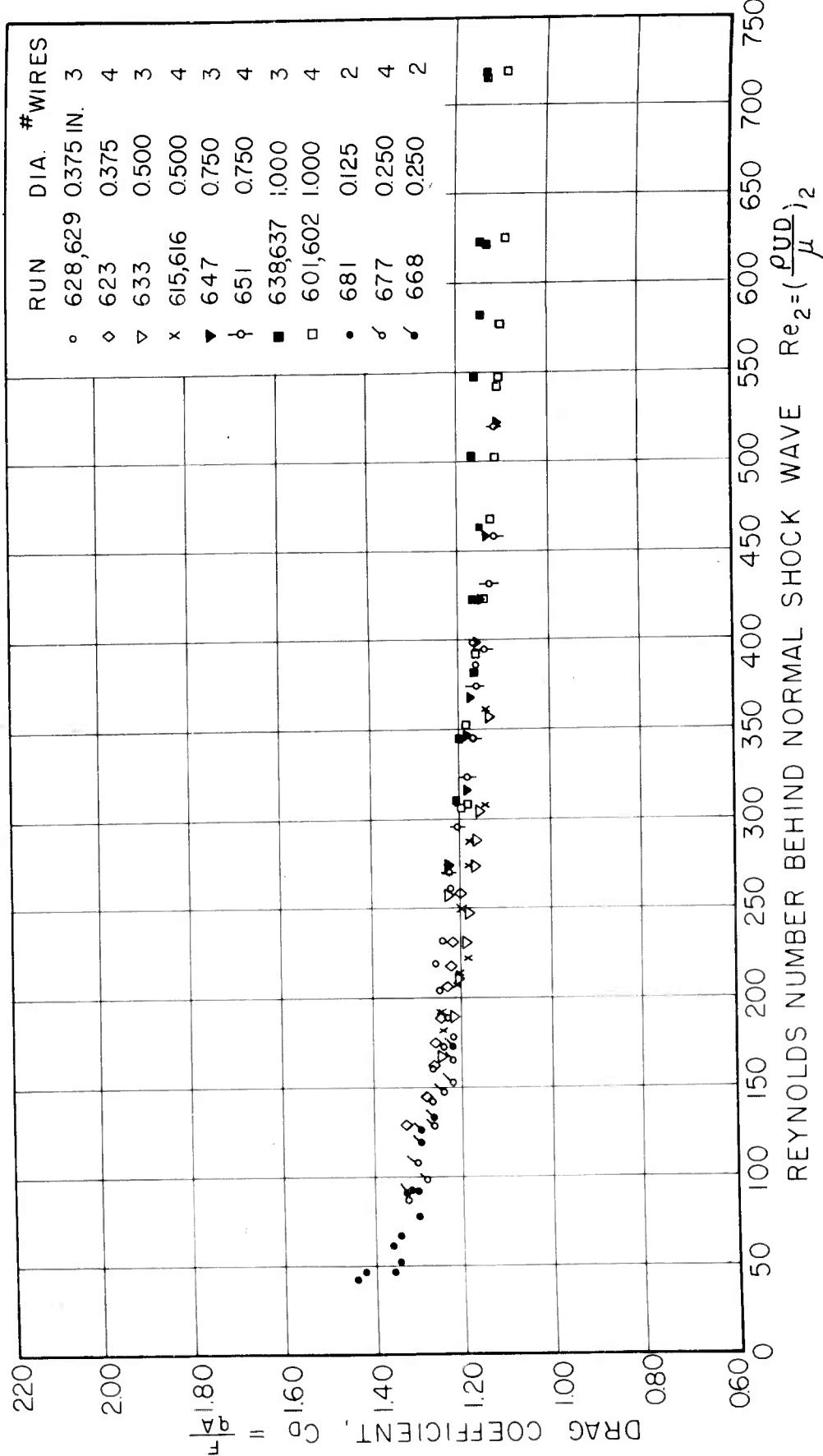
FIG 15 SPHERE DRAG COEFFICIENTS AT M~4 IN AIR [DRAG BALANCE STUDIES]

$\frac{T_w}{T_o} = 1$, No 8 M~4 NOZZLE

HYD 7635
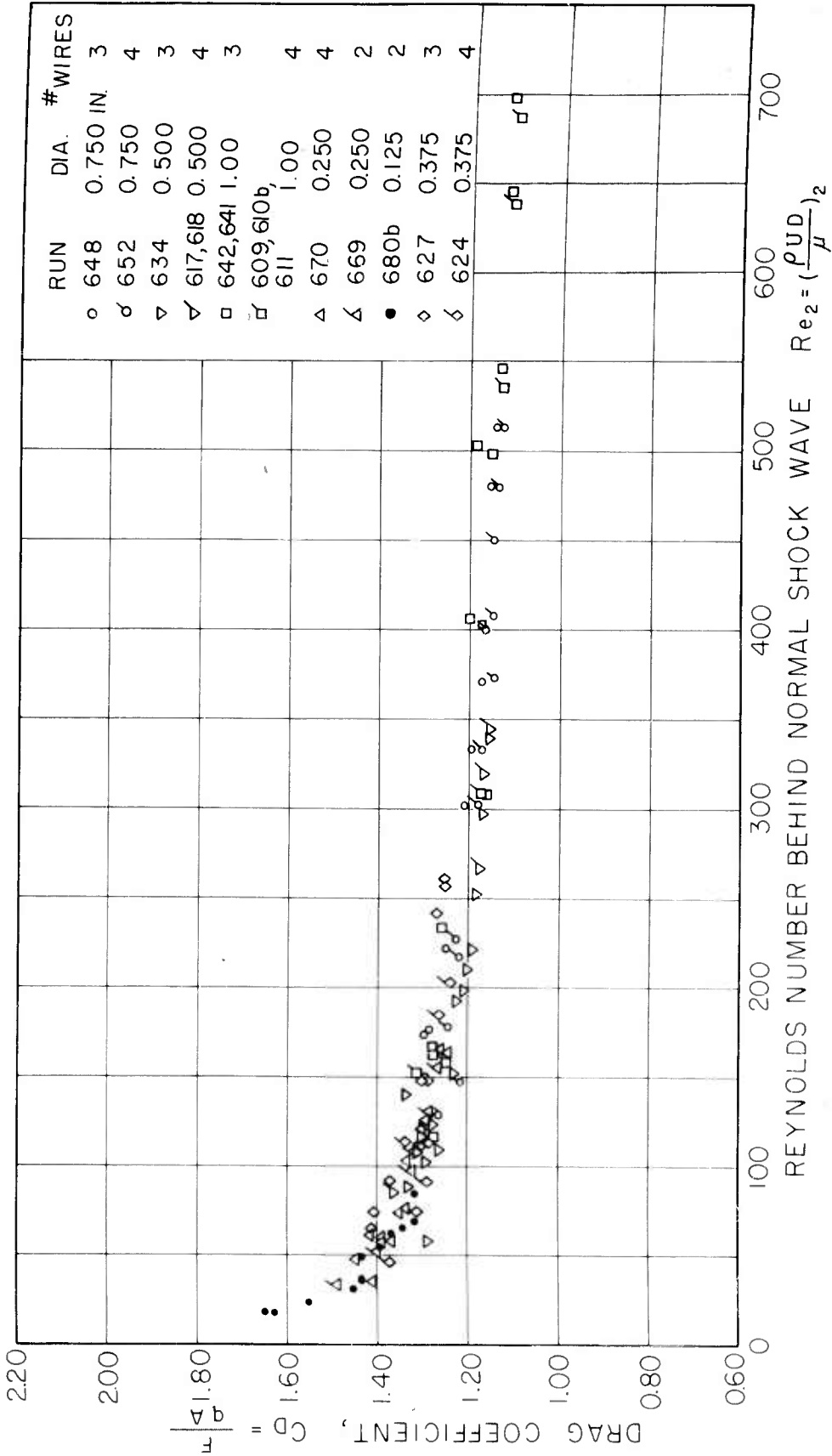
FIG.16 SPHERE DRAG COEFFICIENTS AT M∼4 IN AIR [DRAG BALANCE STUDIES]

$\frac{T_w}{T_o} = 1$, No.14 M∼4 NOZZLE

HYD 7636
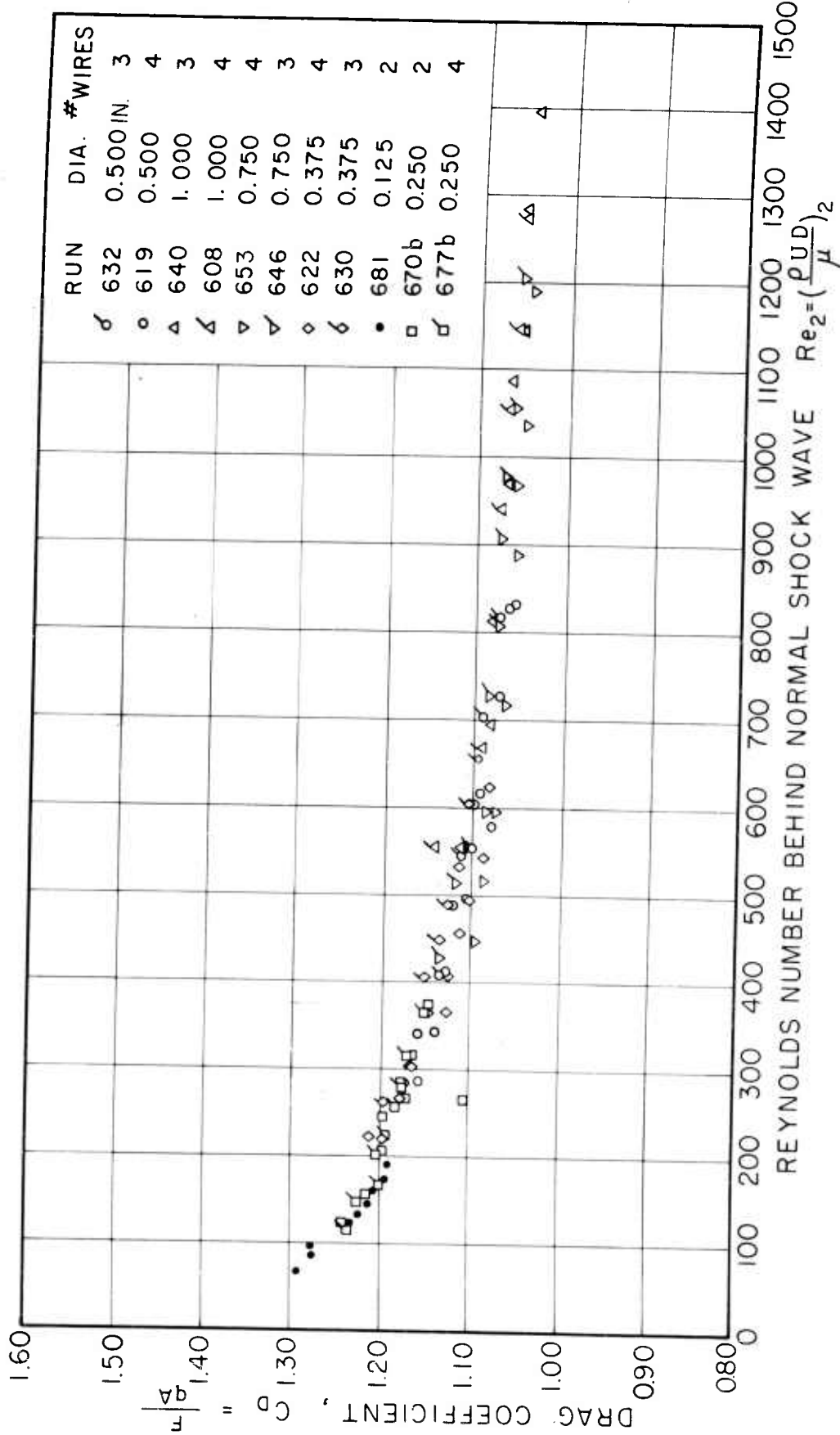
FIG.17 SPHERE DRAG COEFFICIENTS AT M~6 IN AIR [DRAG BALANCE STUDIES]

$\frac{T_w}{T_o} = 1$, No.9 M~6 NOZZLE

REYNOLDS NUMBER BEHIND NORMAL SHOCK WAVE $Re_2 = \left(\frac{\rho UD}{\mu}\right)_2$

DRAG COEFFICIENT, $C_D = \frac{F}{qA}$

	RUN	DIA.	#WIRES
⟆	632	0.500 IN.	3
○	619	0.500	4
◁	640	1.000	3
⟁	608	1.000	4
▷	653	0.750	4
⟐	646	0.750	3
◇	622	0.375	4
⟆	630	0.375	3
●	681	0.125	2
□	670b	0.250	2
⟑	677b	0.250	4
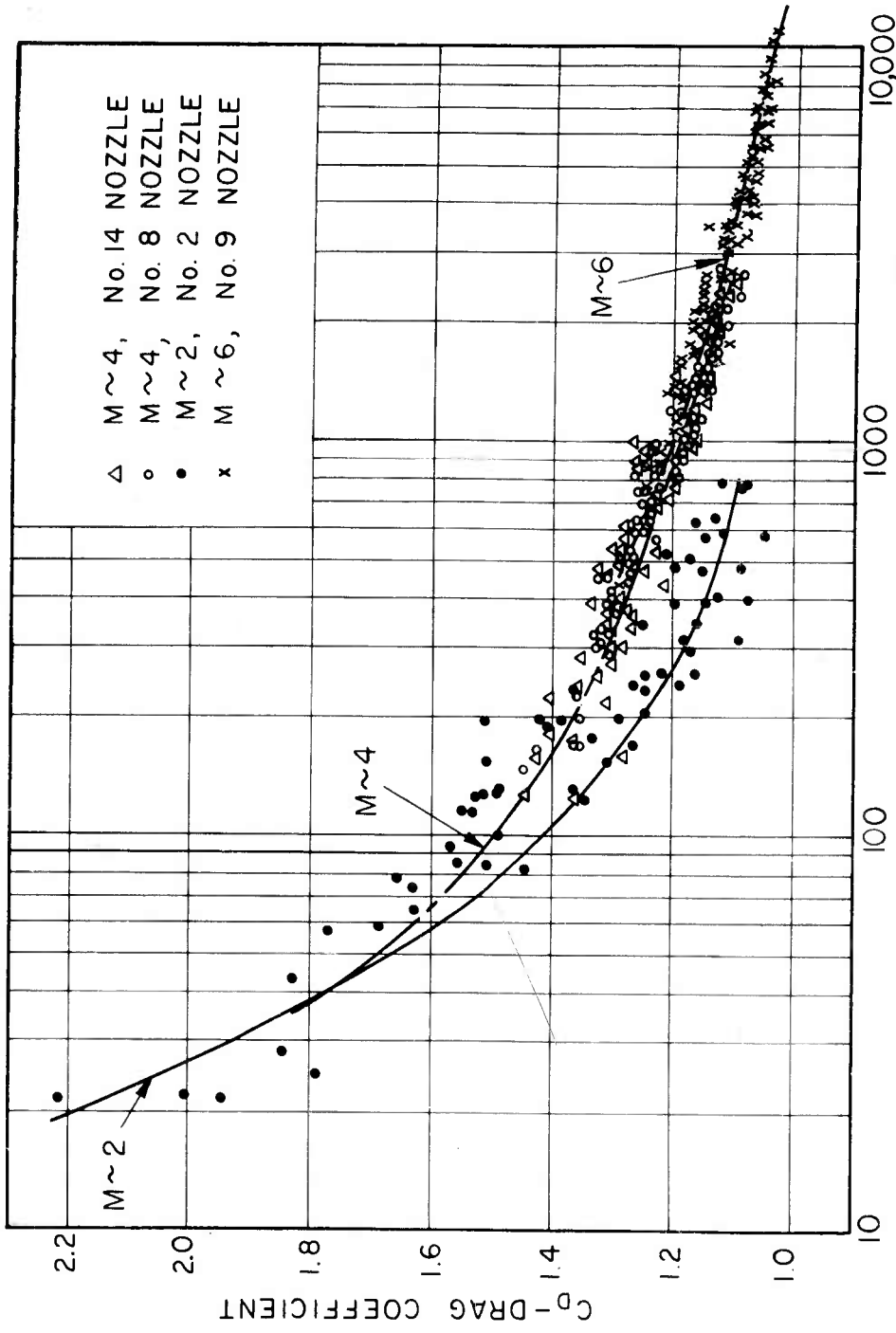
FIG.18 SPHERE DRAG COEFFICIENTS AT M = 2,4,6 AS A FUNCTION OF Re∞

(DRAG BALANCE STUDIES)

FREE STREAM REYNOLDS NUMBER, $Re_\infty = (\frac{\rho UD}{\mu})_\infty$

C_D—DRAG COEFFICIENT

| | M ~ 4, | No. 14 NOZZLE |
△	M ~ 4,	No. 8 NOZZLE
○	M ~ 2,	No. 2 NOZZLE
●	M ~ 6,	No. 9 NOZZLE
×		
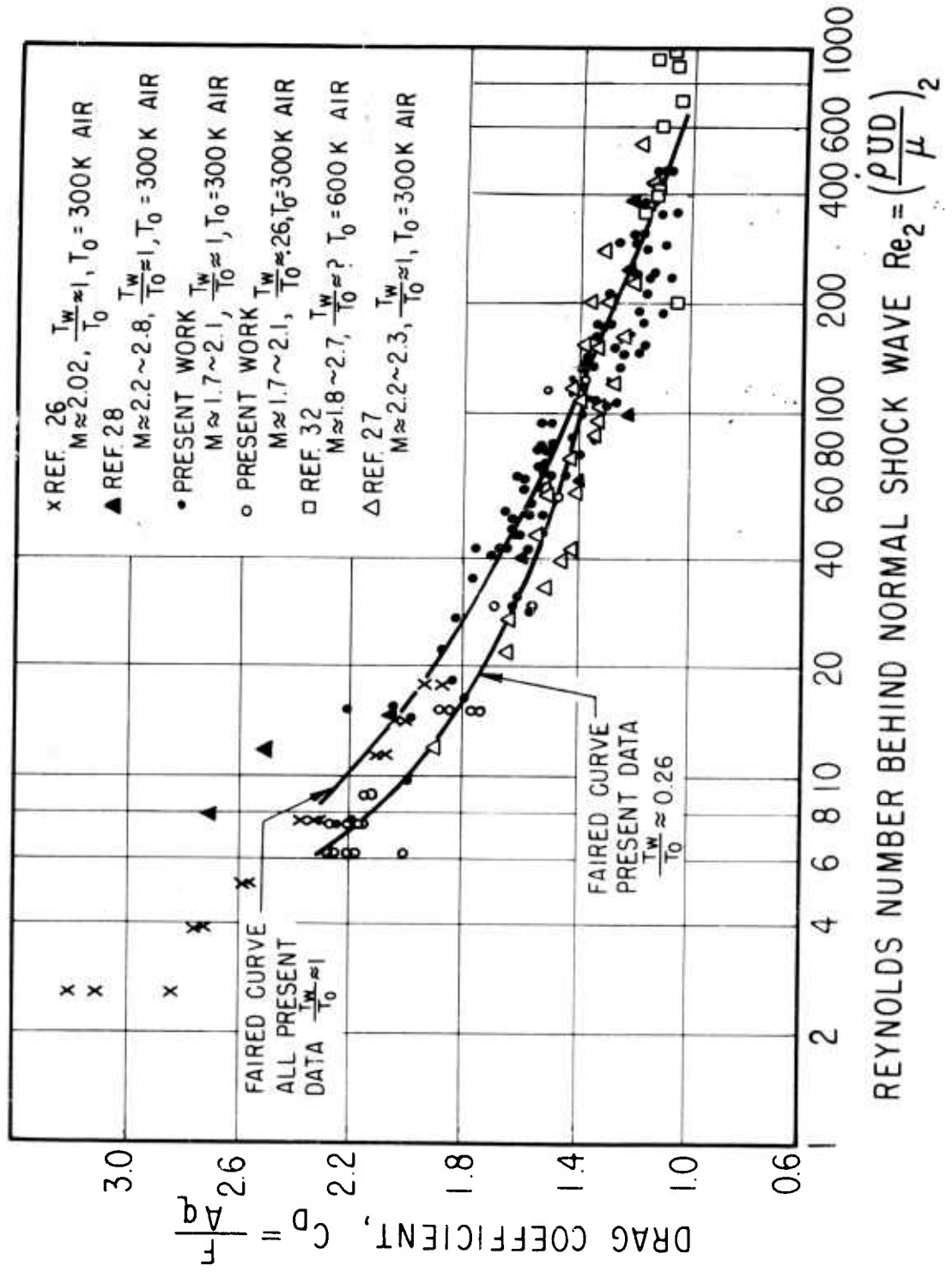
FIG.19 SPHERE DRAG COEFFICIENTS AT M~2

HYD 7639

FIG. 20 SPHERE DRAG COEFFICIENTS AT M ∼ 4

HYD 7640

FIG.21 SPHERE DRAG COEFFICIENTS IN HYPERSONIC FLOW (M > 5)

HYD 7641

NAVY

Chief of Naval Research
Department of the Navy
Washington 25, D. C.
Attn: Code 438   (2)
        Code 419   (1)
        Code 461   (1)

Commanding Officer
Office of Naval Research
Branch Office
150 Causeway Street
Boston, Massachusetts   (1)

Commanding Officer
Office of Naval Research
Branch Office
The John Crerar Library Building
86 East Randolph Street
Chicago 1, Illinois   (1)

Commanding Officer
Office of Naval Research
Branch Office
346 Broadway
New York 13, New York   (1)

Commanding Officer
Office of Naval Research
Branch Office
1030 East Green Street
Pasadena 1, California   (1)

Commanding Officer
Office of Naval Research
Fleet Post Office
Navy No. 100, Box 39
New York, New York   (15)

Commanding Officer
Office of Naval Research
Branch Office
1000 Geary Boulevard
San Francisco 9, California   (2)

Director
Naval Research Laboratory
Washington 25, D. C.
Attn: Code 2021   (6)

Chief, Bureau of Aeronautics
Department of the Navy
Washington 25, D. C.
Attn: Research Division
        Aero & Hydro Branch   (2)

Commanding Officer and Director
David Taylor Model Basin
Carderock, Maryland
Attn: Aerodynamics Laboratory   (1)

Chief, Bureau of Ordnance
Department of the Navy
Washington 25, D. C.
Attn: Code Re 0   (1)
Code Re S1-e   (1)

Commander
Dahlgren Proving Ground
Dahlgren, Virginia
Attn: Technical Library   (1)

Commander
Naval Ordnance Test Station
Inyokern, China Lake, California
Attn: Technical Library   (1)
        Code 501   (1)

Commander
Naval Ordnance Laboratory
White Oak, Maryland
Attn: Hyperballistics Division   (1)
       Aeroballistics Division   (1)
       Aerophysics Division   (1)

Commander
Office of Scientific Research
Air Research & Development Command
P.O. Box 1395
Baltimore 3, Maryland   (1)

Chief, Bureau of Yards & Docks
Department of the Navy
Washington 25, D. C.
Attn: Plans & Research Section   (1)

Superintendent
Naval Postgraduate School
Monterey, California   (1)

NAVY (cont'd)

U.S. Naval Air Material Test Center
Point Mugu, California
Attn: Chief Scientist   (1)

AIR FORCE

Commander
AF Office of Scientific Research
Washington 25, D. C.
Attn: Mechanics Division   (1)

Director
Office for Advanced Studies
AF Office of Scientific Research
Box 2035
Pasadena 2, California   (1)

Commander
Western Development Division
Air Research & Development Command
P. O. Box 262
Inglewood, California   (1)

Commander
Air Force Cambridge Research Center
230 Albany Street
Cambridge-39, Massachusetts
Attn: Geo-Phys. Research
          Library   (1)

Commander
AF Missile Test Center
(AFMTC Tech Library MU-135)
Patrick AFB, Florida   (1)

Arnold Engineering Development
          Center Library
P. O. Box 162
Tullahoma, Tennessee
Attn: Dr. J. Lukasiewicz   (2)

Commander
Wright Air Development Center
Wright-Patterson Air Force Base
Dayton, Ohio
Attn: Aeronautical Research Lab   (1)
          Aircraft Laboratory   (1)

ARMY

Office of Ordnance Research
Department of the Army
Duke Station
Durham, North Carolina   (1)

Ballistics Research Laboratory
Aberdeen Proving Ground
Aberdeen, Maryland
Attn: Dr. R. H. Kent   (1)
          Dr. F. D. Bennett   (1)

Internal Ballistics Laboratory
Aberdeen Proving Ground
Aberdeen, Maryland
Attn: Dr. J. H. Frazer   (1)

Commanding General
Redstone Arsenal, U.S.Army
Redstone Arsenal, Alabama
Attn: Technical Library   (1)

NASA

Director of Research
National Aeronautics and Space
          Administration
1512 H Street, N.W.
Washington 25, D. C.   (5)

Director
Langley Research Center, NASA
Langley Field
Hampton, Virginia   (1)

Director
Ames Research Center, NASA
Moffett Field, California   (1)

Director
Lewis Research Center, NASA
21000 Brookpark Road
Cleveland 35, Ohio   (1)

Western Coordination Office
National Aeronautics and Space
          Administration
7660 Beverly Boulevard
Los Angeles, California   (1)

DEPARTMENT OF DEFENSE

Chief
Armed Forces Special Weapons Project
P. O. Box 2610
Washington 25, D. C.   (1)

Executive Secretary
Weapons System Evaluation Group
Office of Secretary of Defense
The Pentagon
Washington 25, D. C.   (1)

OTHER GOVERNMENT AGENCIES

Director
National Bureau of Standards
Washington 25, D. C.
Attn: Fluid Mechanics Section   (1)
        Electron Physics Section   (1)

U.S. Atomic Energy Commission
Technical Information Service
Washington 25, D. C.
Attn: Technical Librarian   (1)

National Science Foundation
Division of Mathematical, Physical
    and Engineering Sciences
Washington 25, D. C.   (1)

Documents Service Center
Armed Services Technical
    Information Agency
Arlington Hall Station
Arlington 12, Virginia   (10)

Office of Technical Services
Department of Commerce
Washington 25, D. C.   (1)

EDUCATIONAL INSTITUTIONS

Prof. R. F. Probstein
Division of Engineering
Brown University
Providence 12, Rhode Island   (1)

Aeronautical Laboratory
Division of Engineering
Brown University
Providence 12, Rhode Island
Attn.: Dr. Maeder   (1)

Metcalf Laboratory
Brown University
Providence 12, Rhode Island
Attn: Prof. D. F. Hornig   (1)

Los Alamos Scientific Laboratory
University of California
Los Alamos, New Mexico
Attn: Theoretical Division,
        Dr. J. L. Tuck   (1)
        Dr. R. G. Shreffler   (1)
        J-1 Division,
        Drs. Duff and Graves   (1)

Jet Propulsion Laboratory
California Institute of Technology
Pasadena 4, California
Attn: Dr. P. Wegener   (1)

Guggenheim Aeronautical Laboratory
California Institute of Technology
Pasadena 4, California
Attn: Prof. C.B.Millikan, Director (1)
        Prof. Lester Lees   (1)
        Prof. H. W. Liepmann   (1)
        Prof. J. Cole   (1)

Department of Physics
California Institute of Technology
Pasadena 4, California
Attn: Prof. F. Zwicky   (1)

Radiation Laboratory
University of California
Livermore, California
Attn: Dr. S. A. Colgate   (1)
        Dr. R. Post   (1)

Department of Aerodynamics
Case Institute of Technology
Cleveland 6, Ohio
Attn: Prof. G. Kuerti   (1)

Yerkes Observatory
University of Chicago
Williams Bay, Wisconsin
Attn: Prof. S. Chandrasekhar   (1)

Graduate School of Aeronautical
    Engineering
Cornell University
Ithaca, New York
Attn: Prof. W. Sears   (1)
        Prof. E. L. Resler, Jr.   (1)

EDUCATIONAL INSTITUTIONS -(Cont'd)

Cornell Aeronautical Laboratory
4455 Genessee Street
Buffalo, New York
Attn: Dr. A. Hertzberg   (1)

Department of Engineering Sciences
Harvard University
Cambridge 38, Massachusetts
Attn: Prof. G. Carrier   (1)
      Prof. H. Emmons   (1)

Harvard Observatory
Harvard University
Cambridge, Massachusetts
Attn: Prof. F. Whipple   (1)

Dr. H. Kendall Reynolds
Physics Department
The University of Houston
3801 Cullen Boulevard
Houston 4, Texas   (1)

Department of Aeronautical Engineering
University of Illinois
Urbana, Illinois
Attn: Prof. H. S. Stillwell,
      Chairman   (1)

Armour Research Foundation
Illinois Institute of Technology
Chicago 16, Illinois   (1)

Applied Physics Laboratory
Johns Hopkins University
P.O. Box 244 - Rt. 1
Laurel, Maryland
Attn: Dr. F. N. Frenkiel
      Technical Reports Office   (2)

Department of Physics
Lehigh University
Bethlehem, Pennsylvania
Attn: Prof. R. J. Emrich   (1)

Institute for Fluid Mechanics
      and Applied Mathematics
University of Maryland
College Park, Maryland
Attn: Prof. Burgers   (1)

Department of Aeronautics
Johns Hopkins University
Baltimore 18, Maryland
Attn: Prof. F. H. Clauser   (1)

Department of Aeronautical Engineering
Massachusetts Institute of Technology
Cambridge 39, Massachusetts
Attn: Prof. H. G. Stever   (1)
      Prof. L. Trilling   (1)

Department of Mathematics
Massachusetts Institute of Technology
Cambridge 39, Massachusetts
Attn: Prof. C. C. Lin   (1)

Department of Mechanical Engineering
Massachusetts Institute of Technology
Cambridge 39, Massachusetts
Attn: Prof. J. Kaye   (1)

Department of Aeronautical Engineering
University of Michigan
Ann Arbor, Michigan
Attn: Prof. O. Laporte   (1)
      Prof. G. Uhlenbeck   (1)

Department of Astronomy
University of Michigan
Ann Arbor, Michigan
Attn: Prof. L. Goldberg   (1)

Department of Aeronautical Engineering
University of Minnesota
Minneapolis, Minnesota
Attn: Prof. J.D.Akerman,Chairman (1)

Institute of Meteoritics
University of New Mexico
Albuquerque, New Mexico
Attn: Prof. L. LaPaz   (1)

Institute for Mathematics and Mechanics
New York University
25 Waverly Place
New York 3, New York
Attn: Prof. R. Courant, Director (1)
      Prof. J. Stoker   (1)

Guggenheim School of Aeronautics
New York University
New York 53, New York
Attn: Prof. J.F. Ludloff   (1)

Department of Mechanical Engineering
Northwestern University
Evanston, Illinois
Attn: Prof. A. B. Cambel   (1)

EDUCATIONAL INSTITUTIONS -(Cont'd)

Department of Physics
University of Oklahoma
Norman, Oklahoma
Attn: R.G.Fowler   (1)

Dr. Loren E. Bollinger
The Ohio State University
Rocket Research Laboratory
2240 Olentangy River Road
Columbus 10, Ohio   (1)

Aerodynamics Laboratory
Polytechnic Institute of Brooklyn
Freeport, L.I., New York
Attn: Prof. A. Ferri   (1)

Palmer Physical Laboratory
Princeton University
Princeton, New Jersey
Attn: Prof. W. Bleakney   (1)
       Prof. W.C.Griffith   (1)

Princeton University
The James Forrestal Research Center
Princeton, New Jersey
Attn: Prof.S.M.Bogdonoff, Bldg.D (1)

Princeton University
The James Forrestal Research Center
Princeton, New Jersey
Attn: Prof.W.D.Hayes, Sayre Hall (1)

Princeton University Observatory
Princeton, New Jersey
Attn: Prof. L. Spitzer, Jr.   (1)

Department of Aeronautical Engineering
Rennselaer Polytechnic Institute
Troy, New York
Attn: Profs. Harrington & Foa   (1)

Engineering Center
University of Southern California
University Park
Los Angeles 7, California
Attn: Drs.R.Chuan & C.L.Daily   (1)

Guggenheim Aeronautical Laboratory
Stanford University
Standord, California
Attn: Prof. W. Vincenti   (1)

Defense Research Laboratory
University of Texas
P. O. Box 8029
Austin, Texas
Attn: M.J.Thompson   (1)

College of Engineering
University of California, Los Angeles
Los Angeles 24, California
Attn: Dean L.M.K. Boelter   (1)

Department of Physics
University of California, Los Angeles
Los Angeles 24, California
Attn: Prof. J. Kaplan   (1)

Experimental Research Group
University of Utah
Salt Lake City, Utah
Attn: Prof. M.A.Cook, Cirector   (1)

Department of Aeronautical Engineering
University of Washington
Seattle 5, Washington
Attn: Department Librarian   (1)

Department of Chemistry
University of Wisconsin
Madison, Wisconsin
Attn: Prof. J.O.Hirschfelder   (1)

Sterling Chemistry Laboratory
Yale University
New Haven, Connecticut
Attn: Prof. J.G.Kirkwood   (1)

CANADA

Institute of Aerophysics
University of Toronto
Toronto 5, Canada
Attn: Dr.G.N.Patterson, Director   (1)

Division of Mechanical Engineering
National Research Laboratories
Ottawa, Canada
Attn: Dr. K. Orlik, Dr. Ruckemann   (1)

United Aircraft Corporation
Research Department
362 Main Street
East Hartford 8, Connecticut   (1)

INDUSTRIAL ORGANIZATIONS

Aerojet Engineering Corporation
6352 North Irwindale Avenue
Box 296
Azusa, California   (1)

ARO, Inc.
Tullahoma, Tennessee
Attn: Drs. R.W.Perry & R.Smelt   (1)

Miss Spence, Librarian
AVCO Manufacturing Company
Research Laboratories
2385 Revere Beach Parkway
Everett 49, Massachusetts
Attn: Drs. Kantrowitz & Lin   (2)

AVCO Manufacturing Company
Lycoming Division
Stratford, Connecticut
Attn: Dr. J. C. Keck   (1)

Boeing Airplane Company
Box 3107
Seattle 14, Washington   (1)

Borg-Warder Corporation
Research Center
Applied Physics Group
Des Plaines, Illinois
                                    (1)

Chance-Vought Aircraft Corporation
Dallas, Texas   (1)

CONVAIR
San Diego Division
San Diego 12, California
Attn: Dr. W. H. Dorrance   (1)

Air Force Plant Representative
San Antonio Air Material Area
CONVAIR-Astronautics
San Diego 12, California   (1)

Douglas Aircraft Company, Inc.
3000 Ocean Park Boulevard
Santa Monica, California   (1)

Fairchild Engine & Aircraft Company
Guided Missiles Division
Wyandanch, L.I., New York   (1)

Fairchild Engine & Aircraft Company
Fairchild Engine Division
Farmingdale, L.I., New York
Attn: Mrs. C.Minck, Librarian   (1)

Flight Sciences Laboratory, Inc.
1965 Sheridan Drive
Buffalo 23, New York
Attn: Dr. J. S. Isenberg,
         Technical Director   (1)

General Applied Science Laboratories
Meadowbrook National Bank Building
60 Hempstead Avenue
Hempstead, New York
Attn: Jane L.Herod, Librarian   (1)

General Electric Company
Research Laboratory
P. O. Box 1088
Schenectady, New York
Attn: Drs. Nagamatsu, White,
         and Alpher   (1)

General Electric Company
Special Defense Projects Department
3198 Chestnut Street
Philadelphia 4, Pennsylvania
Attn: Aerophysics Lab. Operation
         Dr. J. Farber   (2)

Dr. Gottfried K. Wehner
Mechanical Division
General Mills, Inc.
1620 Central Avenue
Minneapolis 13, Minnesota   (1)

The Glenn L. Martin Company
Department 520, Mail No. 3072
Baltimore 3, Maryland .
Attn: Mr. L. Cooper   (1)

Grumman Aircraft Engineering Corp.
Bethpage, L.I., New York   (1)

Hughes Aircraft Corporation
Research and Development Laboratory
Culver City, California
Attn: Dr. A. E. Puckett   (1)

Hydronautics, Incorporated
200 Monroe Street
Rockville, Maryland
Attn: Mr. Phillip Eisenberg
         Mr. Marshall P. Tulin   (1)

INDUSTRIAL ORGANIZATIONS -(Cont'd)

Technical Information Center, 50-21
Lockheed Missiles and Space Division
P. O. Box 504
Sunnyvale, California   (1)

Marquardt Aircraft Corporation
7801 Havehurst
Van Nuys, California   (1)

Midwest Research Institute
Department of Physics
4049 Pennsylvania Avenue
Kansas City, Missouri
Attn: Mr. K.L.Sandefur   (1)

North American Aviation, Inc.
Aerophysics Department
12214 Lakewood Boulevard
Downey, California
Attn: Dr. van Driest   (1)

Northrop Aircraft, Inc.
Northrop Field
Hawthorne, California   (1)

Technical Librarian
Ramo-Wooldridge Corporation
8820 Bellance Avenue
Los Angeles 45, California
Attn: Drs. M.U.Clauser, Doll,
    & J. Logan   (2)

RAND Corporation
1700 Main Street
Santa Monica, California
Attn: E.P.Williams &
    C. Gazley, Jr.   (1)

Republic Aviation Corporation
Farmingdale, L.I., New York   (1)

Sandia Corporation
Sandia Base
Albuquerque, New Mexico
Attn: Drs. C.C.Hudson, M.L.Merritt,
    & J.D.Shreve, Jr.   (1)

Stanford Research Institute
Poulter Laboratories
Palo Alto, California
Attn: Drs. Poulter & Duvall   (1)

Therm Advanced Research
Therm, Incorporated
Ithaca, New York
Attn: Dr. A. Ritter

SPECIAL ADDITIONAL LIST FOR THEORETICAL PAPERS

Professor M. Holt
Division of Applied Mathematics
Brown University
Providence 12, Rhode Island

Professor H. Lew
Applied Mathematics Group
Mathematics Department
University of California
Berkeley 4, California

Professor D. Gilbarg
Graduate School for Applied Mathematics
Indiana University
Bloomington, Indiana

Librarian
Graduate School for Applied Mathematics
Indiana University
Bloomington, Indiana

Dr. G. Griderley
P. O. Box 186
Fairborn 4, Ohio

SPECIAL ADDITIONAL LIST FOR RAREFIED GASES

Mr. K. M. Siegel
Upper Atmosphere Section
Willow Run Research Center
University of Michigan
Ypsilanti, Michigan

Professor A. H. Kuhlthau
Department of Physics
University of Virginia
Charlottesville, Virginia

Australian Weapons Research Establ.
c/o Defence Res. & Dev. Representa.
Australian Joint Service Staff
P.O. Box 4837
Washington 8, D. C.